Title

Marsh Dynamics: Laboratory and Field Investigations of Gas Transport, Wave Attenuation, and Biosolids Amendment

Author

Foster-Martinez, Madeline

Publication Date

2017

Marsh Dynamics: Laboratory and Field Investigations of Gas Transport, Wave Attenuation, and Biosolids Amendment

by

Madeline Russell Foster-Martinez

A dissertation submitted in partial satisfaction of the
requirements for the degree of
Doctor of Philosophy

in

Engineering - Civil and Environmental Engineering

in the

Graduate Division

of the

University of California, Berkeley

Committee in charge:

Professor Evan A. Variano, Chair
Professor Mark T. Stacey
Professor Laurel G. Larsen

Fall 2017

Marsh Dynamics: Laboratory and Field Investigations of Gas Transport, Wave Attenuation, and Biosolids Amendment

Abstract

Marsh Dynamics: Laboratory and Field Investigations of
Gas Transport, Wave Attenuation, and Biosolids Amendment

by

Madeline Russell Foster-Martinez

Doctor of Philosophy in Engineering - Civil and Environmental Engineering

University of California, Berkeley

Professor Evan A. Variano, Chair

Marshes, and tidal salt marshes in particular, are gaining recognition as critical elements in sustainable shoreline protection (Narayan, Beck, Reguero, *et al.* 2016; Narayan, Beck, Wilson, *et al.* 2016; Spalding, Ruffo, *et al.* 2014; Spalding, McIvor, *et al.* 2014). They contribute to coastal resiliency not only by attenuating wave energy in large storms (Gedan *et al.* 2011; Möller, Kudella, *et al.* 2014), but also by maintaining the existence of coastal land (Kirwan *et al.* 2016), supporting fisheries (Boesch & Turner 1984; MacKenzie & Dionne 2008), sequestering carbon (Ouyang & Lee 2014), and removing contaminants (Dhir *et al.* 2009; Windham *et al.* 2003). These benefits directly contribute to the sustainability of the growing populations in coastal regions (Sutton-Grier, Wowk, *et al.* 2015). With this recognition, there are many ongoing projects to preserve existing salt marshes, restore former marshes, and create hybrids of natural and engineered structures (Pontee *et al.* 2016). These projects require an understanding of the underpinning processes that lead to marsh sustainability. The projects presented in this dissertation are efforts to better understand marsh dynamics. The first project explores the impact of emergent vegetation on gas flux in marsh surface waters. Wind causes the stems of emergent vegetation to wave back and forth, stirring the water column and facilitating gas exchange. To understand the magnitude of this effect, a gas transfer velocity (k_{600}-value) was measured via laboratory experiments. Measuring this transport pathway contributes to a mechanistic understanding of gas flux and can improve models of climatically important gases. The second project examines wave attenuation across a salt marsh. Salt marsh vegetation is effective at reducing wave energy. It is important to understand how this attenuation varies. Through field measurements, wave attenuation is explored as a function of hydrodynamic conditions, season, and vegetation type. The results showed that even fringe marshes, which are common in San Francisco Bay, are effective at reducing wave energy year-round. The last project investigates the viability of using biosolids as an amendment to dredged material in marsh restorations. Biosolids is a reliable and sustainable source of sediment, and more sources of sediment are needed for marsh restoration projects. Both the aboveground and belowground biomass increased when vegetation was grown in soil containing biosolids as compared to only dredged material. Taken together, the three projects discussed here can contribute to improving the success and efficiency of marsh restoration and preservation.

To Charles ‘Pete’ Savoye

May we have his pluck and remember to listen.

Contents

List of Figures

List of Tables

Acknowledgments

Starting at UC Berkeley was daunting. It was a complete unknown, and California was unfamiliar in just about every way. Fast forward 1593 days later, and I'm part of a community that I cherish - one that made this dissertation possible and then helped make it a reality. I won't be able to thank everyone here, or do justice to those I can name, but I hope you know how much you've meant to me.

To the UC Berkeley Environmental Fluid Mechanics and Hydrology group, it's been a joy to be surrounded by you. Thank you for welcoming my fluid mechanics questions that crop up at odd times of the day and helping me prepare (and calm down) for oral exams. Particular thanks to Eli Goodfriend, Rusty Holleman, Lissa MacVean, Diane Taylor, Michelle Hummel, Alex Anderson-Connolly, Olivia Huàng, and Jason Simon for great guidance and discussions. To the Variano lab - Ian Tse, Cristina Poindexter, Ankur Bordorloi, Kim Huynh, Teri Oehmke, Nimish Pujara, Rachel Allen - you're wonderful people. I'm glad I got to be around you. To Megan Williams, you rescued me from more than just geese. Thank you for your time and friendship. To Margaret Byron and Susan Willis, I feel so lucky to have shared an office with you; your love of research and enthusiasm for life diffused my way.

To my dissertation committee, thank you for being supportive not only of my learning but also of my goals for this PhD. To Mark Stacey, your environmental fluid mechanics class is why I am where I am. Thank you for your willingness to talk and provide support. To Laurel Larsen, thank you for great classes and field research and outreach opportunities; you enriched my PhD experience. To my advisor, Evan Variano, thank you for taking me on as your student. The needs of each PhD student are different or even the needs of the same student over the course of a day. Thank you for always being flexible in your advising. Your constant asking what we needed - whether that be going over boot-strapping, hauling dirt in a marsh, recruiting undergraduate lab assistants, or a reflecting on the future of our field - made a world of difference. Thank you for always being ready and willing. To all of my professors - in particular Kara Nelson, Sally Thompson, David Sedlak - thank you for outstanding courses.

To Jessie Lacy, working with you and at USGS was one of the highlights of my time in California. Thank you for your mentorship and advisement and for choosing to work with me in the first place. To all of the USGS and SF NERR people, thank you for making field work fun and for teaching through example how to do good science. To Matt Ferner, thank you for thought-provoking discussions and for valuing my projects. Your encouragement was monumental.

To my PREP family, you made the beginning of August a blast! Thank you to all the PREP students for your eagerness to learn. Y'all were and continue to be my inspiration. To Oscar Dubon, Gian Bruno, and Meltem Erol, your faith in me gave me reassurance when I needed it the most. To Paige Teamey, you always seem to enter my life at just the right moments. Keep it up please?

To Project Touchdown, no matter how my week was going, I knew I would walk out of the doors on Thursday evenings feeling back to myself. Thank you for welcoming me into the program and for always reminding me of what is most important in the world. To Regan Patterson and Bria Crawford, I loved the opportunity to spend time with you, albeit too short. Thank you for always caring about my life.

To my cohort, I truly lucked out by starting Berkeley in Fall 2012. Karina Chavarria, Jennifer Lawrence, Joe Charbonnet, James Barazesh, Kevin Olson, Katya Cherukumilli, Chelsea Preble, Rachel Allen, Will Tarpeh - you have been the best friends. To Chelsea Preble and Jennifer Lawrence, thank you for always being willing to help me out (the existence of my signature page is proof!). I've relied upon all of you for countless last-minute requests. To Michael Levy, I've truly appreciated your insights. Thank you to Rachel Dzombak, whose advice is invaluable, not to mention is the reason I'm able to put words on the page at this very moment. To Will Tarpeh, our conversations kept me grounded in why I went to graduate school and kept me pursuing my goals. You are a true leader, and I feel so fortunate to call you a friend. To Rachel Allen, you should be thanked a million-times over. Your capacity to be a supportive and loving friend has proven to be limitless.

To my Bay Area family - Julien Caubel, Zoe Young, Beryl Bevilacque, Luke Ingoldsby, to name a few. Y'all are the best. Thank you for being an awesome support team, not to mention a whole lot of fun. To Christina Milone and Toby Cumberbatch, I know I would not have had the opportunity to get a PhD without you in my life.

This next part is difficult - family is a source of endless love and support, and mine is an exceptional example. To Matthew, Sarah, and Bee, you have been my cheerleaders my whole life, and I can't imagine who I would be without you. To Mom and Dad, no words describe how grateful I am for you two. You've always led by example, and I hope to continue to follow that example. You're the reason I believe people can enact positive change, and that belief has propelled me to this moment. Thank you, MawMaw and Mom, for sending newspaper clippings; they got me out of the bubble and reminded me why I wanted my work to be applicable. To PawPaw, thank you for being an engineer who loved his work. I'm not sure it's true, but my belief that I got some of your brains because I got your nose gave me confidence in moments I needed it. Thank you to my whole Foster-Knipmeyer-Merrill-Chenier-Perry-Martinez family. I love all of you so much. Thank you for making coming home a thing worth celebrating.

To Connor Perry Martinez, you're my favorite. Thank you for both literally and figuratively getting me to California. You (and Tipper) are the loves of my life.

Lastly, to the person who honks at 8:30 pm while driving down Telegraph Avenue every night, thanks for the reminder.

Chapter 1

Introduction

Coastal marshes are highly complex environments. Occupying the space between terrestrial and aquatic ecosystems, they are adapted to deal with the challenges of living at the lands edge. Marshes can raise their surface elevation to keep pace with sea-level rise and withstand high shear forces that accompany storms. Marsh vegetation takes up nutrients from surface waters, protecting fragile aquatic habitats from eutrophication (Valiela & Cole 2002). Countless species of wading birds and migratory waterfowl to fish and shellfish rely on marshes as habitat for part of their life cycle (Mitsch & Gosselink 2007). These functions are vital for healthy coastlines, yet humans have not always recognized the ways marshes benefit coastal communities. This lack of recognition led to mass destruction of these environments, either through direct conversion (*e.g.* salt pond creation, Patton 2002) or through impeding functioning (*e.g.* access canals, Baustian *et al.* 2009). Many projects of the nineteenth and twentieth centuries that were viewed as engineering feats are now seen as unsustainable disruptors of natural processes (*e.g.* Mississippi River Gulf Outlet, Shaffer *et al.* 2009).

Coastlines are currently experiencing the effects of climate change (Sweet *et al.* 2017). As sea-level rise compounds with storm activity (T. R. Knutson *et al.* 2010; Stocker *et al.* 2014), urgency is increasing to construct nature-based coastal protection (Narayan, Beck, Reguero, *et al.* 2016; Spalding, McIvor, *et al.* 2014). The 2017 hurricane season brought much destruction to southeastern United States, namely Texas, Florida, and Puerto Rico. As these communities contend with rebuilding and others take preventative measures, we have an opportunity to learn from the engineering mistakes of the past. With informed planning, we can build ecologically functioning systems that that allow for continuation of life at our coastlines.

The three projects presented in this dissertation are efforts to increase our understanding of marsh dynamics, thereby informing coastal engineering designs and decisions. The section below describes relevant marsh processes and is followed by brief introductions to each project.

1.1 Background

Marshes are a type of wetland. All wetlands are defined by being flooded during part of the year and by containing vegetation adapted to these inundated conditions (Mitsch & Gosselink 2007). Marshes are further defined as containing herbaceous, emergent vegetation. They differ from other wetlands, such as mangroves and swamps, in that they do not contain trees.

Marshes are categorized by the level of salinity in surface water, ranging from fresh to hyperhaline (Cowardin *et al.* 1979). Since tidal salt marshes are the focus of two of the three projects presented here, the following information pertains this ecosystem. Note, the remaining project more generally addresses all emergent vegetation species and is therefore, also relevant in this discussion.

Marsh vegetation is adapted to live in inundated conditions. Surface water greatly inhibits gas transport as compared to terrestrial systems, making it difficult to transport oxygen to the roots. To overcome this stress, the tissues of marsh vegetation are filled with air. These tissues, called aerenchyma, allow for gases to bypass the surface water and exchange between the atmosphere and belowground sediments (Teal & Kanwisher 1966).

Inundation in marshes can also benefit the vegetation. The process of tidal inundation and draining helps flush out salts and harmful toxins (Weinstein & Kreeger 2000). Surface water can also deliver essential nutrients. Field experiments have examined the relationship between biomass production and the amount of inundation received, or the hydroperiod, for salt marsh species (*e.g.* Snedden *et al.* 2015; J. Morris *et al.* 2013). *Spartina foliosa* (pacific cordgrass), follows a parabolic pattern with both the above- and belowground biomass reaching maximum productivity when inundated about 40% of the time (Janousek *et al.* 2016). *Salicornia pacifica* (pickleweed), which sits higher in the tidal frame than *S. foliosa*, follows an exponential decay with the greatest biomass at the lowest inundation levels (Janousek *et al.* 2016).

Salt marshes are first point of contact as storms move onshore in many locations. Densely packed roots and rhizomes of marsh vegetation, in combination with inorganic material, create soils with shear strengths that exceed 4500 Pa, which is greater than the maximum shear stress caused by Hurricane Katrina (Howes *et al.* 2010). These high strength soils are more resistant to erosion than their low-salinity counterparts. In an undisturbed system, low-salinity and freshwater marshes are located further inland and would not typically encounter erosive forces associated with storms.

Located at the land's edge, salt marshes must manage changes in sea level. A feedback loop allows marsh platforms to keep pace with sea-level rise (Fagherazzi *et al.* 2013). As tidal water floods a marsh, the vegetation imposes a drag force, slowing the speed of the water. As the water slows, suspended sediment settles out and deposits on the marsh surface. If the tidal inundation increases, the amount of suspended sediment brought into the marsh increases. This additional sediment raises the marsh surface, thereby reducing the amount of inundation received. Moderately more inundation also leads to a boost in biomass production, increasing the organic matter contribution to surface accretion. This loop operates within a certain range of sea-level rise rates and suspended sediment concentrations, outside of which this balance is not maintained.

1.2 Outline of Research Chapters

1.2.1 Chapter 2: Gas transport due to marsh vegetation movement

Exchange between wetland surface water and the atmosphere is driven by a variety of motions, ranging from rainfall impact to thermal convection and animal locomotion. Here, we examine the effect of wind-driven vegetation movement. Wind causes the stems of emergent vegetation to wave back and forth, stirring the water column and facilitating air-water gas exchange. To understand the magnitude of this effect, a gas transfer velocity (k_{600}-value) was measured via laboratory experiments. Vegetation-waving was studied in isolation by mechanically forcing a model canopy to oscillate at a range of frequencies and amplitudes matching those found in the field. Measuring this transport pathway contributes to a mechanistic understanding of gas flux and can improve models of climatically important gases.

1.2.2 Chapter 3: Wave attenuation across a tidal marsh

Wave attenuation is a central process in the mechanics of a healthy salt marsh and is often cited as a key motivation for marsh restoration. It is important to understand how wave attenuation varies with vegetation and hydrodynamic conditions. These relationships inform models of other marsh processes that are a function of wave energy (*e.g.* sediment transport) and allow for the incorporation of marshes into coastal protection plans. Here, we examined the evolution of wave height across a tidal salt marsh in San Francisco Bay. Instruments were deployed along a cross-shore transect, starting on the mudflat and crossing through zones dominated by *Spartina foliosa* and *Salicornia pacifica.* This dataset is the first to quantify wave attenuation for these vegetation species, which are abundant in the intertidal zone of California estuaries. Measurements were collected in the summer and winter to assess seasonal variation. By performing a local study on what is in practice a local phenomenon, the results inform designs for marsh restorations and management plans in San Francisco Bay.

1.2.3 Chapter 4: Biosolids as Marsh Restoration Amendment

The typical process of restoring or creating a marsh consists of filling an area of open water with dredged material. The elevation is raised to the point where emergent vegetation can grow. We investigated ways biosolids can be used as an amendment to dredge material to enhance project outcomes. Marsh mesocosms were built in San Francisco Bay and planted with native cordgrass, *Spartina foliosa*. One third of the mesocsoms contained a subsurface layer of biosolids sourced from a local wastewater treatment facility. Biosolids contain organic matter and nutrients, which can be beneficial to plant growth, and are reliably produced in urban areas. By using biosolids in marsh restorations, we are integrating human infrastructure and natural processes.

Chapter 2

Gas Transport due to Marsh Vegetation Movement

2.1 Introduction

2.1.1 Motivation

Gas transport has both direct and indirect influences on the chemical composition of the water column. A direct effect is the diel emission of methane due to nighttime thermal stirring (Poindexter & Variano 2013). An indirect effect is seen in the absorption of oxygen across the air-water interface. The relationship between oxygen concentrations and methane flux has been measured in a number of environments, due to the importance of methane as a greenhouse gas (GHG). At sites in the Okavango Delta an increase in surface-water dissolved oxygen from less than 0.2 to 3.6 mg/L has been shown to accompany an order-of-magnitude decrease in diffusive methane flux, presumably due to an increase in aerobic methanotrophy (Masamba *et al.* 2015). A change in oxygen levels can also lead to a change in decomposition rates, which in turn affects the rate of peat accretion and the ability of the wetland to maintain its elevation relative to sea level (Miller, Fram, *et al.* 2008).

Herein we examine one of the mechanisms influencing gas transport. Our intent is to improve the mechanistic foundations available to predictive modeling efforts. Such improvements can contribute to a better understanding of global carbon cycling (Melton *et al.* 2012), as well as local gas flux. Gas transport models have the potential to replace the direct measurements of flux currently required by methods accredited by the American Carbon Registry for calculating carbon offsets (Mack *et al.* 2012).

2.1.2 Background

While gas transport has been extensively studied in open water environments, such as lakes (MacIntyre *et al.* 2010) and oceans (D. T. Ho, Wanninkhof, *et al.* 2011), wetlands have unique features that prevent the direct application of other methods and findings (Happell *et al.* 1995). Particularly, the presence of emergent vegetation greatly alters the system dynamics. Emergent vegetation is rooted underwater but emerges though the air-water interface. Physically, emergent vegetation shields the water surface from wind and sunlight and acts to couple the atmosphere and the water column. This coupling changes the influence of wind from direct shear, as expected on a lake, to damped bursts of momentum and to wind-driven vegetation movement. Previous work has explored the relative importance of these momentum-bursts for water column mixing and has shown they are non-negligible for wetland environments (Tse *et al.* 2016). Here, we focus on wind-driven vegetation movement and its effect on gas transport.

Wind-vegetation coupling has been studied in a diverse group of disciplines with applications ranging from seed dispersal to computer animation (de Langre 2008). Particular attention has been given to the honami phenomena, in which waves appear to roll along a canopy of vegetation. It was first documented in Inoue (Inoue 1955) through observation of wind on wheat fields. Honamis form in terrestrial canopies as shear layer instabilities cause stalks to spring back and forth in a coherent manner; however, the exact generation mechanism is still debated (Finnigan 1979; Raupach *et al.* 1996). The submerged vegetation counterpart, monami, presents a simpler case due to the restricted scale of the shear layer (Ghisalberti & Nepf 2002). For both honami and monami, peaks in the flow velocity spectra occur at the natural frequency of the vegetation, and the frequency of the vegetation oscillations remains at the natural frequency regardless of the flow velocity (Finnigan 1979; Ghisalberti & Nepf 2002; Py *et al.* 2006; Gosselin & de Langre 2009). A gap in this research exists for systems with emergent vegetation; however, we work under the hypothesis that the natural frequency would continue to dominate the movement in emergent vegetation.

Numerous studies have explored the natural oscillation frequencies of a variety of vegetation types, using equations for slender rods with varying loading situations (Spatz & Speck 2002; Brüchert *et al.* 2003; Speck & Spatz 2004). Yet accurately estimating this frequency for real vegetation has proven challenging and requires a combination of video and analytical techniques (Flesch & Grant 1992; Doaré *et al.* 2004; Py *et al.* 2006). Even for one species, factors such as seasonal senescence, vegetation health, and crowding cause significant variation in morphologies and material properties (Harley & Bertness 1996; Neumeier 2005). For emergent vegetation, the water acts as an additional dampening mechanism, making the frequency a function of the water depth in addition to the vegetation material properties. Due to this complexity and the desire to have generic results that encompass a range of motions, we select a range of frequencies and amplitudes to study, measuring the dependence of gas transfer on both.

2.2 Methods

2.2.1 Thin film model

The thin film model of gas transport describes expected flux across an interface ($\langle J_{\text{interface}} \rangle$) as a function of molecular diffusion (D_m), thickness of an idealized thin-film diffusive boundary layer (λ) and concentration gradient across the thin film:

$$\langle J_{\text{interface}} \rangle \approx \frac{D_{\text{m}}}{\lambda}(\langle C_{\text{Interface}} \rangle - \langle C_{\text{Bulk}} \rangle) \tag{2.1}$$

Where angle brackets represent expectation values. Equation 2.1 has two concentrations of interest, $\langle C_{\text{Bulk}} \rangle$ and $\langle C_{\text{Interface}} \rangle$. We assume that the diffusive processes in the bulk of the fluid are large, creating a homogenous concentration ($\langle C_{\text{Bulk}} \rangle$) everywhere except at the interface. This assumption is supported by laboratory measurements of dissolved oxygen and field measurements of methane (Poindexter & Variano 2013). At the interface, we assume the solute is in equilibrium with the atmosphere, thus $\langle C_{\text{Interface}} \rangle$ can be found using Henry's Law. The molecular diffusion and boundary layer thickness terms are combined to form the gas transfer velocity, $k = D_m/\lambda$.

$$\langle J_{\text{interface}} \rangle \approx k\Delta C = k(\langle C_{\text{Equilibrium}} \rangle - \langle C_{\text{Bulk}} \rangle) \tag{2.2}$$

Gas transfer velocity is a commonly-used parameter for quantifying and comparing gas transport in different environments and caused by different mixing mechanisms. A more active mixing mechanism gives a larger k and thus a larger gas flux. Taking a mass balance through a water column of depth h (with no production or decomposition of solute and flux only at the air-water interface) gives us a solution to Equation 2.2:

$$\Delta C(t) \approx \Delta C(t_0) e^{-(\frac{k}{h})(t-t_0)} \tag{2.3}$$

A time series of ΔC can be collected in the laboratory and used to calculate k. This is the approach used herein. Since k includes the effects of molecular diffusion, it is dependent on the temperature at which the experiment was performed. To account for these thermodynamic effects and to compare with other solutes, k is scaled using an established empirical relationship (Barber *et al.* 1988):

$$k_1 = k_2(\frac{Sc_1}{Sc_2})^{-\alpha} \tag{2.4}$$

Where the Schmidt number (Sc) is defined as

$$Sc \equiv \frac{\nu}{D_m} \tag{2.5}$$

For comparability between studies, k is commonly scaled to a reference Schmidt number of 600, giving k_{600}:

$$k_{600} = k_{exp}(\frac{600}{Sc_{exp}})^{-\alpha} \tag{2.6}$$

The α value in Equation 2.6 is dependent on the surface conditions of the interface. It has been found to range from 1/2 for a clean surface to 2/3 for a no-slip boundary; however, it has been shown that even a low level of surface contamination causes a surface to act similarly to a no-slip boundary in regards to inhibiting gas transport (McKenna & McGillis 2004). As wetlands contain a high level of surfactants (Kadlec & Wallace 2008), the 2/3 exponent seems appropriate.

2.2.2 Experimental Design

By working in a laboratory, we were able to isolate the mechanism of wind-driven vegetation movement and produce results that are not site specific. While honami motion does not occur in isolation in real wetlands, we isolated it here to judge the relative contribution of this mechanism to the total diffusive flux.

Wind-driven vegetation movement was recreated in a laboratory tank (Figure 2.1). Plastic tubes acting as emergent vegetation were anchored at the top and bottom in two plates that were separated by 65 cm; the bottom plate was secured to the bottom of the tank, while the top plate sat on two rollers and was oscillated horizontally in one dimension. These tubes have dimensions similar to *Schoenoplectus acutus*, a common California wetland species known as Tule, with a diameter of 13 mm; they were randomly spaced to give a vegetation density of 2.16 m^{-1}, which is within the range of naturally-grown Tule (Gardner *et al.* 2001; Miller & Fujii 2009). Since we were interested in how the stem acts as a stirring rod at the air-water interface and not in biological interactions, it was not necessary for our laboratory setup to use real vegetation.

A motor was used to move the top plate, and therefore the synthetic vegetation, back and forth at a set frequency and amplitude. The natural frequency of Tule was measured through an in situ video of a single live stem being plucked and was determined to be approximately 1 Hz. Past measurements of terrestrial alfalfa have shown a range of 0.8 to 1.5 Hz and 1.29 to 1.80 Hz for corn (Flesch & Grant 1992; Py *et al.* 2006). A range of stem-waving frequencies was tested in the laboratory to cover a range of natural conditions. Since the water acts to dampen the motion and lower the frequency (S. S. Chen *et al.* 1976), we tested a range of 0.3 - 1.2 Hz.

For the frequencies considered, there were three amplitude scenarios: 0.5 cm (small), 0.8 cm (medium), and 1.3 cm (large). These values encompass a range observed from our in situ video and qualitative observations of vegetation waving at a number of wetland sites with a variety of wetland vegetation. The flow in all experiments was laminar, remaining under the Reynolds number, $Re_d = Ud/\nu$, threshold for turbulent wake structures within an array of cylindrical vegetation (Nepf 1999).

A wave-dampening buffer was added to the perimeter of the study area at the air-water interface. This buffer was meant to prevent the formation of an in-tank seiche and to minimize tank boundary effects. Data collected with and without the buffer is presented.

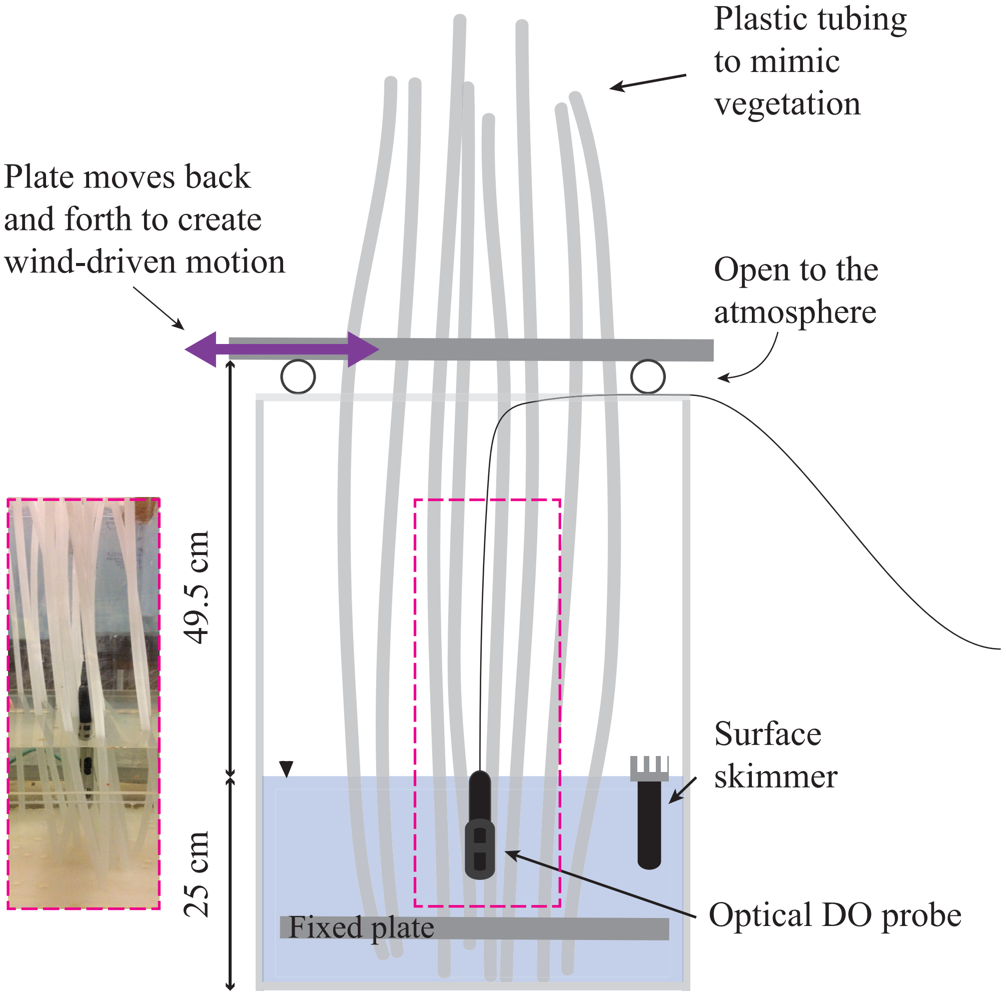

Figure 2.1: Diagram of the laboratory setup. Plastic tubing, mimicking vegetation, was run through two parallel plates; the bottom plate was fixed, while the top plate was oscillated in one dimension. An optical DO probe took measurements in the middle of the water column. The top of the tank is open to the atmosphere. Photograph to the left shows the central area of the tank. Tank buffers are not shown.

2.2.3 Experimental Procedure

Each experiment began by deoxygenating the water using sodium sulfite; cobalt chloride was used as a catalyst. After the reaction was completed, 5 cm were skimmed off the surface to give a final water depth of 25 cm. Skimming this top layer allowed for experimental repeatability but was not expected to produce a surfactant-free surface. Side panels prevented lateral transport to the unvegetated sections of the tank, creating a study area 33 cm wide and 48 cm long.

The frequency for each experiment was determined from videos taken at the beginning and end using ImageJ (available at https://imagej.nih.gov/ij/docs/index.html). The frequency increased over the course of the experiment, which we ascribe to the warming of the motor. The difference between the beginning and ending frequency was kept as small as possible by cooling the motor with an external fan.

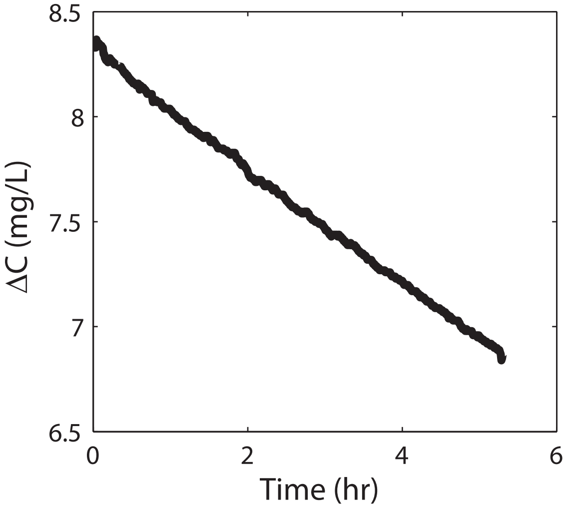

Figure 2.2: Example time series of the change in dissolved oxygen concentration for one experiment. ΔC is defined in Equation 2.2

As the vegetation moved, oxygen diffused into the water, re-equilibrating with the atmosphere. A time series of the dissolved oxygen concentration at the middle of the water column was then recorded using an optical probe (YSI ProODO). An example time series is shown in Figure 2. It was important to use an optical probe, as those which require strong stirring near a membrane (*i.e.* Clark-type probes) may not have received enough stirring in this flow. From the dissolved oxygen time series, we used the thin film model of gas transport to determine the gas transfer velocity, via Equation2.3.

Control experiments with no oscillations were also performed in the experimental setup. With no motion, the gas transfer is driven by ambient thermal convection, which is slow and variable. The greatest value of k_{600} from the no-motion experiments was used as a comparison.

2.2.4 Statistical Analysis

Each dissolved oxygen time series was divided into subsets, where each subset represents an increase in dissolved oxygen of 0.02 mg/L. This gives n subsets per experiment, where n is always greater than 92. A k_{600} value was computed for each subset; k_{600} for the experiment was set as the median across n. The 95% confidence interval was found via bootstrap by resampling 1000 times from n (Efron & Tibshirani 1994).

2.3 Results

Gas transfer velocity is enhanced by the movement of emergent stems. With no motion, the greatest k_{600} in our experimental setup was 0.4 cm/hr, which is the lower bound in Figure 2.3. In Figure 2.3, the vertical error bars show the 95% confidence interval, calculated as described in Section 2.3. The horizontal error bars reflect the difference in frequency from the beginning to end of the experiment. In all experiments, the frequency at the end was higher than at the beginning. The choice of the 2/3 exponent, rather than 1/2 discussed in Section 2.1, caused an average decrease of 4.31.9% in the resulting k_{600}.

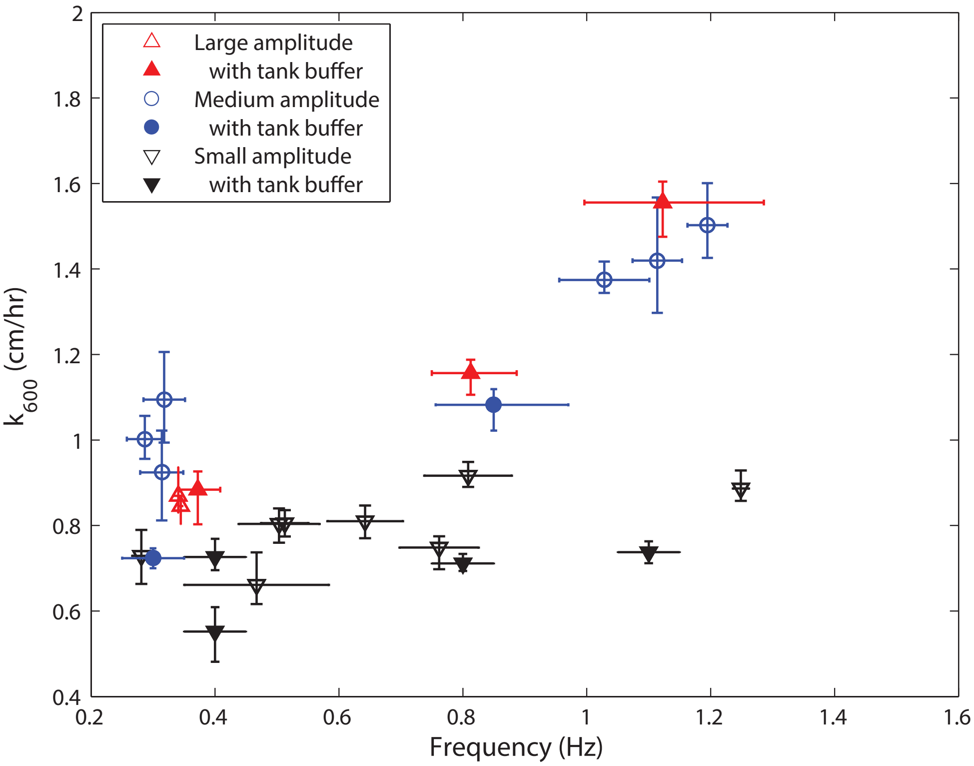

Figure 2.3: Results from gas transfer velocity experiments. Colors and symbols represent the three amplitudes tested. Closed symbols represent experiments run with wave-dampening buffer along the tank perimeter. Vertical error bars encompass 95% confidence interval, and horizontal error bars show the full range of the forcing frequency in each experiment. Small amplitude = 0.5 cm; Medium amplitude = 0.8 cm; Large amplitude = 1.3 cm.

The closed symbols indicate experiments where wave-dampening buffer was placed at the edges of the tank at the air-water interface. The presence of this buffer reduces the tank boundary effects on k_{600}. Linear regression on k_{600} versus frequency for the small amplitude case shows that the slopes are the same with and without the buffer, but intercepts differ, indicating an amplification of k_{600} by 0.15 cm/hr when the buffer is absent. The full dataset is presented and indicates when the buffer setup was used.

For stem-waving frequencies below 0.5 Hz, the results for all amplitude cases are clustered together. Beyond this frequency, the medium- and large-amplitude cases show an increase in gas transfer velocity reaching a maximum of 1.6 cm/hr. The small amplitude case shows little dependence on frequency, remaining less than 1 cm/hr at a frequency of 1.25 Hz.

Our results show that for small-amplitude motions, the stem-waving frequency does not greatly alter the gas transfer velocity. At larger amplitudes, k grows with frequency in a manner that seems linear, or slightly more rapid than linear.

2.3.1 Dimensional Analysis

These results can also be viewed non-dimensionally. Gas transfer velocity is a function of stem-waving frequency (f), amplitude (a), stem diameter (d), and viscosity (ν):

$$k = h(f, a, d,) \tag{2.7}$$

Dimensional analysis suggests the following:

$$\Pi_0 = H(\Pi_1, \Pi_2) \tag{2.8}$$

$$\frac{k}{fa} = H(\frac{d}{a}, \frac{\nu}{fa^2}) \tag{2.9}$$

Our results show that Π_0 is nearly independent of Π_1, allowing it to be combined with Π_2 to produce a Reynolds number:

$$\Pi_0 = G(\Pi_1, \Pi_2) \tag{2.10}$$

$$\frac{k}{fa} = G(\frac{fad}{\nu}), \text{where } Re \equiv \frac{fad}{\nu} \tag{2.11}$$

The data confirm the result of Equation 2.8, as seen in Figure 2.4.

Since G has the form of typical drag coefficients, we rewrite the dimensionalized form as

$$k = fa * C_D(Re) \tag{2.12}$$

Here, we have confined the analysis to only include data from experiments with the tank buffer. This result highlights the importance of both stem-waving frequency and amplitude. Their product (fa) is the maximum velocity of the vegetation stem as it oscillates. When

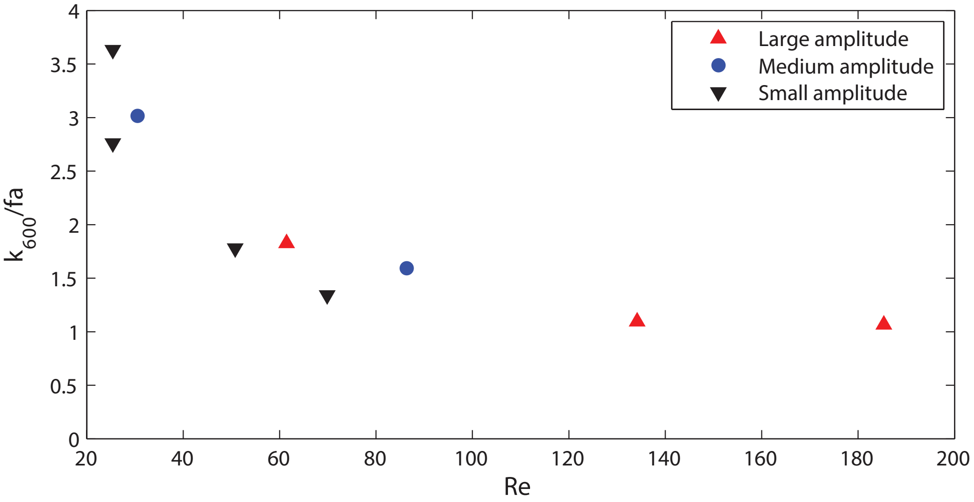

Figure 2.4: Results of dimensional analysis. Gas transfer velocity scaled by fa and given as a function of Re (defined in Equation 2.11). Data shown is only from experiments with the tank buffer.

either the amplitude or frequency is sufficiently large, the gas transfer velocity appears to be linearly proportional to fa.

2.4 Discussion

Having quantified the effect of stirring by vegetation stems, we can put this mechanism into context with the other drivers of wetland air-water exchange. These drivers include rain, water convection due to differential heating, and wind directly shearing the surface. The latter two drivers have been quantified by Poindexter and Variano (Poindexter & Variano 2013), giving k_{600}-values between 0.1 and 4 cm/hr depending on conditions. Even with a k_{600} of 0.6 cm/hr, which is at the lower end of this range, Poindexter showed that air-water exchange is an important pathway in the wetland biogeochemical budget. Since vegetation-waving gives k-values within the same range considered by Poindexter, we can conclude that it has a non-negligible effect on wetlands as well.

This effect of waving on the gas transfer velocity is much smaller than the effect of wind would be in the absence of vegetation. The canopy greatly reduces wind speed (Tse *et al.* 2016), and the small amount of wind shear acting on the surface drives a typical gas transfer velocity around 0.1 cm/hr (Poindexter & Variano 2013). This value is negligible compared to the gas transfer velocities observed in open waters, which are certainly above 1 cm/hr and typically on the order of 10 cm/hr (Crusius & Wanninkhof 2003). The effect of rain has been quantified by Ho *et al.* (D. T. Ho, Zappa, *et al.* 2004); taking measurements in a model ocean, results showed that even with ocean-like forcing the presence of rain can increase k_{600}

from 11.2 to 49.7 cm/hr. Although these are strikingly different conditions, rain is likely to also be significant in wetlands.

When considering these different drivers, the timing and consistency of the events become important. Rain may be the dominant driver during rain events. The tendency of vegetation-waving to be intermittent in time lowers its importance relative to thermal convection, which is driven consistently by the day-night cycle, but the fact that vegetation-waving can occur everywhere in a dense wetland makes it more important than direct wind shear, which is greatly weakened away from canopy edges.

Two open questions remain before the effect of vegetation-waving on wetland biogeochemistry can be fully described. The first is an understanding of how the different drivers acting on the air-water interface combine with each other. The second is a thorough survey of the frequency and amplitude of the waving, and how it varies with wind conditions, canopy density, plant type, and plant life-stage. This first question arises from the fact that these drivers of motion naturally occur simultaneously along with additional mechanisms such as animal motion and seiches, whose effect on gas transfer velocity in wetlands is unknown. Until we understand how these individual k values combine, the relative importance of each phenomena is uncertain. That is, there may be nonlinear interactions in which two stirring phenomena amplify or attenuate each other. At the moment, we can only compare the magnitude of different forcings in isolation and suggest that the strongest forcings be included in predictive models for wetland biogeochemical budgets. Our results can also be used to estimate the bias incurred by flux measurements that use static chambers or other methods which block stirring by wind.

To answer the second question, tools for monitoring vegetation motion are needed. We have explored several options and determined that todays accelerometers are insufficient for recording the motion of a single stem. This is because they are either too heavy or not sensitive enough - existing field data suggest that stems acceleration is on the order of 0.01 m/s2 (or 1 G), and accelerometers with such fine resolution are currently quite large. Cameras can monitor motion to very fine resolution, as long as an optical path can be found through the canopy. One planar view must be selected because stem motions are too small for accurate stereoscopic 3D imaging. We think the best camera configuration is a single camera pointed vertically, monitoring the horizontal motion. Different plant stems, or different locations on a single stem, can be monitored simultaneously in a single image. If the monitoring points are clearly labeled, they can be identified by imaging processing in real time, thus greatly reducing the data storage burden that usually accompanies field-deployment of cameras. Such data management would be essential, as the intermittent nature of vegetation waving demands continuous monitoring over a long time period. This monitoring would reveal the probability distribution of vegetation-waving frequency and amplitude. It could also indicate the dominant causes of vegetation-waving in a wetland. That is, waving will likely be different when generated by gusts in the above-canopy wind field than when it is generated by shear at the canopy top. A range of sites would need to be studied to avoid site-specific results. Factors to consider include but are not limited to the vegetation density, spatial variation of vegetation types, surrounding structures (influencing wind patterns), time of year, and weather conditions.

Herein, we have focused on freshwater wetlands due to their greater production of methane relative to salt marsh species. Salt marsh vegetation will likely have different behavior than the Tule measured here, given their different morphology. Specifically, salt marsh vegetation typically have smaller diameters and greater flexibility than Tule. In terms of flexibility, the maximum stress withstood by stems is an order of magnitude greater for Tule (Groeneveld & French 1995), than for *Spartina alterniflora* and *Salicornia europaea* (Harley & Bertness 1996), two common salt marsh species. In terms of size, the diameter of the Tule modeled here was 13 mm, which is larger than the average of 4.3 mm and 3.6 mm determined for healthy and unhealthy *Spartina alterniflora*, respectively (Feagin, Irish, *et al.* 2011). With smaller stem diameter, the Reynolds number decreases, and motion of vegetation stems is likely to cause a smaller k_{600} as compared to larger stems. However, other linked factors may alter this effect in the opposite way; for example, there may be increased vegetation density with decreased stem diameter.

2.5 Conclusions

We have measured the stirring at an air-water interface caused by waving vegetation stems, inspired by the wind-driven waving that occurs in wetlands. The stirring is quantified in terms of a gas transfer velocity, k_{600}. Results suggest that over a wide range of amplitudes and frequencies, vegetation-waving can contribute significantly to vertical fluxes across the air-water interface. These results underscore the value of performing a thorough field survey of vegetation-waving over space, time, and vegetation characteristics. These results also suggest that the waving of vegetation should be considered when investigating nonlinear interactions of different phenomena which simultaneously act to stir the air-water interface.

Chapter 3

Wave Attenuation Across a Tidal Marsh

3.1 Introduction

Marsh plants attenuate wave energy via frictional drag. This drag has an impact on the overall wave evolution to a greater or lesser degree depending on vegetation and hydrodynamic characteristics (*e.g.* storm track and speed (Wamsley *et al.* 2010) and vegetation patchiness (Temmerman *et al.* 2012)). Understanding how attenuation changes with these conditions informs our understanding of other marsh processes that are influenced by wave energy, such as sediment transport and deposition. Lower wave energy can create conditions conducive to sediment trapping and settling, which is critical to marsh survival. Wave attenuation across marshes has been studied in both the field and laboratory. Tables containing aggregated results can be found in Paquier *et al.* (2016), Guannel *et al.* (2015), and Gedan *et al.* (2011).

It is well established that marshes attenuate wave energy, but the degree of attenuation can greatly vary. Pinsky *et al.* 2013 reprocessed data from nine field studies on marshes using a uniform method. The calculated drag coefficient (C_D), which is a measure of attenuation, ranged from 0.5 to 30 for similar hydrodynamic conditions. This variability is in part due to the presence of different vegetation species and location-specific conditions. Cooper *et al.* (Cooper 2005) lists 23 factors that influence wave attenuation, many of which varied across the marshes in Pinskys analysis. The ways that these factors interact in a location drive the spatial and temporal patterns of marsh effects on waves. Therefore, local measurements focusing on sites of interest are necessary for effective resource management and shoreline protection.

In this study, we measured wave attenuation in a tidal salt marsh in San Francisco Bay. The most abundant salt marsh species are *Salicornia pacifica* (pickleweed) and *Spartina foliosa* (Pacific cordgrass) (Baye 2012). *S. pacifica* and *S. foliosa* are morphologically different; *S. foliosa* is more rod-like, while *S. pacifica* is shorter and highly branched (*i.e.* more shrub-like). The existing wave attenuation literature has focused heavily on *Spartina alterniflora* (smooth cordgrass), as it is dominant along the east coast of the U.S. and the Gulf of Mexico (*e.g.* (P. L. Knutson *et al.* 1982) in the field and (Anderson & Smith 2014 in the lab). *S. foliosa* is distinct from *S. alterniflora* mainly because it is shorter and has less leaf production (Callaway & Josselyn 1992). We also examined the seasonal variation in wave attenuation. Both *S. pacifica* and *S. foliosa* are perennial species; however, the aboveground biomass of *S. foliosa* dies back in the winter months, while *S. pacifica* retains aboveground biomass year-round.

The goal of this chapter is to provide a first look at the wave attenuation and its seasonal variation across vegetated marshes in San Francisco Bay. We investigated how wave attenuation varies as waves progress through the different vegetation zones, as well as how it varies within the zones under different hydrodynamic conditions. We calculated bulk drag coefficients and exponential decay constants to differentiate mechanisms of dissipation. Finally, we discuss the results in the context of projected sea-level rise.

3.1.1 Field Site

San Pablo Bay is the northwestern extremity of the San Francisco Bay system. It is characterized by broad shallows with a deep channel along the southeastern edge that connects the Pacific Ocean to the ports and industries of the Sacramento-San Joaquin Delta (Figure 3.1). The shores of San Pablo Bay contain about 80% of the remaining marshes of San Francisco Bay (Beagle *et al.* 2015). The Mediterranean climate in the region creates a strong seasonal signal; the winters are marked by episodic storms followed by periods of calm, while the summers are dry with consistent afternoon sea breeze (Cloern & Nichols 1985). In the center of San Pablo Bay, the sea breeze generates significant wave heights of about 0.5 m, and storms can generate significant wave heights up to 0.8 m (Lacy & MacVean 2016).

The study area is a 96.7 hectare tidal salt marsh within China Camp State Park, a component of the San Francisco Bay National Estuarine Research Reserve (Takekawa *et al.* 2013). The bayward portion of the salt marsh was created by sediment delivery from mining activities near the end of the 19th century and is characterized by nearly straight tidal creeks, while the landward portion is prehistoric and has a complex and sinuous channel network (Baye 2012; Goman *et al.* 2008). This polyhaline to hyperhaline site has a semidiurnal tidal cycle with a mean tidal range of 1.4 m (Callaway, Borgnis, *et al.* 2012; Takekawa *et al.* 2013). Outside the marsh, there are extensive intertidal mudflats that extend into San Pablo Bay. These mudflats reduce incoming wave energy (Lacy & MacVean 2016), and the marsh location shields it from southerly waves. Cores dated with ^{137}Cs show the site has been keeping pace with sea-level rise over the last half century with a vertical accretion rate of 0.63 cm/yr in the low marsh and 0.36 cm/yr in the mid marsh (Callaway, Borgnis, *et al.* 2012). These accretion rates and vegetation patterns are considered indicative of a healthy marsh in this region.

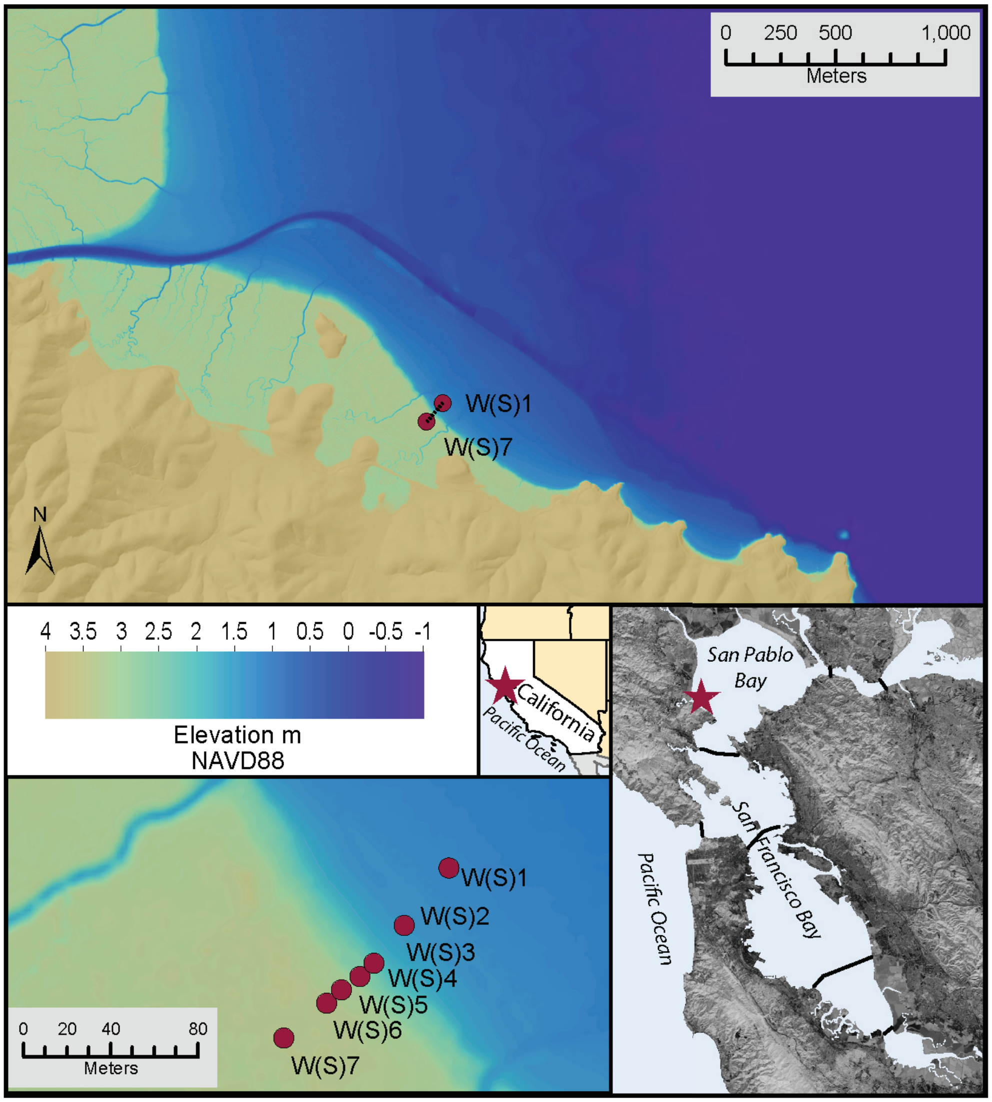

Figure 3.1: Bathymetry of San Pablo Bay with the stations of the cross-shore transect. Inset shows San Pablo Bay and China Camp State Park (star) within the San Francisco Bay system.

The low marsh is characterized by a narrow fringe of *S. foliosa*, a zone that typically spans elevations of 0.4 to 1.1 m relative to mean low water (MLW) (Swanson *et al.* 2014; Takekawa *et al.* 2013). There are portions of San Pablo Bay without this fringing *S. foliosa* and other areas where it is up to 50 m wide (Baye 2012). Baye (Baye 2012) observed that this zone width grows after calm winters, suggesting the zone width is controlled in part by storm activity. In the upper marsh (generally +1.3 m MLW), the dominant vegetation is *S. pacifica* (Baye 2012; Takekawa *et al.* 2013). The transition zone contains both *S. foliosa* and *S. pacifica* and extends from approximately +0.7 to +1.3 m MLW (this study). The spring-neap cycle is important at this site, as the upper marsh is primarily inundated only on high spring tides.

3.2 Methods

3.2.1 Field Data Collection

To capture differences in vegetation and wave conditions, we conducted two field campaigns. The first was in December 2014 and January 2015 (winter dataset), and the second was in May and June 2016 (summer dataset). Each campaign included a vegetation survey and deployment of instrumentation to measure wave evolution.

3.2.1.1 Vegetation Surveys

Vegetation surveys were conducted on January 23, 2015, and June 6, 2016; both surveys occurred while instruments were deployed. One-meter quadrats were analyzed for percent cover of each vegetation species present, average canopy height, and maximum canopy height. A quarter-meter quadrat (0.0625 m^2) was then used for stem count and stem diameter measurements. Stem counts were done for *S. foliosa* but not for *S. pacifica*; *S. pacifica* has a high number of branching stems, making the number of stems connected to the ground not representative of the vegetation density. Instead, for *S. pacifica*, estimates were made of the porosity, or the solid volume fraction occupied by vegetation. These estimates were made in the field and were based on visual inspection from three researchers. The stem count was then back-calculated from porosity assuming cylindrical stems and using the measured stem diameter. Destructive biomass sampling in the area from previous studies, as well as documented growth patterns of *S. pacifica*, indicate that the number of stems does not greatly change with the season (Mahall & Park 1976). Therefore, the value that was estimated for summer was also used in winter. Photographs were taken of each quadrat at the time of the surveys.

Information on the vertical structure of vegetation is important to characterizing the drag but is not part of standard vegetation surveys. To gather more information on the distribution of drag elements, additional vegetation surveys were conducted on September 29, 2016 (at the site) and May 31, 2017 (section of the marsh adjacent to the study area). The length, width, and spacing along the stem of *S. foliosa* leaves were measured.

3.2.1.2 Wave Attenuation Measurements

We deployed instruments on a cross-shore transect (Fig. 3.2). This transect started on the mudflat 35 m outside of the start of vegetation and ended 75 m into the vegetation in the upper marsh. The stations were placed to mark changes in the dominant vegetation type, creating four zones: mudflat, *S. foliosa*-dominated, transition between *S. foliosa* and *S. pacifica* (transition zone), and *S. pacifica*-dominated. We measured the precise position and elevation of each instrument station using RTK-GPS; the GPS base station was located on an established benchmark 0.5 km away (precision of 0.02 m in the horizontal and 0.01 m in the vertical directions). Because the outer station on the mudflat was not accessible by foot, the elevation was taken from bathymetry data. There is a 1.4 m elevation gain from the first station to the last. We measured the topography of the transect on foot using Trimble R7 and R10 GNSS backpack-mounted receivers and taking readings approximately every 2 m along the transect at the time of the vegetation surveys.

Instrument deployments along the marsh transect spanned periods of perigean spring tides, the greatest inundation depths of the year. A timeline of deployments can be found in Figure 3.3. For both the winter and summer, the stations bordering the mudflat were deployed longer than stations in the marsh. In winter, there were two separate marsh deployments. The first contained six instrument stations, and the second repeated the locations of the first with an additional station in the transition zone. In the summer, there was a single deployment that occupied approximately the same locations of the second winter deployment. During the summer deployment, one station (S4) had a battery failure and collected no data; thus, the winter transition zone is resolved into two sections, and the summer contains one.

We deployed a high-frequency pressure sensor (6 or 8 Hz) at each instrument station. A burst of measurements were taken at 10 or 15 minute intervals; each burst was 2048 measurements, which is approximately 5 min depending on the sampling frequency. Each station also contained temperature sensors and optical turbidity sensors, whose results will be communicated in a future publication.

The elevation of the pressure sensors was measured when the sensors were installed. Stations bayward of the vegetation had sensors positioned 0.16 - 0.27 m above the bed, and stations in the vegetation were positioned less than 0.05 m from the bed. The pressure data was converted to water depth by averaging over one burst, assuming a constant water density, subtracting atmospheric pressure, and adding the elevation of the sensor above the bed. For the winter dataset, atmospheric pressure was measured at the site with a TWR-2050 pressure sensor, and for the summer dataset, measurements were obtained from the NOAA RCMC1 weather station (11.5 km from the site).

There is evidence that some instrument stations settled over time, particularly those outside of the vegetation. Adjustments were made to the depth measurements by examining the water-surface elevations over the course of the deployment. In both datasets, slight (<5 cm) adjustments were made to correct for vertical movement. In the winter, W2 drifted horizontally by approximately 10 m during the deployment; we corrected its position in our data.

Only data from inundated bursts were used for wave analysis, where inundation is defined as the burst-mean depth being 2 cm above the height of the pressure sensor. Wave statistics, including root-mean-square wave height (H_{RMS}), and peak period (T_p), were calculated from the pressure frequency spectra following the methods of Wiberg and Sherwood (Wiberg & Sherwood 2008). The pressure timeseries had linear trends removed and were corrected for attenuation with depth below the water surface. We used a low-frequency cutoff of 0.2 Hz. The high frequency cutoff was calculated as follows for each burst:

$$f = \sqrt{\frac{g}{4\pi(h - h_s)}} \tag{3.1}$$

where h is the mean depth for the burst, and h_s is the height of the pressure sensor. This frequency defines the highest frequency that penetrates to the depth of the sensor. Orbital velocity (u_b) was calculated from H_{RMS} and T_p. These calculations, as well as the high frequency cutoff, are based on linear wave theory. Wave attenuation was determined from simultaneous bursts from two adjacent stations when both had $H_{RMS} >0.001$ m, which is 5 times greater than the resolution of the instrument.

3.2.2 Modeling Wave Attenuation

Vegetative resistance is commonly modeled as a drag force. Dalrymple *et al.* ((1984)) derived an expression for energy dissipation of monochromatic waves through a vegetated field, treating the vegetation elements as rigid cylinders. Mendez and Losada ((2004)) modified this expression for a random wave field. They also developed an analytical solution for monochromatic shallow-water waves on a sloped plane, where depth is not constant. Here, we start with this latter solution:

$$H_{RMS} = H_{0,RMS} K_s K_v \tag{3.2}$$

where

$$K_s = \frac{h_0^{1/4}}{h^{1/4}} \tag{3.3}$$

$$K_v = \frac{1}{1 + 2\frac{A_2}{m} H_{0,RMS}(K_S - 1)} \tag{3.4}$$

$$h = h_0 - mx \tag{3.5}$$

x is the distance between the two stations, and m is the bed slope. The 0 subscript indicates the offshore station. K_s is a shoaling coefficient (Greens law (Dean & Dalrymple 1991)), which describes the increase in wave height due to the decrease in water depth, and

K_v is the vegetative-dissipation coefficient. We then apply the modification for a random wavefield (Méndez & Losada 2004), assuming a Rayleigh distribution of wave heights:

$$A_2 = \frac{2C_D N b_v \alpha}{3\pi} * \frac{3\sqrt{\pi}}{4} = \frac{C_D N b_v \alpha}{2\sqrt{\pi}} \tag{3.6}$$

b_v is the diameter of the vegetation stem, N is the number of vegetation stems in a square meter, α is the ratio of the vegetation height to the water depth (h_v/h), and C_D is the drag coefficient. Given our data, C_D is the only free parameter. Since the vegetation is in reality flexible, C_D is assumed to account for vegetation motion as part of the drag force. These expressions ignore nonlinear processes, such as wave reflection and interaction between stems. They were originally derived for submerged vegetation but have been used for emergent conditions (Anderson & Smith 2014). Other models for calculating C_D were also explored (see Appendix for details). We found that Equation 3.2 is preferable, as it is a conservative approach that incorporates the effects of bottom slope.

By linearizing the force acting on the vegetation, Kobayashi *et al.* (1993) showed the change in wave height can be approximated as an exponential decay:

$$\frac{H_{RMS}}{H_{0,RMS}} = e^{-k_i x} \tag{3.7}$$

This model assumes constant depth. Although our site has a non-zero bed slope, we use Equation 3.7 to examine the bulk attenuation per unit distance for pairs of adjacent stations.

3.3 Results

3.3.1 Tidal and Wave Conditions

The wave conditions during the study were typical of the San Francisco Bay system. The winter deployment captured periods of calm (*e.g.* January 21 in Fig. 3.4b) with sporadic storms (*e.g.* January 22 in Fig. 3.4b), and the summer had a consistent generation of waves from the afternoon seabreeze (Fig. 3.4e). The marsh platform was inundated more frequently during the summer deployment, but because the summer tides are not as energetic, the marsh was inundated to a greater depth in the winter. Larger waves were observed at the marsh edge during the winter deployment with a maximum H_{RMS} of 0.27 m versus a maximum of 0.12 m in the summer. Ninety-six percent of all waves just outside of the vegetation (at W(S)2) were classified as shallow or intermediate ($h/L_\infty < 1/20$ where $L_\infty = (g/2\pi)T_p^2$ deep-water wavelength). Typical peak period was 1.8 s in the summer and 2.1 s in the winter. No waves included in our analysis met the wave-breaking criteria (H_{RMS}>$0.7h$); the wave heights were less than $0.6h$ in the winter and $0.3h$ in the summer.

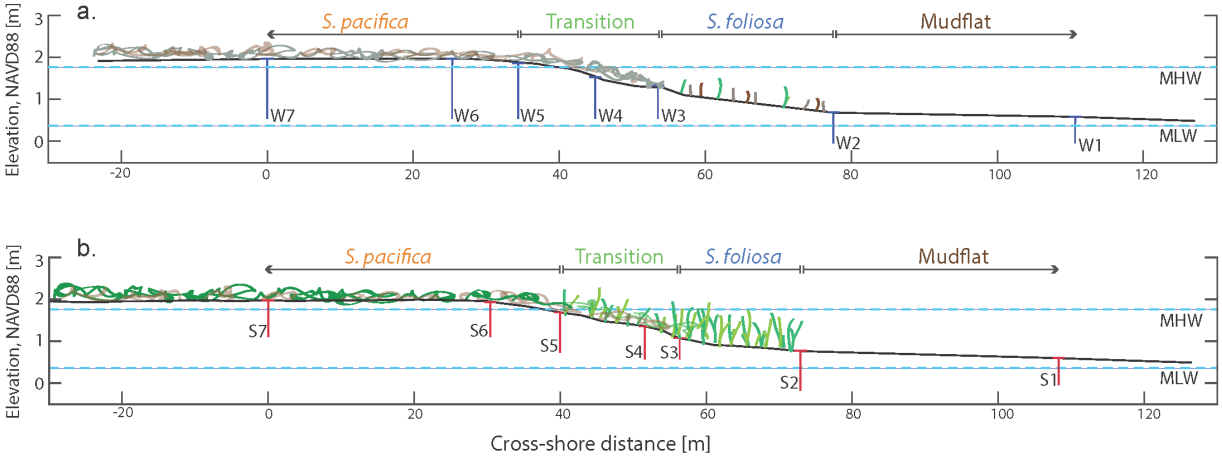

Figure 3.2: Instrument locations and vegetation zones along the cross-shore transects for (a) winter and (b) summer deployments. Datums relative to NAVD88: MLLW = 0.06 m (not shown); MLW = 0.37 m; MSL = 1.01 m (not shown); MHW = 1.77 m; MHHW = 1.95 m (not shown) Swanson *et al.* 2014. Sketch of vegetation depicts the general morphology and condition but is not an exact representation.

Season	**Vegetation Zone**	b_v **(m)**	N **(m^{-2})**	**Porosity**	h_v **(m)**	$h_{v,max}$ **(m)**	$N * b_v$ **(m^{-1})**
Summer	*S. foliosa*	0.0047	440	-	0.48	0.75	9.5[a]
Summer	*S. pacifica*	0.0034	$4.4\text{x}10^4$ [b]	0.4[c]	0.25	0.50	150
Winter	*S. foliosa*	0.0027	312	-	0.16	0.35	0.8
Winter	*S. pacifica*	0.002	$4.4\text{x}10^4$ [b]	-	0.22	0.50	88.3

Table 3.1: Vegetation parameters from summer and winter deployments: b_v = stem width, N = number of stems per m^2, Porosity = solid volume fraction of vegetation, h_v = vegetation height. Measured in the field unless otherwise noted. [a]Includes stem width and width of two leaves (8 mm each). [b]Back-calculated from the porosity assuming cylindrical stems. [c]Estimated by visual inspection in the field.

Season	**Vegetation Zone**	***S. foliosa*** **%**	***S. pacifica*** **%**	$N * b_v$ **(m^{-1})**
Summer	Transition	70	17	32.1
Winter	Transition 1	20	15	13.4
Winter	Transition 2	5	55	48.5

Table 3.2: Percent coverage of *S. foliosa* and *S. pacifica* in transition zones for summer and winter deployments. $N * b_v$ as defined in Table 3.1.

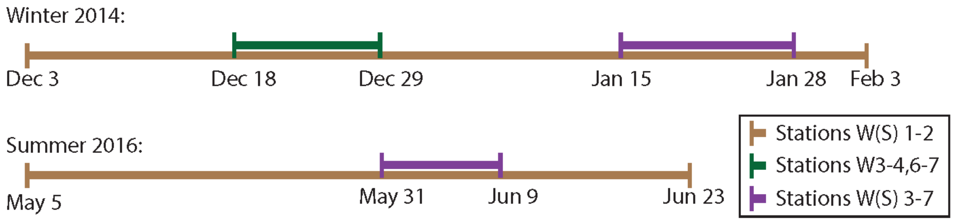

Figure 3.3: Timeline of instrument deployments. Portions in purple and green are marsh stations and in brown are mudflat stations. The location of these stations is shown in Figure 3.2.

3.3.2 Vegetation characteristics

Key features of the two dominant vegetation species during both seasons are given in Table 1. The product of stem density and width ($N * b_v$) is a direct input in our calculation of drag coefficients and is a measure of the width taken up by vegetation in the water column. *S. foliosa* changes dramatically between the seasons (Fig. 3.5a and b). In the winter, most leaves are lost, and the vegetation consists of shorter stems and stubble; whereas in the summer, *S. foliosa* is taller and has many leaves. To account for these leaves, the summer $N * b_v$ includes two leaf widths (8 mm each), as our field data (details given in Section 3.2.1.1) showed on average two overlapping leaves at a given point along the stem. By contrast, *S. pacifica* retains much of its aboveground biomass in the winter months, and the height and structure between the seasons are similar (Fig. 3.5c and d). In the winter, much of the *S. pacifica* biomass has senesced, decreasing the diameter of the stems. Due to the narrower stem width the $N * b_v$ value decreases by a factor of two. The back-calculated stem count is high, but it includes all of the volume taken up by *S. pacifica* and is comparable to stem counts of *Salicornia europea* (N = 10,000 (Ellison 1987)). In the winter and summer, the $N * b_v$ values for *S. pacifica* are an order of magnitude larger than *S. foliosa*.

Seasonal changes also occur in the transition zone, which contains a combination of *S. foliosa* and *S. pacifica*. The parameters used for the transition zone are a weighted average of the values from the *S. foliosa* and *S. pacifica* zones. These averages were weighted by the percent coverage of the two species from observations in the field. The percent coverages are different for the two segments within the winter transition zone. The second segment, or transition zone 2, is mainly *S. pacifica*, but for our analysis we classify it as transition if the zone contained any amount of both species.

3.3.3 Evolution of Wave Height

Wave heights decreased as waves moved onshore across the marsh. As seen in Fig. 3.6, some waves grew in height across the mudflat and *S. foliosa* zones due to shoaling or local wave generation. No wave growth was observed across the transition and *S. pacifica* zones

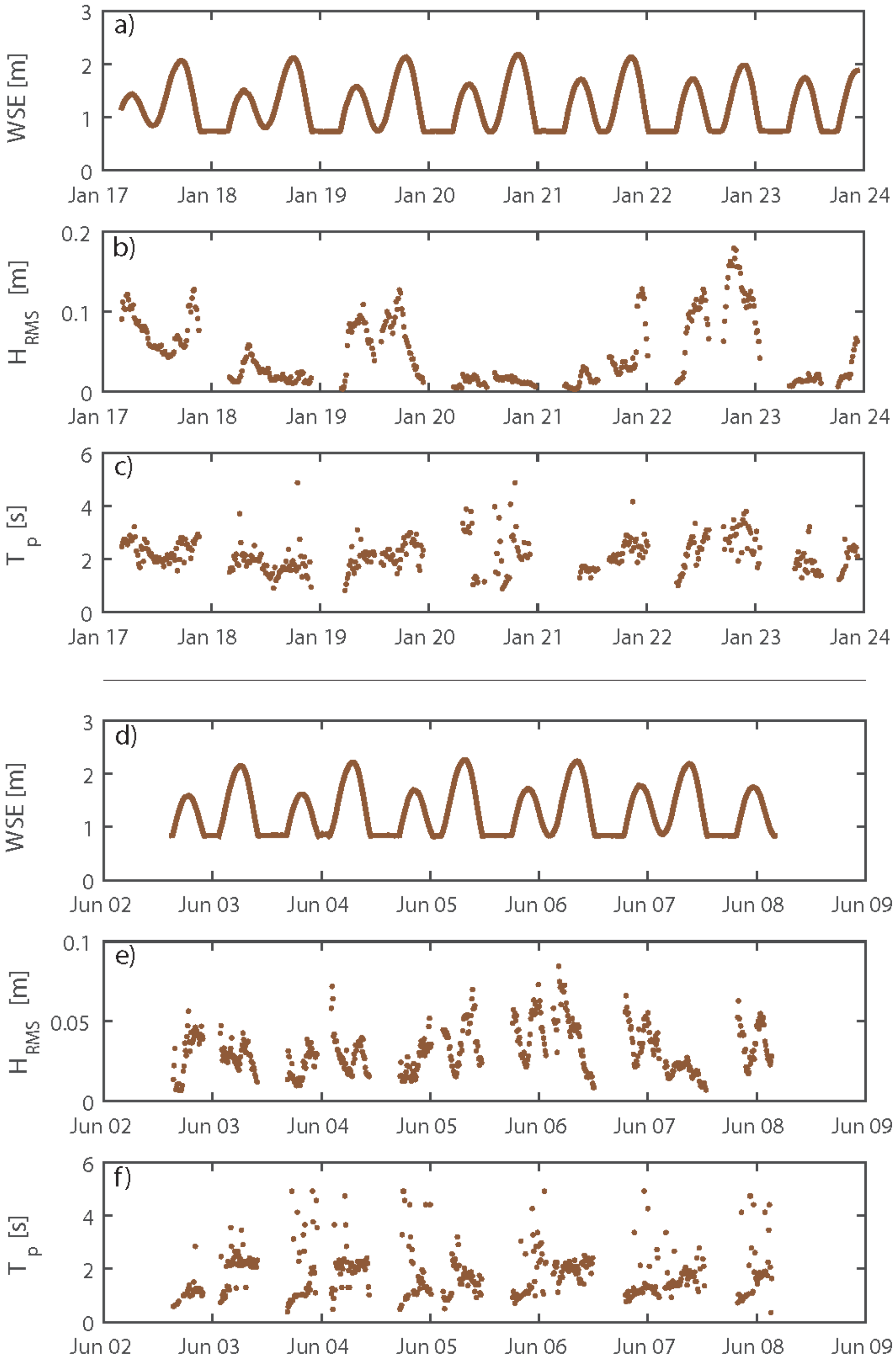

Figure 3.4: Example hydrodynamic characteristics at W1 (a-c) in winter and S1 (d-f) in summer. WSE = water surface elevation; H_{RMS} = root mean square of wave height; T_p = peak period.

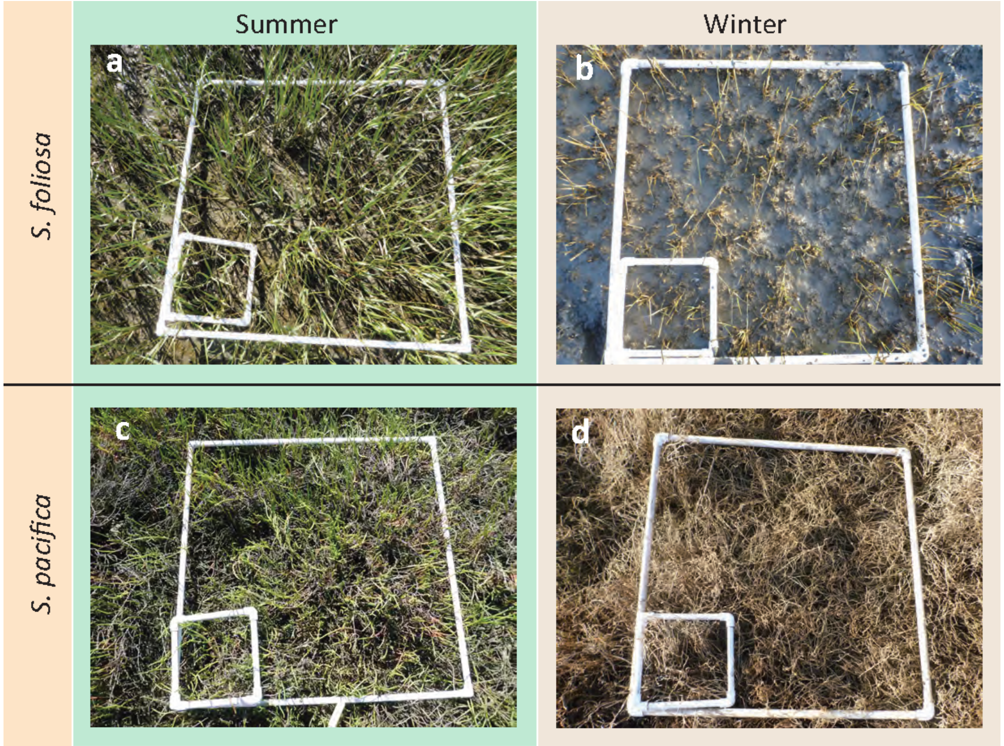

Figure 3.5: Photographs of example vegetation quadrats from winter (b, d) and summer (a, c). Larger quadrats are 1 m x 1 m, and smaller quadrats are 0.25 m x 0.25 m.

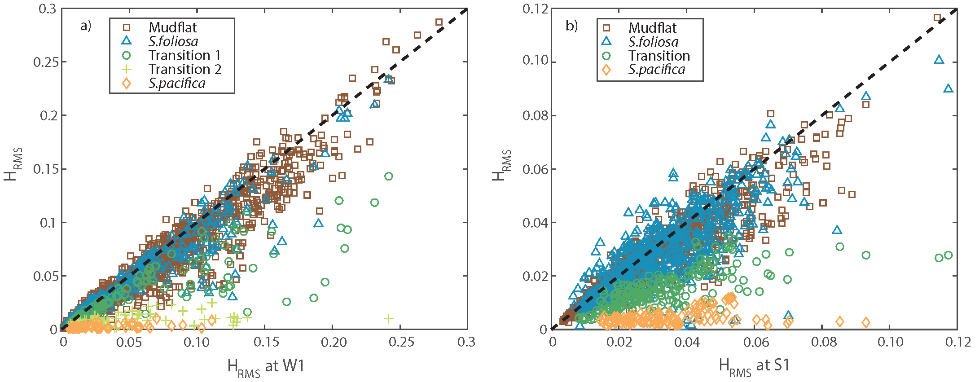

Figure 3.6: H_{RMS} at W(S)1 versus the H_{RMS} recorded at the end of each respective zone for (a) winter and (b) summer. Note the different axes scales. The dashed line indicates 1:1 correspondence.

Station ID	**Zone**	**No. of wave attenuation measurements**
W1 to W2	Mudflat	2887
W2 to W3	*S. foliosa*	793
W3 to W4	Transition 1	529
W4 to W5	Transition 2	140
W5 to W6	*S. pacifica*	155
W6 to W7	*S. pacifica*	0
	Total	4505
S1 to S2	Mudflat	1303
S2 to S3	*S. foliosa*	214
S3 to S5	Transition	215
S5 to S6	*S. pacifica*	126
S6 to S7	*S. pacifica*	0
	Total	1858

Table 3.3: Number of wave attenuation measurements in winter (W1-W7) and summer (S1-S7).

in either season. Complete attenuation was observed approximately 75 m into the vegetated marsh, as no waves greater than 0.001 m were recorded at the farthest landward station in either season (W(S)7). The mean percent reduction from W(S)2 to W(S)6, a distance of 51.3 m in winter and 42.6 m in summer, was 89±7% and $86 \pm 6\%(\pm std\%)$ respectively.

There was a total of 4504 attenuation measurements in the winter and 1858 in the summer (detailed in Table 3.3). These are not the numbers of bursts containing waves, but rather, the number of occurrences when simultaneous bursts from adjacent stations had waves, allowing the tracking of wave height.

3.3.4 Exponential Decay Constant

Wave attenuation varied between the vegetation zones. The decay constants increase by approximately an order of magnitude with each zone from the mudflat into the marsh (Fig. 3.7). Across the mudflat and *S. foliosa* zone, the k_i-values are on the order of 10^{-3}, while the transition and *S. pacifica* zones values are on the order of 10^{-2} and 10^{-1} respectively. Based on these k_i-values, at a water depth of 0.4 m in each zone, 115 m of mudflat would be needed at achieve a 50% reduction in wave height, versus 6 m of *S. pacifica*. For the depths observed, the *S. pacifica* was the most effective at reducing wave heights.

3.3.5 Evolution of Wave Energy Spectra

Spectra seen in Fig. 3.8a-b are an average of all bursts with wave heights between 0.02 and 0.04 m and peak wave periods between 2 and 3 s. The spectra were generated using Welch's method with a Hanning window. We do not see strong preferential attenuation at certain frequencies but, rather, a decrease across the spectrum. Isolating the stations bordering the *S. foliosa* zone, the seasonal difference becomes apparent, particularly at high frequencies (Fig. 3.8c-d). In the winter, the wave energy grows across this zone with a difference of up to two orders of magnitude. The denser vegetation in the summer counteracts this growth, and the wave energies are largely unchanged at high frequencies.

3.3.6 Drag Coefficient, C_D

Drag coefficients allow us to isolate the attenuation due to vegetation. They were determined using the expressions described in Section 3.2.2. Since vegetation, wave, and topography parameters were measured, C_D could be directly solved. Each zone of the transect had unique vegetation parameters; therefore, a separate C_D was calculated for each zone. These C_D values were then binned by the wave Reynolds number (Re). The wave Reynolds Number is defined as $Re = (u_b b_v)\nu$, where ν is kinematic viscosity and u_b is the orbital velocity at the top of the vegetation.

The general trend is a decrease in C_D with an increase in Re (Fig. 3.9). The data was binned such that each bin contains the same number of data points. This binning scheme causes some bins cover a wider range of Re than others. The winter *S. pacifica* has the highest overall C_D values but is measured at relatively low Re.

The results from winter *S. foliosa* were not described well using this model; the 95% confidence interval at low Re spanned two orders of magnitude. The wave attenuation for this zone was comparable to that for the unvegetated mudflat and was better described by bed friction. The bed friction was calculated assuming a turbulent wave boundary layer, which is true for the San Pablo Bay mudflats (Lacy & MacVean 2016), and a flat bottom slope, following Dean & Dalrymple 1991:

$$K_f = \left[1 + \frac{8f_w}{6\pi}\frac{k_p^2 H_{0,RMS}\Delta x}{(2k_p h + \sinh(2k_p h))\sinh(k_p h)}\right]^{-1} \tag{3.8}$$

Where k_p is the wavenumber associated with peak period, and f_w is the wave friction factor defined as (P. Nielsen 1992) :

$$f_w = exp\left[5.213\left(\frac{2\pi k_b}{T_p u_B}\right)^{0.194} - 5.977\right] \tag{3.9}$$

k_b is the roughness length scale and u_B is the orbital velocity at the bed. The winter *S. foliosa* results best fit the model:

$$H = H_0 K_f K_s \tag{3.10}$$

with a k_b of 0.04 m. This model and k_b value also described the summer *S. foliosa* data well. The difference between the measured and predicted wave height reductions ($H_{RMS}/H_{0,RMS}$) had a root-mean-square error (RMSE) of 0.2. However, the vegetation dissipation model was preferred for this zone since it fit the data better (RMSE = 0.1) and is more physically meaningful. To assess the importance of bed friction in the absence of vegetation, Equation 3.10 was applied to all of the zones with a k_b of 0.01 m, which was previously measured in the vicinity of our study site (Lacy & MacVean 2016). The effect was negligible with high RMSE on the wave height predictions that ranged from 0.43 to 0.96 (see the Appendix for details).

3.4 Discussion

3.4.1 Variations within China Camp Salt Marsh

Measurements of wave attenuation through the *S. foliosa* and into the *S. pacifica* zones show that these species attenuate wave heights to different degrees. The exponential decay constants for *S. pacifica* are two orders of magnitude greater than those for *S. foliosa*, meaning greater attenuation occurred across this zone. The vegetative drag modeling, however, shows the two species have similar C_D values. Thus, differences in attenuation are due to slope or vegetation density, not single stem morphology. For example, this result indicates that under the same hydrodynamic conditions, 1 cm wide section of *S. foliosa* provides a similar drag as 1 cm of *S. pacifica*.

Yet due to their presence in different elevations of the marsh, these species rarely experience the same hydrodynamic conditions. The maximum depth at W(S) 6, in the *S. pacifica* zone, was 0.32 m in the summer and 0.34 m in the winter, meaning α (the ratio of vegetation height to water depth) had a minimum value of 0.67. *S. foliosa*, occupying a lower elevation in the marsh, was inundated to a greater depth and had minimum values of α of 0.33 in the summer and 0.10 in the winter.

The seasonal signal in wave attenuation is dominated by the changes in frontal area of the vegetation. Möller and Spencer (2002) documented seasonal changes in marshes on the Dengie Penninsula and found greater attenuation in summer months when more biomass was present. It is interesting that the degree of attenuation across the *S. foliosa* zone does not change much between summer and winter, despite the dramatic change in vegetation density and height. One possible explanation is a seasonal shift in the mechanism of wave generation. The summer sea breeze may cause more local wave generation or re-generation that leads to increased wave propagation through the *S. foliosa* zone.

The exponential decay coefficients can be used to predict the complete profile of wave height evolution across the marsh, shown in Fig. 3.10 for a given set of offshore wave height and depth conditions. Differences between the seasons occur across the mudflat, *S. foliosa*, and transition zones. These different states of wave energy likely affect in the local sediment dynamics, but since complete attenuation is reached at similar distances regardless of season, these differences do not greatly influence the final outcome. Many of San Francisco Bays marshes do not have fringing *S. foliosa* and have conditions more similar to the winter year-round.

3.4.2 Dependence on relative depth

A dependence on water depth can be seen in both the decay constants and drag coefficients. Our findings demonstrate that there is greater attenuation when vegetation is emergent than when it is submerged. This behavior is most visible across the *S. foliosa* zone (Fig. 3.11). There is a marked decrease in the decay coefficient when the water level at the upland end of the zone is at or above the vegetation. In the summer, the k_i-value decreases by an order of magnitude at this point (Fig. 3.11 depths past solid vertical line), and in the winter, most bin medians become negative, indicating wave growth (Fig. 11 depths past dotted vertical line). Even for the short *S. foliosa* stems, it makes a difference if they are deeply submerged. This result agrees with findings of Augustin *et al.* (2009), who studied wave attenuation in a laboratory under emergent and near-emergent conditions. With emergent vegetation, the wave attenuation was 50% to 200% greater per wavelength (Augustin *et al.* 2009).

The vegetative drag model accounts for the height of the vegetation relative to the water depth via the parameter; therefore, C_D should not be a function of *alpha*. Yet *alpha* can change with vegetation motion, and this motion is not in the model (Méndez & Losada 2004). Möller *et al.* (Möller, Kudella, *et al.* 2014) measured the change in plant posture with varying wave conditions and found that more attenuation occurred when stems were more upright. We examined the summer *S. foliosa* results as a function of α (Fig. 3.12) and found greater drag coefficients when the vegetation was emergent ($\alpha \geq 1$) and presumably upright. We did not find this trend with α for *S. pacifica*, likely because the morphology of *S. pacifica* prevents the stems from greatly changing with depth conditions. Augustin *et al.* [43] did not find a large difference between the C_D values of rigid cylinders and flexible material. However, the flexible material did not bend past 20from vertical, suggesting it is only beyond this point that the stem bending affects the drag. The attenuation in the summer *S. foliosa* zone decreases with greater submergence both because less of the water column is influenced by vegetative drag and because stem bending is greater.

The vegetation heights reported here are an average measured visually in the field, and they do not account for spatial variability in the α values for individual plants. This variability occurs in most field studies, as vegetation is not typically uniform. Furthermore, a sloped marsh profile means that the water depth, and thereby the α value, varies in the cross-shore direction. Studies often point to α as a central parameter for determining the effectiveness of a salt marsh at attenuating waves, so it may be important to understand these local variations and sources of uncertainty when interpreting or applying these results (Narayan, Beck, Wilson, *et al.* 2016).

3.4.3 Variations among vegetation species

Drag coefficients have been measured for a range of vegetative and hydrodynamic conditions both in the lab and in the field. Constant C_D values have been found to overestimate attenuation because C_D decreases with increasing wave energy (Pinsky *et al.* 2013). The dependence on wave energy is typically represented by expressing C_D as a function of Re or the KeuleganCarpenter number ($KC = u_b T_p / b_v$). Other studies (*e.g.* Möller, Kudella, *et al.* 2014; Pinsky *et al.* 2013; Anderson & Smith 2014; Kobayashi *et al.* 1993; Jadhav, Q. Chen & Smith 2013) have found the relationship $C_D = a + (b/Re)^c$ to describe results well. We apply that fit to the binned data for each zone type (with the exception of winter *S. foliosa*). Fig 13 shows this empirical relationship between C_D and Re for selected studies alongside the results of this study. The coefficients for our empirical fits as well as those of other authors are given in the Appendix. The results are applicable over the range of Re in each study; hence the functions are only shown where they overlap the range of Re measured in this study (Re<800). This requirement limited the number of comparable studies, as the conditions that we observed here were less energetic.

For a given Re, the C_D values in Fig. 3.13 vary by two orders of magnitude. The two studies that focus on *S. alterniflora*, Anderson and Smith (lab study using polyolefin tubing, (2014)) and Jadhav *et al.*(field study, Jadhav & Q. Chen 2012), exhibit the greatest C_D values. These results are followed by Pinsky *et al.* Pinsky *et al.* 2013, which is a combination of the results from 14 marsh attenuation studies with varying vegetation species, and Moller *et al.*Möller, Kudella, *et al.* 2014, who used real vegetation, primarily Elymus athericus and Puccinellia maritima, in a laboratory flume.

It is likely that material differences between these species drive the differences in C_D. For example, stiffer plants may exert more drag, though the existing data is both noisy and seems to point in the opposite direction. Published values of Youngs modulus are greater for *E. athericus* (2696.3 m 1963.8 MPa (Möller, Kudella, *et al.* 2014)) than for *S. alterniflora* (1410 ± 710 MPa (Feagin, Irish, *et al.* 2011)).

The comparatively low C_D values in our study may be due in part to differences in modeling the vegetation parameters. The stem counts for *S. pacifica* were back-calculated from estimates of porosity and therefore, include all of the biomass encountered by incoming waters. A similar approach was used for the *S. foliosa*, and the leaves in addition to the stems were included in the $N * b_v$ parameter. If we instead restrict it to the rigid stem alone, the C_D values increase because the observed attenuation is then attributed to a smaller area of vegetation.

Another source of uncertainty arises from the initial assumption of uniform vegetation characteristics. Our vegetation surveys revealed heterogeneity even within monocultures. We used the smallest and largest measurements of $N * b_v$ in the summer *S. foliosa* zone to show the sensitivity of C_D to vegetation parameters (Fig 14). Allowing $N * b_v$ to range from 3.5 (stem width = 3 mm; leaf width = 3 mm) to 13.8 (stem width = 8 mm; leaf width = 10 mm) produced an order of magnitude difference in C_D at low Re and shifted the results to larger range of Re values.

We can also compare the vegetation through measurements of exponential decay. Ysebaert *et al.* Ysebaert *et al.* 2011 and Paquier *et al.*Paquier *et al.* 2016 measured attenuation across *S. alterniflora* in the Yangtze estuary and Chesapeake Bay, respectively. They reported exponential decay constants that vary from 0.02 to 0.12 m^{-1} with increasing depth, which correspond to much greater attenuation than the k_i-values for *S. foliosa* measured here. These different values support the idea that the structural differences between the Spartina species produce the differences in C_D values, rather than differences in modeling alone. San Francisco Bay contains non-native Spartina species, including *S. alterniflora.* While it has decreased by 96% in recent years (Rohmer *et al.* 2015), the difference between our results and those for *S. alterniflora* suggests that attention should be given to the species present when modeling wave attenuation in a specific area.

We can also compare transition zone and *S. pacifica* zone to *S. alterniflora.* The attenuation rates increased greatly moving into the transition zone and are comparable to the sparse (N=97 Paquier *et al.* 2016) *S. alterniflora.* The *S. pacifica*-zone rates were the highest measured, exceeding those of dense (N=334 Ysebaert *et al.* 2011) *S. alterniflora.* The higher drag coefficients indicate that on a per width basis, *S. alterniflora* exerts a greater drag than *S. pacifica.* However due to the high amount of *S. pacifica* biomass, a larger portion of the water column is occupied by vegetation, and *S. pacifica* attenuates wave energy in shorter distances compared to *S. alterniflora.* Recall the conditions studied cover a limited range of α-values for this zone (α>0.67). Deeply submerged conditions should be tested to better understand the attenuation capacity of *S. pacifica.* Since it is typically found in the high marsh (+1.3 m MLW), encountering deeply submerged conditions is rare at this site.

3.4.4 Implicit vs. explicit representation of vegetation

Wave dissipation over the *S. foliosa* zone was well described with a bottom friction model by increasing the roughness length scale, k_b, to 0.04 m. Other studies, primarily those of seagrasses, have also used this approach to implicitly represent dissipation due to vegetation. k_b-values ranging from 0.03 m (*Zostera marina* Nowacki *et al.* 2017) to 0.4 m (*Posidonia oceanica* Infantes *et al.* 2012) have been found to agree well with attenuation observations. The stem densities for those studies tended to be much higher ($N = 600\ \ 4600$); although perhaps the increased rigidity of *S. foliosa* compensates for the decreased density, making the apparent roughness similar. Nowacki *et al.*(2017) showed that an implicit formulation, following the methods of Collins (Collins 1972) with $C_f = 0.4$, was able to out-perform the explicit representation of vegetation following the methods of Mendez and Losada (Méndez & Losada 2004). The explicit representation may be viewed as advantageous because it is a more mechanistic approach and can be implemented using standard vegetation measurements. It is not yet clear how to estimate the equivalent roughness length scale, which can vary over an order of magnitude. However, as seen with the winter *S. foliosa* characterized in our study, not all vegetation data can be modeled with the explicit formulation.

3.5 Conclusions

We measured wave height evolution in the summer and the winter across a tidal salt marsh in San Francisco Bay. The marsh vegetation dissipated wave energy, and complete attenuation was reached less than 75 m into the vegetation. Attenuation rates followed seasonal shifts in biomass. Wave attenuation was greater when more vegetation occupied the water column either because of shallower inundation, denser vegetation, or both. The greatest rates of attenuation occurred in the *S. pacifica* zone, which did not experience high levels of inundation. As a low-marsh species, *S. foliosa* was exposed to greater wave heights and water levels, and net wave growth occurred across this zone when the plants were deeply submerged (α<0.3 in the winter and α<0.4 in the summer). Under similar conditions, published attenuation rates for *S. alterniflora* are greater than and less than those found here for *S. foliosa* and *S. pacifica*, respectively.

We presented drag coefficients and exponential decay constants expressed as functions of Re and water depth, respectively. These relationships can be used to predict wave height in locations with vegetation and hydrodynamics similar to our study site. Using the exponential decay constants requires the same amount of vegetation present, as well as the same slope, but they can be used as a first-order approximation, especially for *S. pacifica* which occupies a narrow range of elevations. Use of the C_D values requires more information on the hydrodynamics (*i.e.* Re) and vegetation parameters (*i.e.* stem diameter and density). The application of this model to *S. pacifica* would be greatly improved with a standardized method for measuring the volume occupied by the vegetation, ideally one that is nondestructive.

Predictive models have been run for future scenarios of sea-level rise for China Camp Salt Marsh. Results from the WARMER model show that with 1.05 m of sea-level rise (projected for 2090), the whole marsh will be converted to mudflat (Takekawa *et al.* 2013; Swanson *et al.* 2014). At a constant depth of 0.5 m, a 0.20 m wave would propagate well over 1 km across mudflat before dissipating. Along some shorelines, such elevated wave heights could then have an impact on the surrounding seawalls and levees. Datasets, like the one from this study, can help inform these future scenarios and be used to develop best practices for coastal land management.

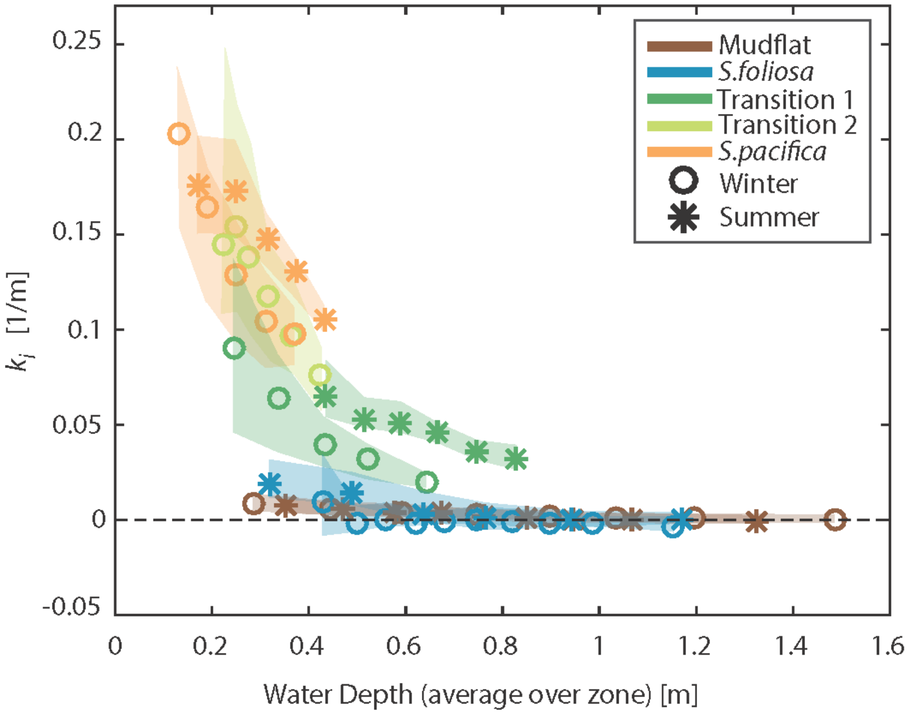

Figure 3.7: Wave height exponential decay constants binned by depth. Shaded regions are the interquartile range, and markers are at the bin median.

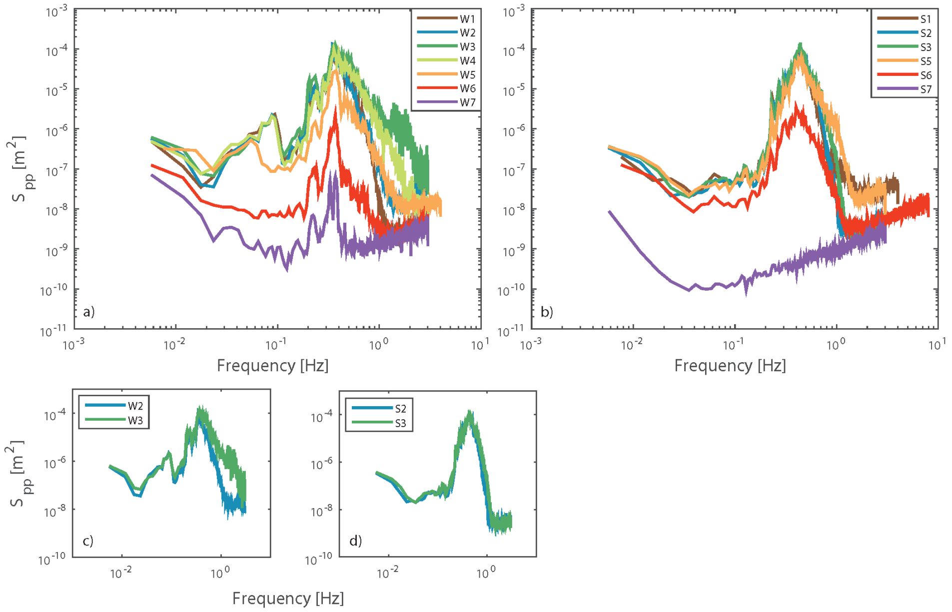

Figure 3.8: Wave energy spectrum for bursts with wave height $0.02H_{RMS} < 0.04$ m and wave period $2 < T_p < 3s$; a) All winter zones, n = 16 bursts; b) All summer zones, n = 9 bursts; c) Winter *S. foliosa* zone; d) Summer *S. foliosa* zone.

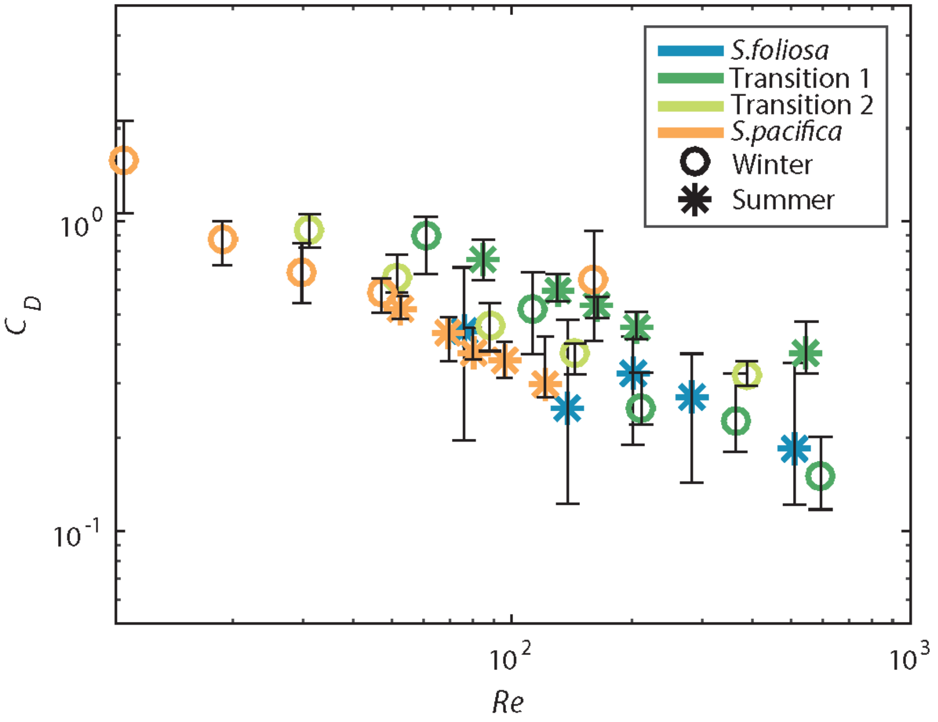

Figure 3.9: C_D as a function of Re. Error bars show interquartile range.

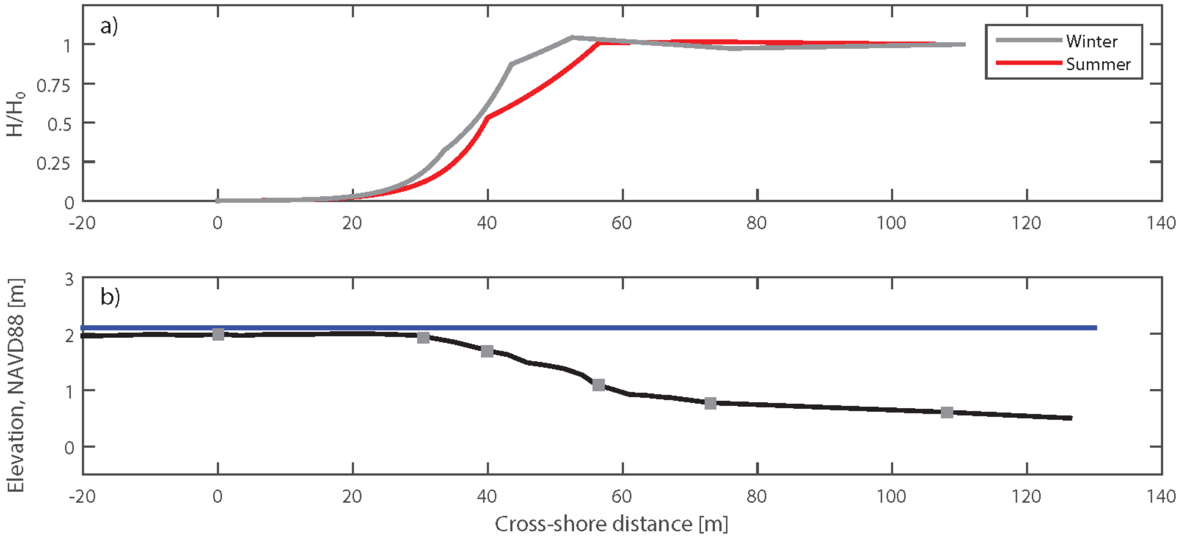

Figure 3.10: a) Predicted wave attenuation for with a depth of 1.5 m at W(S)1 for summer and winter. Predictions are made from the exponential decay constants for each zone of marsh. b) Cross-shore bathymetry and water level. Stations are marked by squares.

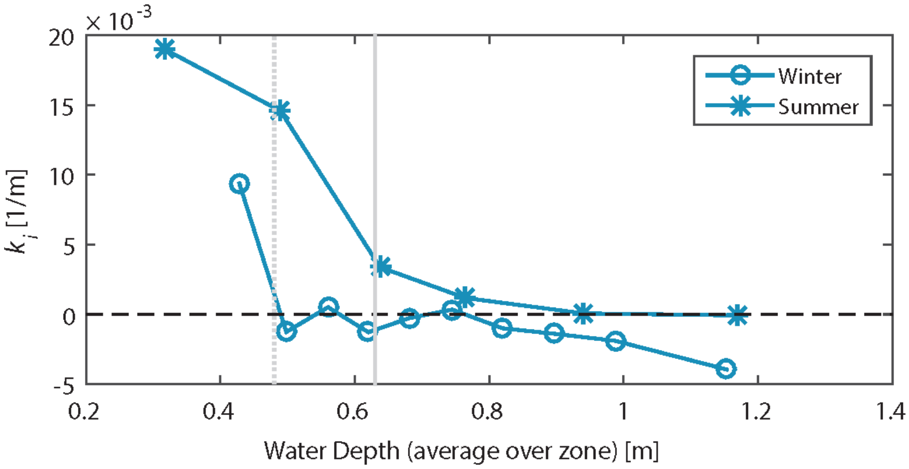

Figure 3.11: Wave height exponential decay constants for the *S. foliosa* zone in winter and summer. Vertical gray lines indicate the transition from emergent vegetation to submerged in winter (dotted line) and summer (solid line).

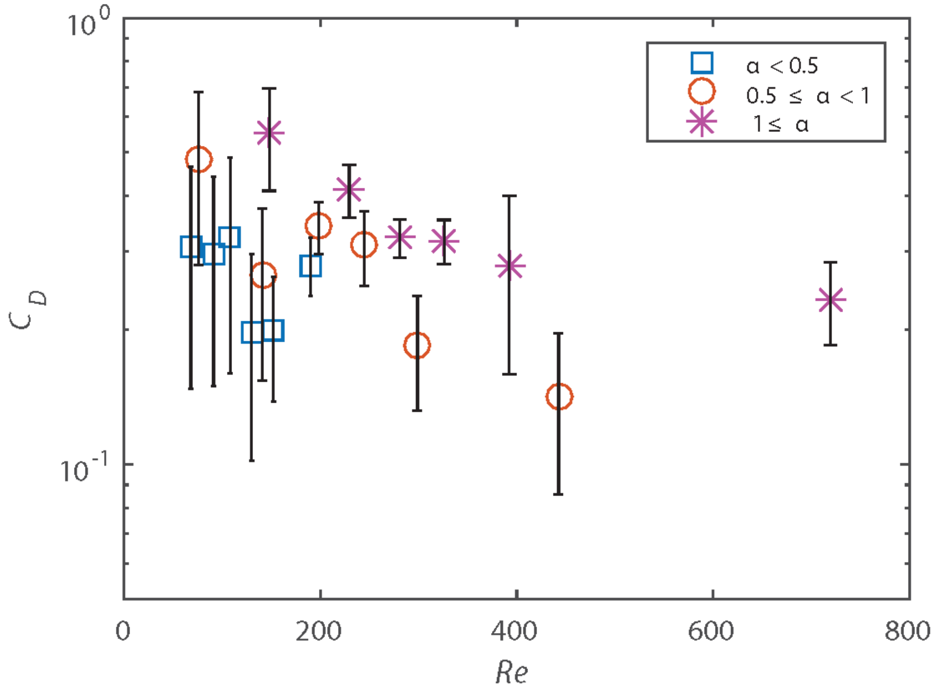

Figure 3.12: C_D as a function of Re for summer *S. foliosa*. Symbols show different values of α ($\alpha = h_v/h$). For $\alpha > 1$, vegetation is emergent, and for $\alpha \leq 1$, vegetation is submerged. Error bars are standard error.

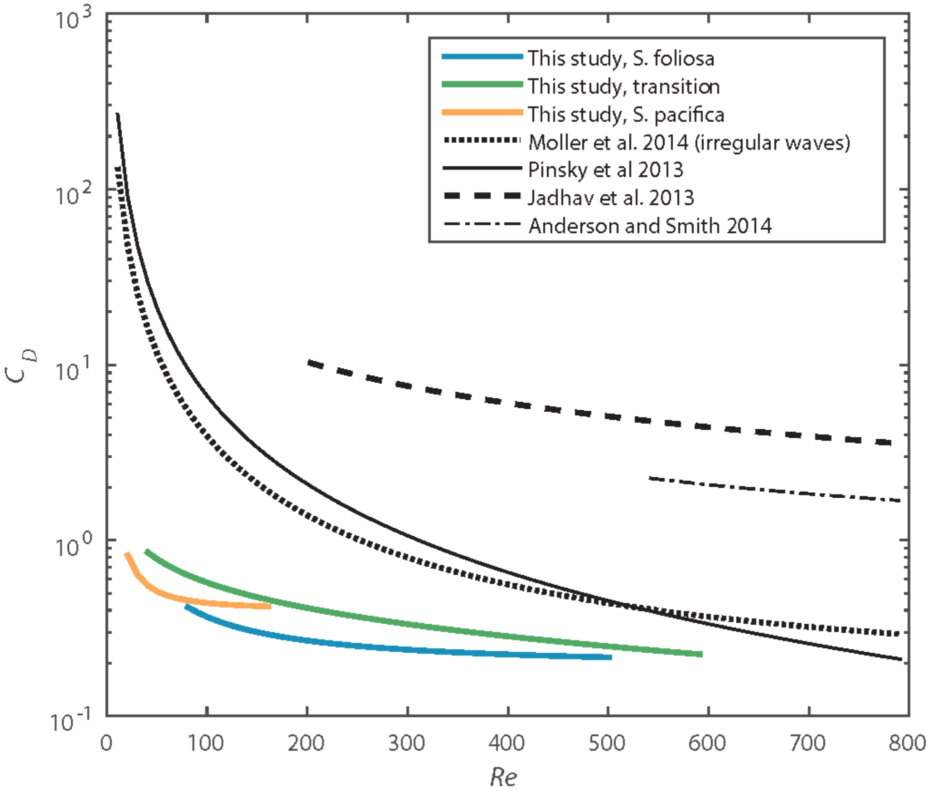

Figure 3.13: Relationship between C_D and Re ($C_D = a + (b/Re)^c$) for four published studies along with this study.

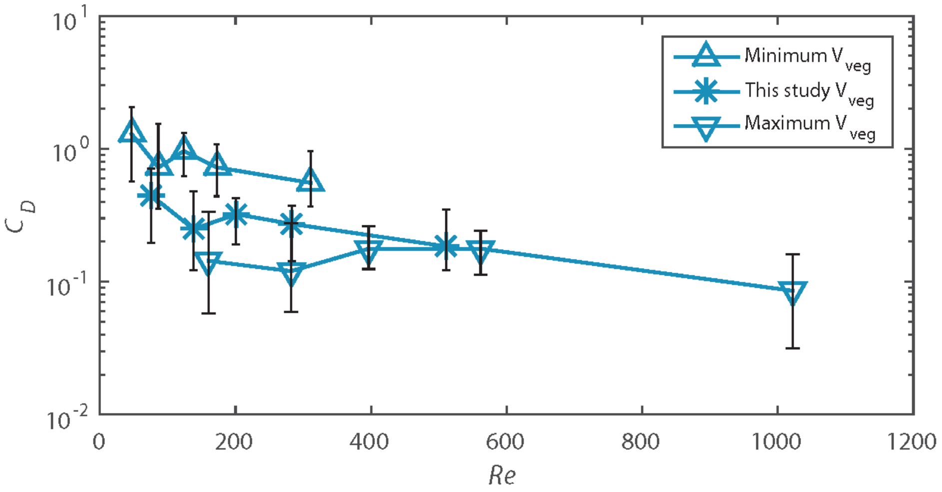

Figure 3.14: Relationship between C_D and Re ($C_D = a + (b/Re)^c$) for *S. foliosa*. Minimum volume of vegetation (V_veg) uses the smallest vegetation parameters measured in the field, and maximum V_veg uses the largest. Error bars are interquartile range.

Chapter 4

Biosolids as a Marsh Restoration Amendment

4.1 Introduction

In an effort to reverse marsh loss, marsh restoration and creation projects are becoming more common. These projects typically consist of raising the elevation of an area of open water to the point where emergent vegetation can take hold; this process requires a large input of sediment. Material dredged from waterways is most commonly used, and the reuse of this dredged material is encouraged by federal agencies (U.S. Environmental Protection Agency & U.S. Army Corps of Engineers 2007). Another possible source of sediment is biosolids. Biosolids are the solids product of modern wastewater treatment and are ubiquitous in populated areas. Depending on their properties and the properties of the receiving waters, biosolids fit into one of three categories: 1) source of fill material; 2) beneficial amendment to other fill material; 3) harmful material not to be used. Here, we investigate this second category, using biosolids as an amendment to dredged material.

4.1.1 Background

4.1.1.1 Marsh Restoration and Sediment Amendments

Dredged material is one of the only sources of sediment suitable for marsh restoration projects that is available in the quantities needed. Dredged material tends to have a high sand content, which aides the dewatering and consolidation processes but also creates soil properties different from established marshes. Reflecting this sand content, dredged-material marshes tend to have lower organic matter, lower water content, and higher bulk density (Armitage *et al.* 2014; Fearnley 2008; Streever 2000; Edwards & Proffitt 2003; Feagin, Lozada-Bernard, *et al.* 2009). As typical with newly restored marshes, dredge-material marshes tend to have less belowground biomass (Tong *et al.* 2013; Armitage *et al.* 2014; Streever 2000; Boyer *et al.* 2000). Streever *et al.* (2000) performed a review of restorations, examining characteristics of sites ranging from 1 to 24 years post-construction; in regards to organic matter content, they studied 19 sites and found no evidence that levels in dredge-material marshes were increasing over time to reach levels of established marshes.

Mimicking edaphic conditions of established marshes can help restore driving physical processes (Zedler 2001). For example, soil properties are important for regulating infiltration, which can determine the presence of oxygenated zones in the soil (Marani *et al.* 2006). Sediment amendments ranging from compost to direct nutrient addition have been suggested and tested for accelerating marsh restoration (Cain & Cohen 2014; Kelley & Mendelssohn 1995; Fearnley 2008). Increased nutrients can help overcome other stressors (*e.g.* salinity (Cavalieri & Anthony H. C. Huang 1979)). In southern California, rototilling kelp compost was found to significantly increase the height and stem density of *Spartina foliosa* (O'Brien & Zedler 2006). Products like the Gulf Saver® bag use compost in an effort to increase the survival of the vegetation transplants (Sullivan 2010). Some biosolids-derived compost products are already being used in restorations (*e.g.* in a riparian wetlands (Sutton-Grier, M. Ho, *et al.* 2009)).

4.1.1.2 Biosolids in Salt Marshes

The term "biosolids" was recognized by Water Environment Federation in 1991 in response to advances in treatment technology that produced material safe for reuse (Lu *et al.* 2012). The term "sludge" now typically refers to the solids portion of wastewater while undergoing treatment, but prior to 1991, it referred to the solids at any treatment stage. Biosolids are continuously produced in all populated areas. In 1998, approximately 6.2 million dry metric tons (6.9 million U.S. tons) were produced in the U.S. (Agency 1999), and in California, 688,000 dry metric tons were produced in 2014 (of Sanitation Agencies 2015). These figures increase as the population increases. The composition of biosolids varies depending on the specific treatment processes (*e.g.* anaerobic digestion, chemical stabilization, composting) and waste streams being treated (*e.g.* industrial, residential), but they are characterized by containing organic matter and nutrients, as well as heavy metals. Land application of biosolids is common. By following U.S. EPA regulations on land application, land owners can take advantage of the well-established soil-improving benefits of biosolids application, while preventing potentially harmful accumulation of contaminants (Lu *et al.* 2012; García-Orenes *et al.* 2005; Tian *et al.* 2013).

Biosolids in wetlands are often thought of in the fresh water context, as there are extensive resources on the use of wetlands to treat wastewater (*e.g.* (Kadlec & Wallace 2008). While that practice is beneficial and can be used in conjunction with restoration (*e.g.* freshwater assimilation wetlands (Day *et al.* 2004), it is not our focus. We focus on the use of biosolids as part of the substrate in salt marshes.

There are a few studies that have looked specifically at the impact of biosolids in salt marshes. In the 1970s, I. Valiela, J.M. Teal, and coauthors sought to understand the potential consequences of sewage sludge contamination. They measured vegetation and nutrient responses to a bi-weekly broadcast of sewage sludge in a *Spartina alterniflora* and *Spartina* *patens*-dominated salt marsh in Massachusetts. During the first tide post-fertilization, about 14% of NH_4-N and 6% of PO_4-P was lost from the marsh (Valiela, Teal & W. Sass 1973). They measured an increase in aboveground biomass (Valiela, Teal & W. J. Sass 1975), decrease in root mass, and no effect on rhizomes (Valiela, Teal & Persson 1976). The lead concentrations in fertilized vegetation was twice as high as concentrations in control plots (Banus *et al.* 1974). Haines (1979) performed a similar experiment in Georgia, applying dried sewage sludge to a *S. alterniflora*-dominated salt marsh. Within a few weeks of fertilization, aboveground biomass increased in fertilized plots and remained greater through the experiment. There was also an increase in belowground biomass. Twenty months after the fertilization ended, half of the sludge nitrogen remained in the soil.

Vance *et al.* (Vance *et al.* 2003) investigated the potential of converting sewage oxidation ponds to marshes. At an abandoned sewage oxidation pond in Southern California, they measured growth of salt marsh vegetation, *Salicornia virginica* and *Frankenia gradifolia*, in pots with varying levels of aged sewage sludge. The site had previously been a salt marsh, and some plants had begun to grow naturally. Due to its aged nature, this sludge contained about 2% organic matter, which was less than the ambient wetland soil. They found no statistical difference in final plant mass between samples grown in 0% and 70% sewage sludge.

Results from previous studies indicate that a biosolids amendment, containing organic matter and nutrients, could be beneficial to vegetation, especially at early stages of marsh development. Working with local constraints, we designed one possible implementation technique for San Francisco Bay and tested it with in situ mesocosms. We present the vegetation responses, measuring both below- and aboveground biomass. Using biosolids as an amendment in restoration projects provides an opportunity to connect human infrastructure and natural coastal processes.

4.2 Methods

4.2.1 Study Site

The study site for the field experiments was Western Stege Marsh. It is a 0.04 km^2 tidally influenced salt marsh in Richmond, California, and is part of the San Francisco Bay system. The mean tidal range is 1.3 m, and the two dominant vegetation species are *Spartina foliosa* (Pacific cordgrass) in the low marsh and *Salicornia pacifica* (pickleweed) in the mid to high marsh (Inc 2010).

4.2.2 Mesocosms

To study the effect of biosolids as an amendment, an array of marsh mesocosms was constructed (Figure 4.1). In situ mesocosms are recommended for testing new restoration techniques (Callaway, Zedler, *et al.* 1997). This array consisted of 24 PVC pipes each with

Figure 4.1: Photograph of the mesocosm array (6x4 15 cm diameter PVC pipes). Photograph was taken while approaching high tide. The tops of the pipes are level with the surrounding marsh. The plastic mesh is to prevent herbivory.

a 15 cm diameter that was open to the bottom sediment. The array of pipes was built into the bank of a tidal creek, adjacent to the marsh platform. The top of the pipes had an elevation even with the surrounding marsh, which was confirmed using a laser level. This design allowed for control of the pipe substrate, while exposing the vegetation to natural conditions. It was inspired by “marsh organs,” a well-documented design for measuring primary production of marsh vegetation (Fahey & Knapp 2007).

Each pipe was filled with a particular substrate, described in Section 4.2.3, and planted with *S.foliosa* sourced from the surrounding marsh. The shock of transplanting vegetation from one environment to another is commonly damaging. At the beginning of the experiment, dead vegetation transplants were replaced until all pipes had one live stem at least 10 cm tall. Shoots were individually tracked over the course of multiple site visits, which allowed us to determine at the end of the experiment if shoots were old (*i.e.* transplanted from the marsh) or new growth. Two 4 mm holes were drilled 10 cm from the top of each pipe to prevent ponding. The entire array was wrapped in a plastic mesh to prevent herbivory.

4.2.3 Substrate

Since a typical rooting depth of *S. foliosa* is 30 cm (Callaway & Josselyn 1992), the top 30 cm of each pipe was the focus of the experiment. From 30 cm to the ground (61.4 cm total), the pipes were filled with dredged material sourced from Martinez Harbor (Martinez, CA) or clean sand. This material had been used for remediation of the marsh platform in 2004, and we used leftovers that had been stored in the upland area of the site. A layer of burlap was used to denote the 30 cm mark.

Of the 24 pipes, 16 were control pipes. The top 30 cm of control pipes were filled with dredged material obtained from the Hamilton Wetlands Restoration Project site. This material was sourced from the Port of Oakland deepening project and began dewatering in 2008. We collected this material on December 15, 2015.[1]

The remaining 8 pipes contained the same dredged material as the controls plus an 8 cm layer of biosolids starting 12 cm beneath the surface (Figure 4.2). The biosolids were obtained from the East Bay Municipal Utility District (EBMUD) Wastewater Treatment Plant on December 11, 2015. This facility produces Class B biosolids, which are used in agricultural fields and as daily cover in landfills. The biosolids had a soil-like consistency. Chemical properties of the biosolids at the facility were measured 11 days prior and 18 days after our collection date as part of routine monitoring. These results are used for characterizing the biosolids used here because the tests show low monthly variability in the biosolids properties. These tests also revealed the biosolids met the fecal coliform standards for Class A Biosolids (2015 annual maximum <1000 MPN/g).

Dredged Material Management Office (DMMO) is the regulating authority for the reuse and dumping of dredged material in San Francisco Bay. Only the biosolids' mercury concentration exceeded the set limits. Mercury in San Francisco Bay is more strictly regulated than other water bodies because there is an elevated concentration from mining in the watersheds that feed the Bay (J. A. Davis *et al.* 2012). The concentration was approximately twice the set total maximum daily limit (TMDL), but it was 57 times less than U.S. EPA land application limit (Institute 2015; Freitas & Chakrabarti 2015). When considering the total concentration over the top 30 cm of substrate, the concentration was under the limit.

At the end of the experiment, chemical and physical properties of the substrate material was analyzed by the University of California Davis Analytical Laboratory. Samples were composites of material from multiple pipes, sampled at the locations shown by the numbered boxes in Figure 4.2. The following concentrations were measured using standard operating procedures: total nitrogen, total carbon, ammonium-nitrogen, nitrate-nitrogen, extractable phosphorus, exchangeable potassium, and organic matter. Proportions of sand, silt, and clay were also determined.

---

[1] The results presented here are from the second trial of experiments. The first trial resulted in high mortality rates of vegetation in control pipes. Informed by this result, one of the original biosolids treatments was removed to have twice as many control pipes.

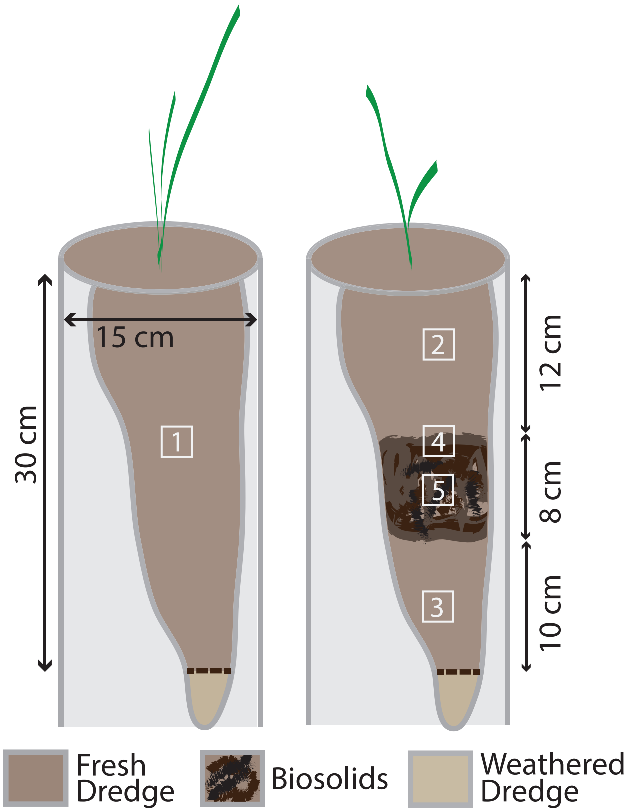

Figure 4.2: Diagram illustrating the dimensions and contents of the two types of pipe: control pipes with only dredged material (left) and treatment pipes with dredged material and biosolids (right). Numbered boxes show the substrate sampling locations. The dashed line at the 30 cm mark represents the burlap.

4.2.3.1 Subsurface Layer of Biosolids

The biosolids were placed as a subsurface layer for four main reasons. First is to prevent mixing substrates. Mechanically mixing multiple substrates is costly and logistically challenging for large-scale marsh restoration projects. Second is to increase rooting depth. Studies have found that roots are more prolific in areas of high nutrient availability ((Hodge 2004)). If nutrients are available near the surface, a shallow root system may develop, which is more prone to erosion (Darby & Turner 2008). Third is to prevent rapid loss of nutrients and organic matter. Burying the biosolids can reduce loss from tidal exchange and aerobic decomposition of organic matter (Valiela & Teal 1979). Fourth is to reduce interaction with fauna. The most biologically active soil layer is thought to be the top 15 cm, and as an additional precaution, the biosolids are largely removed from this zone (J. A. Davis 2004).

Here, the thickness of the subsurface layer was determined by the nutrient and mercury content of the biosolids. The total N content in the top 30 cm was made to match the high end of measurements from an established salt marsh in the area (approximately 1.1% Total N (Ryan & Boyer 2012). Local studies on background nutrient and metal concentrations should be used to understand what concentrations are appropriate for a particular project.

4.2.4 Biomass Characteristics

Peak aboveground biomass for *S. foliosa* in San Francisco Bay is typically reached in October to November depending on timing of rainfall (Mahall & Park 1976). The aboveground biomass was clipped at the sediment surface on November 5, 2016, and collected in labeled paper bags. The samples were then sorted and transferred to a forced-air oven for drying. They were sorted into four categories: old and alive, old and dead, new and alive, and new and dead. The samples were dried at 60°C for 48 hours, which proved sufficient for reaching a constant mass.

The pipes were removed intact on November 11, 2016, and refrigerated until they could be processed. The top 30 cm of each pipe was sectioned into 2 cm slices (in the vertical direction). Biosolids could be differentiated by eye due to their darker color. During processing, notes were kept regarding which layers contained biosolids and at what proportions to determine the amount by which the biosolids had compacted. Each layer was then washed through 2 mm and 0.5 mm sieves to separate the belowground biomass. The belowground biomass was sorted by dead and alive following the criteria described in Darby and Turner (2008) and dried in the same manner as aboveground biomass.

4.2.5 Statistical Analysis

Statistical tests for significance were performed using MATLAB (R2104b). Two sample t-tests were applied to the data assuming equal variances in the two populations. A significance level of 0.05 was used to reject the null hypothesis.

4.3 Results

4.3.1 Biomass

At the end of the growing season, there was more alive biomass in the treatment pipes than the controls. In the treatment pipes, the mean value for alive aboveground biomass was significantly greater (Figure 4.3 panel 1) and the mean value of dead aboveground biomass was significantly less than control pipes (Figure 4.3 panel 2). There was no statistical difference between the pipes when considering total (alive + dead) aboveground biomass (Figure 4.3 panel 3).

The growth of shoots was tracked over the course of the experiment. Significantly more new shoots sprouted and survived in treatment pipes (Figure 4.3 panel 4). The maximum for both groups was four new shoots. In the six days between clipping aboveground growth

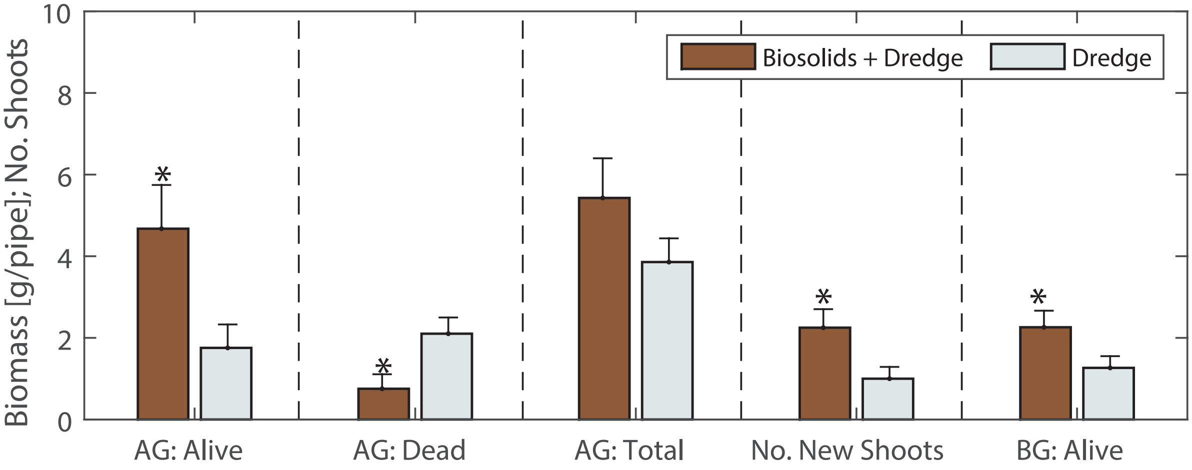

Figure 4.3: Metrics of biomass for the treatment and control pipes (AG = Aboveground, BG = Belowground). Mass is given as mass per pipe (cross-sectional area = 1.7x10^{-2} m^2). Error bars show standard error. Metrics with statistically significant difference ($p<0.05$) are marked with an asterisk.

and retrieving the pipes, shoots regrew in 13 of the pipes. Of these 13, 7 were pipes with biosolids. This regrowth was not included in the biomass or shoot measurements.

Figure 4.4a shows the vertical distribution of belowground biomass. In only one layer, 6-8 cm, were the means significantly different between the substrates. The treatment pipes had significantly more total belowground biomass (Figure 4.3 panel 5). However, it was more concentrated in the upper portion of the soil column. While not statistically different, the average rooting depth was greater in control pipes (Figure 4.4b). Dead belowground biomass could not be well distinguished from macro-organic matter and was not included.

The root to shoot ratio (R:S) is often used to investigate the effect of nutrients on growing patterns. We present this ratio two ways: roots to alive aboveground biomass (Alive R:S) and roots to total aboveground biomass (All R:S). Alive R:S was inflated by a few pipes with low values of alive aboveground biomass. All R:S had less variability (Figure 4.5). There was no statistical difference between the pipes for either ratio, but there was a slight decrease in R:S with biosolids amendment. The p-values for this and all other tests for significance are given in the Appendix.

4.3.2 Chemical and Physical Properties

The carbon to nitrogen (C:N) ratios show a greater difference between the old and new vegetation than between the vegetation grown in the different substrates. The old aboveground biomass had higher C:N values than the new, indicating the old vegetation has more refractory organic matter (Table 4.1). No distinction was made between the stems and leaves.

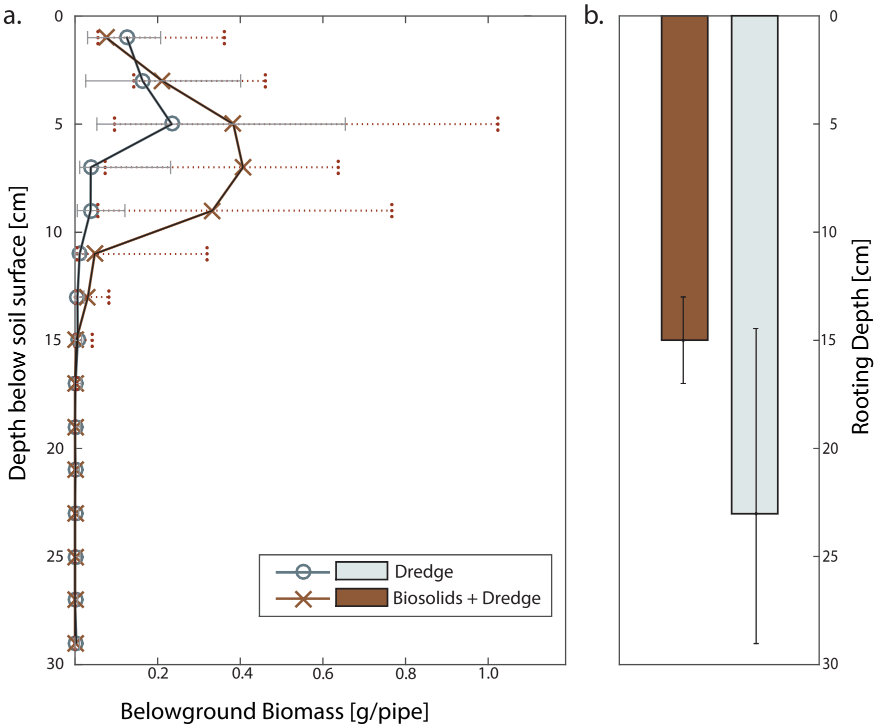

Figure 4.4: a) Belowground biomass vertically resolved by 2 cm increments for the treatment (brown) and control (gray) pipes. Symbols mark the median values and are shown at the center of the increment (*e.g.* biomass from 0-2 cm is marked at 1 cm). Mass is given as mass per pipe (cross-sectional area = 1.7x10^{-2} m^2). b) Median total rooting depth. Error bars for both show the interquartile range. All levels, except 6-8 cm (marked with an asterisk), and the rooting depths were not significantly different ($p>0.05$).

The nutrient concentrations in the biosolids decreased over the course of the experiment. Initially, the biosolids contained 1.3x10^4 mg/kg of NH_4-N; this value decreased to 1.0x10^{-3} mg/kg. A similar trend is seen in the NO_3-N and total N concentrations. For most concentrations measured, the result at Location 4 (edge of biosolids layers) indicates that this material is a mix of mainly biosolids and some dredged material (Table 4.1). The NO_3-N concentration is an anomaly at Location 3 (dredged material below the biosolids). The concentration there is measured to be twice the initial concentration in the biosolids. This high concentration is likely pooling of the NO_3-N; its negative charge allows it to move easily through negatively-charged soil.

In the aboveground biomass, copper (Cu) concentrations were highest in old vegetation and lowest in the new shoots. Although the Cu concentrations were higher in the biosolids than the dredged material by a factor of 10, the new shoots from the treatment pipes had the lowest concentrations.

The tests of physical properties revealed that the different substrates had the same soil

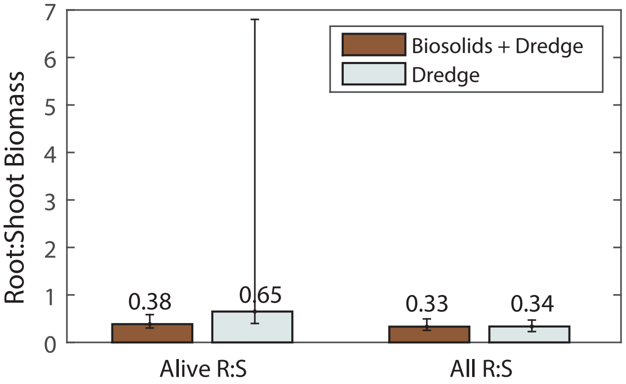

Figure 4.5: Root to shoot (R:S) ratio shown two ways: alive biomass only (left) and total (dead + alive) biomass (right). Values are the median, and error bars show interquartile range. Values were not statistically significant ($p>0.05$).

texture. Both are classified as sandy loam based on the proportions of sand, silt, and clay. The biosolids are measured to be 80% sand; this material is likely not all silica, but rather particles that are the same size as sand grains (Haynes *et al.* 2009). At the end of the experiment, the organic matter content of the biosolids was greater than the dredged material by two orders of magnitude. Statistical significance was not tested for the chemical and physical metrics due to a lack of replicates.

The amounts of compaction were variable between the pipes. Five out of 8 of the treatment pipes did not show signs of compaction, and biosolids were found in four 2 cm layers. The other 3 pipes had biosolids in three 2 cm layers, indicating 2 cm of compaction. Compaction could not be estimated for the dredged material, as any loss could be attributed to either compaction or export from the top of the pipe. Sediment deposition may have occurred, but it was not measured.

4.4 Discussion

4.4.1 Biomass

Our results support findings that increasing nutrient levels to be more similar to established marshes causes an increase in the production of above- and belowground biomass. We measured greater stem density and alive aboveground biomass in treatment pipes. This increased biomass can lead to increased wave attenuation (Pinsky *et al.* 2013) and sedimentation (Bouma, De Vries, *et al.* 2005). These processes, in turn, can allow the marsh platform to increase elevation, thereby keeping pace with sea-level rise, as well as increase carbon sequestration. The increased number of new shoots could mean that marshes restored with this technique require less vegetation transplants or that natural recruitment would be more successful, both of which could reduce project costs. The increased nutrients in the treat-

	n	C (total)	N (total)	C:N	NH_4-N	NO_3-N	[a]Olsen-P	[b]X-K	Cu
		%	%		mg/kg	mg/kg	mg/kg	mg/kg	mg/kg
*Initial Biosolids	2	-	5.7**	-	13000	5	-	-	355
DM (loc. 1)	2	0.20	0.022	9.3	2.76	0.32	11.1	242	12
DM (loc. 2)	1	0.31	0.032	9.7	3.95	0.36	22.7	239	13
DM (loc. 3)	1	0.26	0.034	7.7	0.93	10.49	40.5	290	12
BS (loc. 4)	3	4.50	0.584	7.7	422.31	0.86	93.2	505	67
BS (loc. 5)	2	11.97	1.530	7.8	1040.74	0.88	144.4	839	155
Old Veg $_{\text{BS}}$	1	32.40	1.400	23.1	-	-	-	-	22
Old Veg $_{\text{DM}}$	2	29.25	1.175	24.9	-	-	-	-	25
New Veg $_{\text{BS}}$	2	41.05	2.360	17.4	-	-	-	-	9
New Veg $_{\text{DM}}$	1	35.10	1.840	19.1	-	-	-	-	19

[a] Measures ortho-phosphate

[b] Measures exchangeable potassium

*Average of November and December 2015 values from EBMUD monthly monitoring (**Freitas˙annual˙2015**)

**Sum of Total Kjeldahl Nitrogen (TKN) and NO_3-N

Table 4.1: Properties of the substrate and vegetation material (DM = dredged material, BS = biosolids). Samples are composites, and substrate sampling locations are described in Figure 4.2. For the vegetation, subscripts indicate the substrate in which it was grown. "New" refers to new shoots, and "old" refers to shoots transplanted from the surrounding marsh. With the exception of initial biosolids, all tests were performed by the UC Davis Analytical Laboratory. All values are reported on a dry weight basis.

Substrate Type	% OM	% Sand	% Silt	% Clay
Dredged material	0.55	78	10	12
Biosolids	19.54	80	10	11

Table 4.2: Properties of dredged material (n=4) and biosolids (n=2) as measured at the conclusion of the experiment. Organic matter was measured as loss on ignition. Both substrates are classified as sandy loam (Schoeneberger *et al.* 2012. Samples are composites taken from multiple pipes.

ment pipes did not cause a decrease in belowground biomass, but rather, these pipes had significantly greater biomass. Other fertilization experiments with *S. foliosa* have found no statistical difference in belowground biomass (Boyer *et al.* 2000; Tyler *et al.* 2007).

The increased aboveground biomass outweighed the increase in belowground biomass, causing the R:S to decrease with the biosolids treatment. This difference was not statistically significant. R:S calculated with both the alive and dead material was more similar between the substrates and had less variability for the control pipes. The variability when only including the alive biomass may indicate that the aboveground biomass had died recently. Regardless of formulation, the values measured here were less than those for *S. foliosa* in established marshes in Northern and Southern California whose average values were greater than 2 (Mahall & Park 1976; Boyer *et al.* 2000). Wong *et al.* (2015) report the changes in R:S from 14 studies of nutrient additions and show that often a decrease in R:S is due to an increase in shoot biomass, rather than a decrease in root biomass. Our findings support those of Merino *et al.*(2010) and Wong *et al.*(2015) that increased nutrients does not significantly change the R:S.

The aboveground biomass in the treatment pipes was at the low end of the range found for established marshes in the San Francisco Bay area (180-689 g/m^2), while the biomass in the control pipes was below this range (Callaway & Josselyn 1992; Mahall & Park 1976). The belowground biomass, however, was much lower for both substrates when compared to established marshes (677-941 g/m^2 in the top 25 cm) (Mahall & Park 1976). This result is expected as younger marshes require time to build up belowground biomass. The plant growth may have also been affected by the experimental apparatus (*i.e.* being grown in pipes). The values for above- and belowground biomass are similar to other marsh organ experiments in the area (Janousek *et al.* 2016). Marsh organ experiments on the East and Gulf of Mexico Coast demonstrate that *S. alterniflora* has far greater biomass than *S. foliosa* (Snedden *et al.* 2015; J. Morris *et al.* 2013).

Since all samples were grown in pipes, any effect should not impact the comparison between the substrates. We attribute differences to the presence of biosolids, but it should be noted the growth is also influenced by other environmental factors. The mesocosm array allowed for influencing factors (*e.g.* salinity, hydroperiod) to be the same between the pipes, but it is possible that we did not control for everything (*e.g.* disease).

One possible reason we observed a significant response to nutrient input is that the starting *S. foliosa* biomass was low. Other studies have shown that when *S. alterniflora* biomass is low, there is a greater response to nutrient enrichment than when biomass is high (J. T. Morris *et al.* 2013). A low starting biomass is, however, true of any restoration or creation project. There is a maximum biomass at which additions of nutrients would not have an effect, but typical starting biomass levels are far below this amount (Cameron 1972). This initial increase in biomass could boost survival rates and project outcomes, particularly in storm-prone areas.

4.4.2 Fate of Nutrients

About 92% of the NH_4-N and 82% of NO_3-N were lost from the biosolids over the course of the experiment. Some nutrients were assimilated by the vegetation; the treatment vegetation had about 20% more tissue nitrogen. The remaining concentrations in the biosolids were still greater than those found in the dredged material. With one growing season of data, we cannot definitively say how long these nutrient pools will last or how they will develop over time.

Typically, added nutrients are lost quickly (*e.g* (Wong *et al.* 2015). Marsh environments, having both aerobic and anaerobic zones, foster nitrification and denitrification, which cause a loss of NH_4)-N and NO_3/NO_2 (Mitsch & Gosselink 2007. Soil texture and organic matter content determine cation exchange capacity, which largely control nutrient retention. In a dredge-material marsh (63% sand), Gibson *et al.* (Gibson *et al.* 1994) reported 50-66% of nitrogen was lost within the first two weeks after application. Mendelssohn and Kuhn (Mendelssohn & Kuhn 2003) measured higher retention of potassium and phosphorous in substrate with finer-grained sediments and recommended that future sediment additions have higher clay and silt portions (sand <25%). Similar recommendations of adding fine grained material and organic amendments were made for restored *S. foliosa* marshes in Southern California to improve nutrient retention (Boyer *et al.* 2000).

Compared to established salt marshes in San Francisco Bay, the percentage of organic matter in the biosolids at the end of the experiment (19.54%) is similar to samples from mid and high marsh zones (18.0% and 15.3%, respectively) and greater than that from low marsh zones (10.3%) (Callaway, Borgnis, *et al.* 2012). The biosolids have values similar to established *S. alterniflora* marshes in Louisiana (Stagg & Mendelssohn 2010). It takes time to develop soil carbon and nitrogen pools equivalent to those in established marshes. Whether or not a restoration is developing these pools appears to be site specific with some studies have showing an increase towards established marshes over time and others showing stagnation (Craft *et al.* 1988; Zedler & Callaway 1999; Edwards & Proffitt 2003; Streever 2000).

While the addition of nutrients in dredged-material marshes has been shown to be beneficial, we acknowledge the concern that excess nutrients leads to deterioration of the ecosystem (Deegan *et al.* 2012). Eutrophication of coastal waters is a problem (Assessment 2005). The addition of nutrients to restoration sites is to bring concentrations in nutrient-poor substrates up to levels found in the soils of established marshes. These nutrients should be added in a way that does not lead to nutrient pollution of waterways. Once vegetation is established, the marsh can become a net sink of nutrients, increasing water quality (Valiela & Cole 2002). A full review of nutrients in coastal marshes can be found in Morris *et al.* (J. T. Morris *et al.* 2013).

4.4.3 Effect of Subsurface Layer

The biosolids were placed as a subsurface layer rather than being mixed into the top soil. Burying the biosolids was thought to encourage roots to grow to this nutrient-rich layer. The rooting depth was not significantly different between the substrates. Biomass in treatment pipes often reached the biosolids layer (7 out 8 pipes) but was never found past it. The maximum rooting depth was the 16-18 cm layer, as opposed to the control pipes with maximum rooting depth at the end of sampling range (28-30 cm). The minimum rooting depth for both the control and treatment pipes was the 8-10 cm layer. The biomass for both substrates was concentrated from the surface to 10 cm down. The increased aboveground biomass and decreased rooting depth, although not statistically significant, could create conditions for plant uprooting (Turner 2011). Evidence of uprooting was not observed here, but wave energy and shear stress at the site should be considered in future implementations.

Howes *et al.* (Howes *et al.* 2010) hypothesized that discontinuities in the soil column caused sections of marsh to bifurcate during Hurricane Katrina. For the area studied, these discontinuities were layers of inorganic sediment in organic freshwater marsh substrate. Although biosolids here were applied to a saltwater environment, it is possible that in the event of great shear stress at the marsh surface, the biosolids layer could act as a discontinuity, and slippage could occur.

4.4.4 Contaminant Concerns

The fate of metals should be further investigated as it pertains to the application of biosolids as a sediment amendment. Here, we measured Cu concentrations to understand the trend in Cu transport. The Cu concentrations were highest in the old vegetation. Since the old vegetation was transplanted from the surrounding marsh, this implies the ambient marsh sediments are contaminated with Cu and potentially other metals. A similar outcome was found by Vance *et al.* (Vance *et al.* 2003); sediments thought to be clean embankment fill had higher concentrations of metals than the sewage sludge being investigated. These results highlight how common metal-contaminated sediments are in coastal environments.

By taking up metals into their tissues, marsh vegetation can have a remediating, or at least stabilizing, effect on metal concentrations. Previous studies of *S. alterniflora* have shown that the majority of metals accumulate in the root material with smaller amounts in the stems and leaves (Windham *et al.* 2003; Redondo-Gomez 2013). Since roots are largely recalcitrant in a marsh environment, this leads to permanent burial. In our experiment, the Cu concentrations in the biosolids decreased by over 50% over the course of one growing season. Some of this Cu was measured in the aboveground biomass, but it is likely the concentrations were much higher in the root material. It is unclear why the aboveground biomass grown in control pipes had higher Cu concentrations than the treatment pipes considering the biosolids material had much higher Cu concentrations, even at the end of the experiment.

This study did not specifically address public health. Yet, there are many emerging contaminants of concern. Some of which are largely hydrophilic (*e.g.* pharmaceuticals) and are currently disposed in waterways via wastewater effluent (Richardson & Kimura 2017). Other compounds, such as flame retardants, are removed from wastewater and have been found in biosolids (E. F. Davis *et al.* 2012). All potential contaminants should remain a consideration, especially as technologies advance for removing these compounds from wastewater. We rely upon U.S. EPA regulations to prevent an unhealthy build-up of metals and other potential contaminants when biosolids are applied on land. In the same way, regulations could be created for the application of biosolids to marshes.

4.4.5 Future Implementation

The way biosolids were added to dredged material here is just one of a multitude of possible designs. We modeled the process off a restoration area that has not been opened to tidal action and is in the process of dewatering the dredged material. However, every restoration project will have particular constraints, and the application of this concept should be considered on a case by case basis. The implementation needs to be tailored for the characteristics of the biosolids, other substrates being used, and receiving waters. For example, the number, thickness, and depth of layers are all parameters that could be tuned. Other strategies of application could be explored, such as hydraulically pumping low solids-content biosolids or using a subsurface injection. The biosolids may need to undergo additional treatment before they can be used. For example, Reimers *et al.* (Reimers *et al.* 2015) filed a patent for a treatment process with iron salt and heat application to create a stable product that could be used in this manner.

The location of biosolids production also makes them attractive for application to marshes. Wastewater treatment plants are often in low lying areas close to water. Transporting biosolids to restoration sites may be less costly and produce less emissions than transporting them to landfills or agricultural land, especially as future regulations may limit disposal options (*e.g.* California SB 1383).

4.5 Conclusions

Our results indicate a biosolids amendment can have a beneficial effect on biomass production in dredge-material marshes. With increased the above- and belowground biomass, salt marshes can become more stable and self-regulating. Although restoration success depends on many factors, the organic matter and nutrient additions can help the vegetation establish and restore key physical processes that drive marsh evolution. To our knowledge, this field study is the first of biosolids application with the intent to inform a full-scale marsh restoration. The potential for scaling this concept is great; biosolids are a reliability-produced source of sediment, and by using biosolids as a dredged material amendment, it creates a sustainable sediment source for marsh restorations. Marshes, in turn, can increase a community's resilience with sea-level rise. By integrating our urban infrastructure with natural coastal processes, using a biosolids amendment in marsh restorations is a mutually beneficial process that meets the goals of ecological engineering (Mitsch & Jørgensen 2004).

Chapter 5

Conclusion

5.1 Summary and Implications

5.1.1 Gas Transport

The wind-driven motion of emergent vegetation facilitates hydrodynamic gas transport. Since emergent vegetation is unique to wetlands, so is this mixing mechanism. Our results support previous work that hydrodynamic transport is an important pathway for gases in wetland environments. Other mechanisms, such as rain and thermal convection, are larger drivers of mixing, and therefore, it is unlikely that this stirring of vegetation stems is often the dominant driver of mixing. Further research is needed to understand how different mixing mechanisms interact or combine in natural environments. Current models of wetland biogeochemistry only consider one dominant form of mixing or ignore the effects of mixing all together. This incomplete representation of the physics may be contributing to the error observed in these models. As these models improve, they may be used to calculate carbon credits for wetland environments (i.e. an incentive for conservation and restoration) and inform management decisions to optimize carbon sequestration.

5.1.2 Wave Attenuation

Salt marsh vegetation is effective at reducing wave energy. As waves pass through or over vegetation, vegetative drag acts to reduce the wave height. Shoaling, bed friction, and many other forcings are also at work in a marsh environment and influence the evolution of a wave as it moves onshore. Measuring wave attenuation in San Francisco Bay, we observed many relationships measured in other marshes and laboratory experiments. Namely, greater attenuation occurred when more biomass filled the water column. For the conditions and vegetation studied, *Salicornia pacifica* was the most effective at attenuation. This species is densely packed close to the ground; due to its position high in the marsh, it is not inundated frequently and is emergent during most inundation events. *Spartina foliosa* is lower in the marsh frame and is often completely submerged at some point in the tidal cycle. S. foliosa also dies back in the winter months, changing the patterns of wave energy across the marsh. This change likely impacts sediment mobility and transport to the marsh platform. Our results showed that even fringe marshes of *S. pacifica*, which are common in San Francisco Bay, are effective at reducing wave energy year-round. If marshes are not able to move inland, there are many places were current *S. pacifica* mashes will transition to low marsh species or mudflat; both of which are less effective at reducing wave energy. This transition could bring larger waves to currently protected shorelines.

5.1.3 Biosolids Amendment

Biosolids added to dredge material were shown to increase vegetation growth. Both the aboveground and belowground biomass increased when vegetation was grown in soil containing dredge material with an 8 cm layer of biosolids. The biosolids also decreased vegetation mortality, which can increase the likelihood of restoration success. As we recognize the great benefits to restoring coastal marshes, more sediment sources are needed to complete restoration projects. Biosolids is a reliable and sustainable source of sediment. Not all biosolids will be suitable for reuse; however, wastewater treatment processes could be altered to create a biosolids product tailored to reuse in marshes. While restoring natural sediment sources and hydrology would be ideal, humans have altered these processes beyond restoration in many ways. Using biosolids represents a new way to use the human influence to mimic natural sediment sources, which cannot be restored.

5.2 Future Work

5.2.1 Belowground Processes

Much of my work has pointed to the importance of belowground biomass and belowground processes. A healthy marsh system has robust belowground biomass that contributes to vertical accretion; roots that create oxygenated zones, allowing for aerobic microbial processes in an otherwise anaerobic system; and rhizomes that anchor vegetation stems. It is likely that if belowground processes function well, most other marsh processes will also function (Turner *et al.* 2004).

Conversely, the deterioration of belowground biomass can start trigger feedbacks that lead to marsh drowning. If roots die, the air-filled spaces collapse and become water-logged. Belowground compaction then increases, inhibiting gas exchange (Laan *et al.* 1989) and causing the loss of elevation. Once the aboveground vegetation dies, there is increased open water, leading to greater fetch and wind stress. The weaker, water-logged soils are more susceptible to wave-action and physical erosion may occur.

While these feedbacks are well understood, there are knowledge gaps in our understanding of belowground processes. One such gap is root growth strategies (Bouma, van Belzen, *et al.*

2014). I propose investigating root growth strategies in the field, as well as their vegetation- and landscape-scale ramifications.

Theoretical models provide clear reasoning for different root growth schemes. Two classes commonly used to describe root topology are dichotomous branching and herringbone branching (Fitter 1991). Dichotomous branching is more complex with multiple levels of branching, or higher-order laterals. Conversely, Herringbone is characterized by an increased number of first-order laterals but not many higher-orders. Herringbone structures, being less branched, have the advantage of less radial oxygen loss, important to survival in a marsh environment. However since they cover less area, there is less opportunity for nutrient acquisition, making dichotomous branching more advantageous in nutrient-poor environments (Bouma, K. L. Nielsen, *et al.* 2001; Bouma, Koutstaal, *et al.* 2001). The width, length, and connectivity of roots and rhizomes can alter the nutrient and gas exchange with the surrounding sediment (Segers & Leffelaar 2001) and soil shear strength. Figure 5.1 shows examples of different rooting patterns observed in the biosolids-amendment experiment described in Chapter 4.

Bouma *et al.* (2001) was the first to study the root topology of marsh plants in detail. They grew many species common to European marshes in a greenhouse with different levels of nutrients and inundation. For *Spartina angelica*, larger root diameters were observed in some part of the root system with increased inundation and with increased nutrients. While none of the results directly contradicted the theories of root morphology with inundation, not all expected differences were observed or were statistically significant.

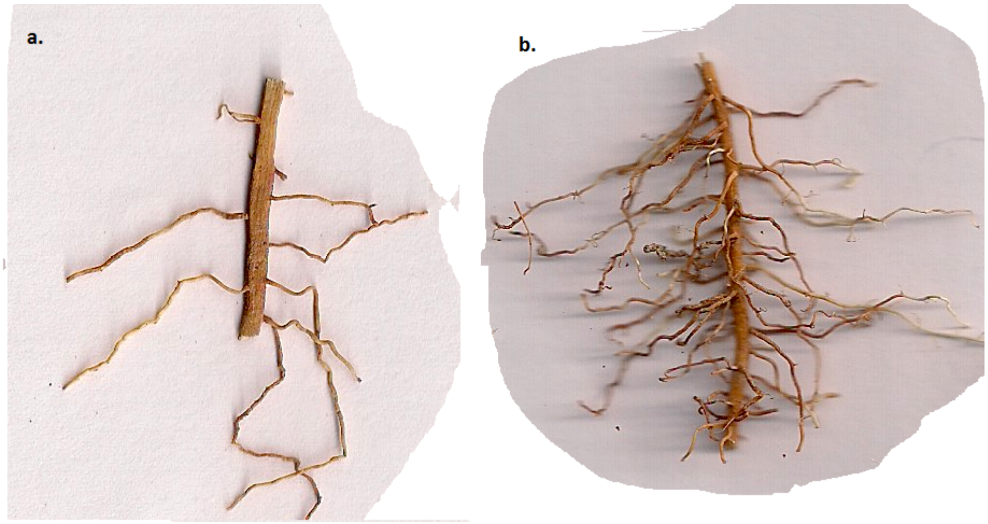

Figure 5.1: Examples of different rooting patterns. Samples are from the experiment described in Chapter 4.

I propose measuring the root topology of natural cores taken from locations with different environmental conditions but the same vegetation species. Environmental conditions to be studied include wave action, inundation, nutrient availability, and pollutants. The primary aspects of root topology will be measured, namely rooting depth and distribution, branching-order, and root and rhizome dimensions. Measurements will also be taken of vertically resolved soil shear strength, and the locations of coring will be monitored for vegetation uprooting. Thresholds will be determined for belowground biomass and root topology, after which point the vegetation becomes more vulnerable to uprooting. Follow-up studies on vegetation-uprooting thresholds could be performed in a laboratory setting, informed by these field observations.

By connecting root topology and belowground biomass to environmental conditions, these results will inform management plans in coastal areas. In particular, they could inform how to operate sediment diversions, which is a current marsh restoration strategy that causes dramatic changes in environmental conditions.

5.2.2 Restoration Implementation

It is important to remember that information on marsh ecosystems alone will not bring about action to preserve, restore, or integrate them. As coastal municipalities grapple with how to handle the current sea-level rise and prepare for the future increases, there are many influencing factors that will determine the action, or lack thereof, taken. Figure 5.2 shows a simple system map of these main drivers. There are countless factors that feed into these four.

I propose performing a systems-level analysis of five different municipalities that have either taken action or considered taking action on coastal projects related to marshes, or more generally, wetlands. By analyzing them with the same framework, we can see how differences in the situations lead to differences in outcome. We can then apply that understanding to new places and use it to inform plans and possible interventions.

5.3 Concluding Thoughts

The projects presented here cover a range of marsh dynamics. The improved understanding of these dynamics can decrease uncertainty in decision making, inform innovative solutions, and help communicate likely project outcomes. Decisions regarding our coastlines have far-reaching and lasting impacts, not only on the fate of the land itself but also on the people and cultures that thrive on it. I look forward to being a part of the work to create resilient communities that work with rather than against natural processes.

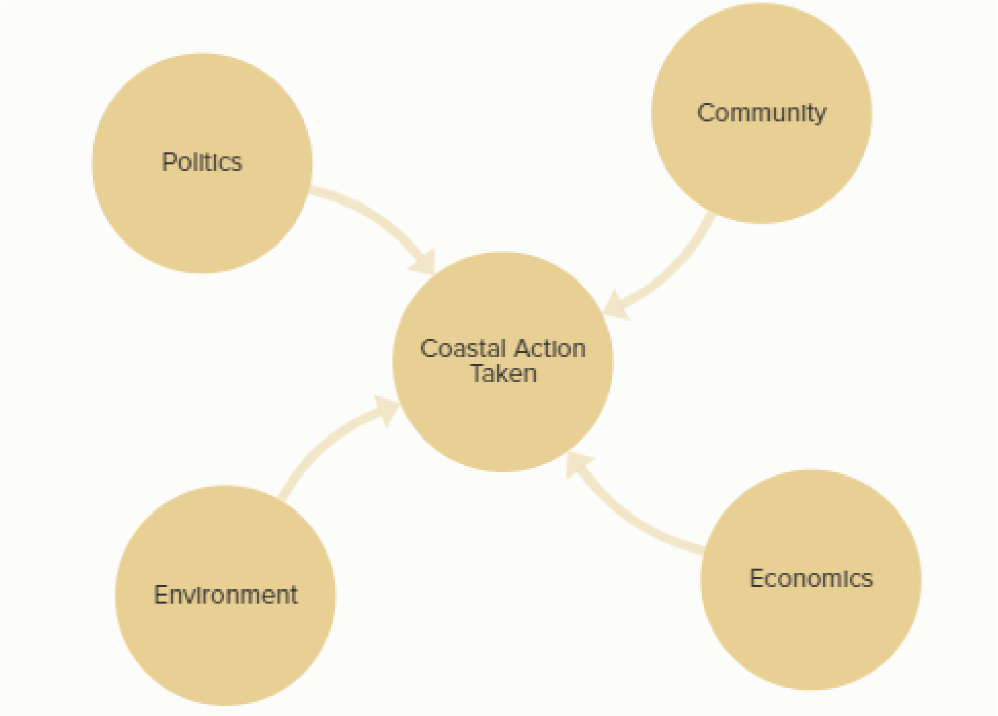

Figure 5.2: Simple network map of factors that influence the coastal action taken (i.e. marsh restoration or integration, hard shoreline approach, no action, etc).

Appendix A

A.1 Models for calculating C_D

To determine the drag coefficient, we follow the derivation of Mendez and Losada (2004) for energy dissipation due to vegetation. They present derivations for random waves along a flat-bottom, as well as monochromatic, shallow water waves along a sloping bottom. Here, we combine these derivations to show three ways to analytically determine the drag coefficient for vegetation: Case 1 - Random waves along a flat bottom; Case 2 Random shallow water waves along a flat bottom; Case 3 Random shallow water waves along a sloping bottom. Case 1 is derived in Section 2.3 of Mendez and Losada (2004), and Case 2 is a simplification of the Case 1 result for shallow water waves. Case 3 is shown below.

Wave energy is dissipated due to vegetative drag:

$$\frac{\partial E c_g}{\partial x} = -\langle \epsilon_v \rangle \tag{A.1}$$

Where E is the energy density $(1/8gH_{RMS}^2)$ and c_g is group velocity, which can be approximated as $\sqrt{gh}$ for shallow conditions. H_{RMS} is the root mean square of the wave height for a given burst, and g is the gravitational constant. For a random wave field that follows a Rayleigh distribution, the following are true:

$$\int_0^\infty H^3 p(H) dH = \frac{3\sqrt{\pi}}{4} H_{RMS}^3 \tag{A.2}$$

And

$$H_{RMS}^2 = \int_0^\infty H^2 p(H) dH \tag{A.3}$$

H is the time-varying wave height from which H_{RMS} originates. We can write the dissipation due to vegetative drag as:

$$-\langle \epsilon_v \rangle = -\Big(\frac{2}{3\pi}\Big) C_D b_v N \Big(\frac{g k_p}{2\sigma_p}\Big)^2 \frac{\sinh^3 k_p \alpha h + 3 \sinh k_p \alpha h}{3 k_p \cosh^3 k_p h} \frac{3\sqrt{\pi}}{4} H_{RMS}^3$$

(A.4)

$$-\langle \epsilon_v \rangle = -\frac{C_D b_v N g^{1/2} \alpha}{16\sqrt{\pi} h^{1/2}} H_{RMS}^3 \tag{A.5}$$

Where Eq. A.5 has been simplified for shallow conditions. Here, b_v is the diameter if the vegetation stem (m), N is the number of vegetation stems in a square meter (m^{-2}), α is the ratio of the water depth to the vegetation height (h_v/h), k_p is the wavenumber associated with the peak period, σ_p is the wave frequency associated with the peak period, and C_D is the coefficient of drag. Substituting Eq.A.2 and Eq.A.4 into Eq.A.1 gives:

$$\frac{1}{8} g^{2/3} \frac{\partial (H_{RMS}^2 h^{1/2})}{\partial x} = -\frac{C_D b_v N g^{2/3} \alpha}{16\sqrt{\pi} h^{1/2}} H_{RMS}^3 \tag{A.6}$$

Because h varies with distance x, it cannot be pulled out of the derivative. Rearranging, this gives:

$$\frac{\partial (H_{RMS}^2 h^{1/2})}{\partial x} = -A_2 \frac{H_{RMS}^3}{h^{1/2}} \tag{A.7}$$

where

$$A_2 = \frac{2 C_D b_v N \alpha}{3\pi} * \frac{3\sqrt{\pi}}{4} = \frac{C_D b_v N \alpha}{2\sqrt{\pi}} \tag{A.8}$$

Solving Eq. A.7 with boundary conditions ($H_{RMS} = H_{0,RMS}$ at x_0) gives:

$$H_{RMS} = H_{0,RMS} K_s K_v \tag{A.9}$$

where

$$K_s = \frac{h_0^{1/4}}{h^{1/4}} \tag{A.10}$$

$$K_v = \frac{1}{1 + 2\frac{A_2}{m} H_{0,RMS}(K_s - 1)} \tag{A.11}$$

and

$$h = h_0 - mx \tag{A.12}$$

This result is identical to that of Mendez and Losada (2004) for shallow water waves with monochromatic wave height over a sloping beach with the exception of the constants in the A_2 term. K_v is the vegetation damping coefficient, and K_s is the coefficient of shoaling. Table A.1 gives the resulting equations for each case.

	Conditions	Resulting Equations
Case 1	Random waves along a flat bottom	$H_{RMS} = \frac{H_{0,RMS}}{1+\tilde{\beta}x}$ $\tilde{\beta} = \frac{1}{3\sqrt{\pi}} C_D b_v N H_{0,RMS} k \frac{\sinh^3 k\alpha h}{(\sinh 2kh + 2kh)\sinh kh}$
Case 2	Random shallow water waves along a flat bottom	$H_{RMS} = H_{0,RMS} K_v$ $K_v = \frac{1}{1+\frac{A_2 H_{0,RMS}}{2h}x}$; $A_2 = \frac{C_D b_v N \alpha}{2\sqrt{\pi}}$
Case 3	Random shallow water waves along a sloping bottom	$H_{RMS} = H_{0,RMS} K_v K_s$ $K_v = \frac{1}{1+\frac{A_2 H_{0,RMS}}{2h}x}$; $A_2 = \frac{C_D b_v N \alpha}{2\sqrt{\pi}}$ $K_s = \frac{h_0^{1/4}}{h^{1/4}}$

Table A.1: Summary of the resulting equations for the change in wave height in the three cases explored.

We then applied these models to the data, calculating C_D values for each case and vegetation zone. Simplifying the governing equations to assume shallow water waves resulted in a decrease in drag coefficients (Case 1 compared to Case 2). Allowing the water depth to vary with position, thus incorporating the effects of bottom slope, caused an increase in drag coefficients (Case 2 compared to Case 3). The values from Case 3 are, however, greater than those from Case 1, indicating the net effect of the inclusion of slope was an increase in wave height due to shoaling. By not including this wave-growth process, the attenuation is underestimated. Overall, the changes between the cases were small (less than 30%) for all zones. An example of the results from these cases for the summer transition zone is shown in Fig A.1.

A.2 Effect of Bottom Friction

Following the methods outlined in Section 3.3.6, we assessed the importance of bottom friction across the study transect. Eq. 3.10 was applied to all zones to predict the change in wave height ($H_{RMS}/H_{0,RMS} = K_s K_f$) in the absence of vegetation. We used a roughness lengthscale, k_b, of 0.01 m, which was measured in San Pablo Bay by Lacy and MacVean (2016). The predicted values were then compared to the measured values. The winter *S. foliosa* results are not included here and are discussed in the text. For all other zones, an average of wave growth was predicted, but wave attenuation was measured. The minimum

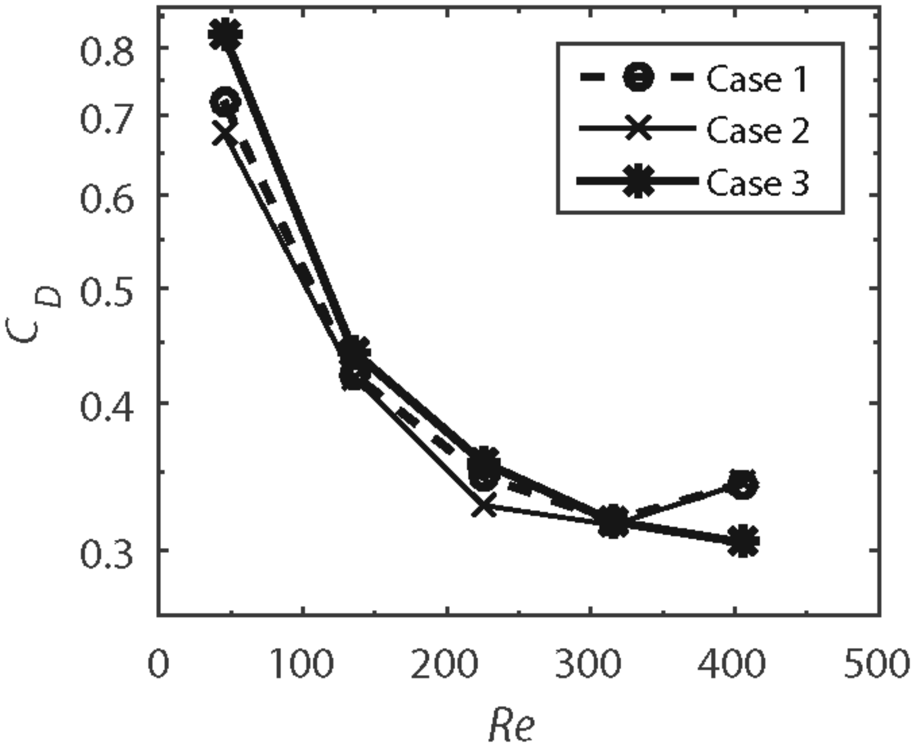

Figure A.1: C_D as a function of Re from the summer transition zone calculated with three different models; Case 1: Flat and not shallow; Case 2: Flat and shallow; Case 3: Sloped and shallow.

average difference was 18.5% for summer *S. foliosa*; only accounting for shoaling and bottom friction predicted an average wave growth of 7.5%, whereas on average waves were attenuated by 11%. The maximum difference of 94% occurred in the transition zone in the winter; average of 26% of wave growth was predicted, and wave attenuation average of 86% was measured. We also assessed bottom friction alone ($H_{RMS}/H_{0,RMS} = K_f$). While bottom friction in the absence of shoaling does predict wave attenuation, the measured attenuates rates were much larger. The difference between them was on average the smallest for the *S. foliosa* zone (5% difference) and the greatest (64% difference) for the summer *S. pacifica*. An example comparison for the winter transition zone 2 is shown in Fig. A.2.

As a further check, we calculated C_D values adding bottom friction to the vegetation dissipation model as follows:

$$H_{RMS} = H_{0,RMS} K_s K_v K_f \tag{A.13}$$

Including bottom friction caused a decrease in the C_D values by an average of 18%. The results for all vegetation zones were fit to the relationship $C_D = a+(b/Re)^c$ with and without

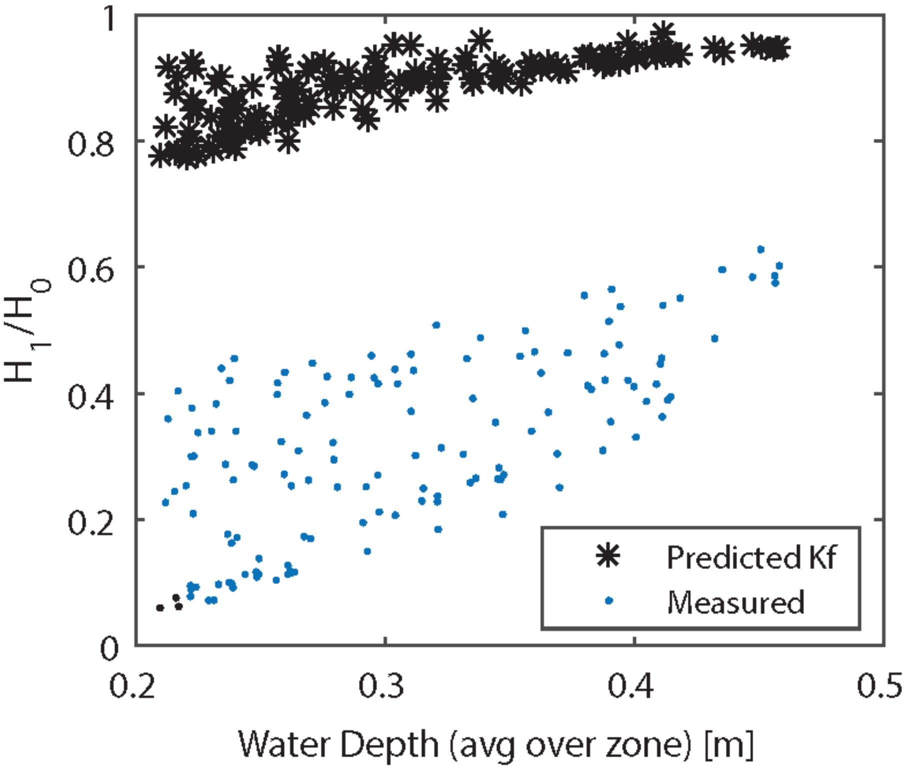

Figure A.2: Ratio of wave height at W4 to W5 (border transition zone 2) measured and predicted from the model of bottom friction alone.

the bottom friction term (Fig. A.3). The 95% confidence intervals for these two fits overlap.

A.3 p-values from Mesocosm Statistical Tests

Statistical tests for significance were performed using MATLAB (R2014b). Two sample t-tests were applied to the data assuming equal variances in the two populations. A significance level of 0.05 was used to reject the null hypothesis. The following table contains the p-values of all tests performed.

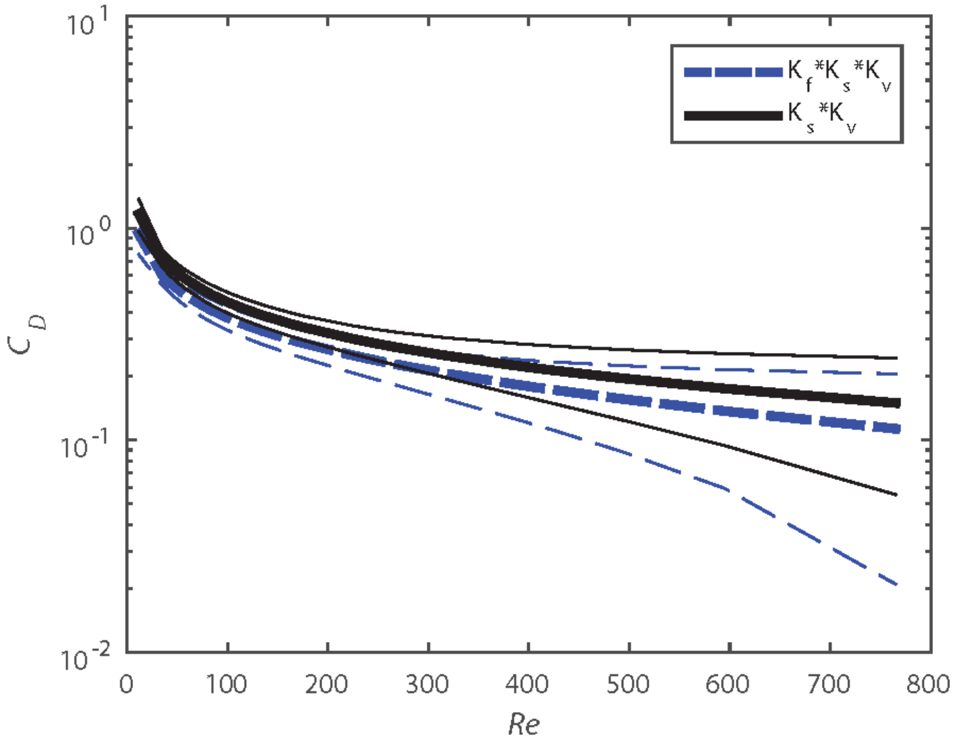

Figure A.3: C_D as a function of Re with and without including bottom friction. The thin lines show 95% confidence interval on the fit.

$C_D = a + (b/Re)^c$	**a**	**b**	**c**	**Range of** Re
*Current Study, *S. foliosa*	0.187	22.2	1.14	76-511
Current Study, *S. pacifica*	0.402	11.9	1.53	10-170
Current Study, Transition	-0.176	44.4	0.354	31-594
Möller *et al.* 2014 (irregular waves)	0.159	227.3	1.615	0-1200
**Jadhav *et al.* 2013	0.02	4000	0.78	200-3500
Pinsky *et al.* 2013,*S. foliosa*	0	311.1	1.67	10-3000
Anderson and Smith 2014, *S. foliosa*	0.187	744.2	1.27	533-2296

Table A.2: $C_D - Re$ fit coefficients. *Fit to the summer dataset only. All others are a fit to both the winter and summer datasets. **Obtained from Guannel *et al.* (2015).

Vegetation type	r^2
S.foliosa	0.77
Transition	0.79
S.pacifica	0.93

Table A.3: Correlation coefficients for the empirical fits to binned data.

	p-value
Total Aboveground Biomass	0.1552
Alive Aboveground Biomass	**0.0149**
Dead Aboveground Biomass	**0.0402**
Alive Belowground Biomass	**0.0423**
No. of New Shoots	**0.0246**
Root:Shoot (alive+dead)	0.3758
Root:Shoot (alive only)	0.2223
Rooting Depth	0.3874
Belowground Biomass (0-2 cm)	0.5362
Belowground Biomass (2-4 cm)	0.8394
Belowground Biomass (4-6 cm)	0.2691
Belowground Biomass (6-8 cm)	**0.0228**
Belowground Biomass (8-10 cm)	0.0851
Belowground Biomass (10-12 cm)	0.2962
Belowground Biomass (12-14 cm)	0.1791
Belowground Biomass (14-16 cm)	0.6813
Belowground Biomass (16-18 cm)	0.2953
Belowground Biomass (18-20 cm)	0.1770
Belowground Biomass (20-22 cm)	0.1674
Belowground Biomass (22-24 cm)	0.2453
Belowground Biomass (24-26 cm)	0.1605
Belowground Biomass (26-28 cm)	0.3078
Belowground Biomass (28-30 cm)	0.2842

Table A.4: p-values for the tests for significance. Significant p-values ($p<0.05$) are shown in bold.

Bibliography

1. Agency, U. E. P. *Biosolids Generation, Use, and Disposal in The United States* EPA530-R-99-009 (1999).
2. Anderson, M. E. & Smith, J. M. Wave attenuation by flexible, idealized salt marsh vegetation. *Coastal Engineering* **83,** 82–92. ISSN: 0378-3839 (Jan. 2014).
3. Armitage, A. R., Ho, C.-K., Madrid, E. N., Bell, M. T. & Quigg, A. The influence of habitat construction technique on the ecological characteristics of a restored brackish marsh. *Ecological Engineering* **62,** 33–42. ISSN: 0925-8574 (Jan. 2014).
4. Assessment, M. E. *Ecosystems and Human Well-being: Synthesis* (Island Press, Washington, DC, 2005).
5. Augustin, L. N., Irish, J. L. & Lynett, P. Laboratory and numerical studies of wave damping by emergent and near-emergent wetland vegetation. *Coastal Engineering* **56,** 332–340. ISSN: 0378-3839 (Mar. 2009).
6. Banus, M., Valiela, I. & Teal, J. Export of lead from salt marshes. *Marine Pollution Bulletin* **5,** 6–9. ISSN: 0025326X (Jan. 1974).
7. Barber, T. R., Burke, R. A. & Sackett, W. M. Diffusive flux of methane from warm wetlands. *Global Biogeochemical Cycles* **2,** 411–425. ISSN: 08866236 (Dec. 1988).
8. Baustian, J. J., Turner, R. E., Walters, N. F. & Muth, D. P. Restoration of dredged canals in wetlands: a comparison of methods. *Wetlands Ecology and Management* **17,** 445–453. ISSN: 0923-4861, 1572-9834 (Oct. 1, 2009).
9. Baye, P. R. Tidal Marsh Vegetation of China Camp, San Pablo Bay, California. *San Francisco Estuary and Watershed Science* **10.** ISSN: 1546-2366. `http://www.escholarship.org/uc/item/9r9527d7` (2012).
10. Beagle, J., Salomon, M., Baumgarten, S. & Grossinger, R. *Shifting Shores: Marsh Expansion and Retreat in San Pablo Bay* Prepared for the US EPA San Francisco Bay Program and the San Francisco Estuary Partnership Publication #751 (San Francisco Estuary Institute, Richmond, CA, June 2015).
11. Boesch, D. F. & Turner, R. E. Dependence of Fishery Species on Salt Marshes: The Role of Food and Refuge. *Estuaries* **7,** 460. ISSN: 01608347 (Dec. 1984).

12. Bouma, T. J., De Vries, M. B., *et al.* Trade-Offs Related To Ecosystem Engineering: A Case Study on Stiffness of Emerging Macrophytes. *Ecology* **86,** 2187–2199. ISSN: 0012-9658 (Aug. 2005).
13. Bouma, T. J., Nielsen, K. L., Van Hal, J. & Koutstaal, B. Root system topology and diameter distribution of species from habitats differing in inundation frequency. *Functional Ecology* **15,** 360–369. ISSN: 1365-2435 (June 1, 2001).
14. Bouma, T. J., Koutstaal, B. P., Dongen, M. v. & Nielsen, K. L. Coping with low nutrient availability and inundation: root growth responses of three halophytic grass species from different elevations along a flooding gradient. *Oecologia* **126,** 472–481. ISSN: 0029-8549, 1432-1939 (Feb. 1, 2001).
15. Bouma, T. J., van Belzen, J., *et al.* Identifying knowledge gaps hampering application of intertidal habitats in coastal protection: Opportunities & steps to take. *Coastal Engineering. Coasts@Risks: THESEUS, a new wave in coastal protection* **87,** 147–157. ISSN: 0378-3839 (May 2014).
16. Boyer, K. E., Callaway, J. C. & Zedler, J. B. Evaluating the progress of restored cordgrass (Spartina foliosa) marshes: Belowground biomass and tissue nitrogen. *Estuaries* **23,** 711–721. ISSN: 0160-8347 (Oct. 1, 2000).
17. Brüchert, F., Speck, O. & Spatz, H.-C. Oscillations of plants' stems and their damping: theory and experimentation. *Philosophical Transactions of the Royal Society of London. Series B: Biological Sciences* **358,** 1487–1492. ISSN: 0962-8436, 1471-2970 (Sept. 29, 2003).
18. Cain, J. L. & Cohen, R. A. Using sediment alginate amendment as a tool in the restoration of Spartina alterniflora marsh. *Wetlands Ecology and Management,* 1–11. ISSN: 0923-4861, 1572-9834 (2014).
19. Callaway, J. C., Borgnis, E. L., Turner, R. E. & Milan, C. S. Carbon Sequestration and Sediment Accretion in San Francisco Bay Tidal Wetlands. *Estuaries and Coasts* **35,** 1163–1181. ISSN: 1559-2723, 1559-2731 (Sept. 2012).
20. Callaway, J. C. & Josselyn, M. N. The introduction and spread of smooth cordgrass (Spartina alterniflora) in South San Francisco Bay. *Estuaries* **15,** 218–226. ISSN: 0160-8347 (June 1, 1992).
21. Callaway, J. C., Zedler, J. B. & Ross, D. L. Using Tidal Salt Marsh Mesocosms to Aid Wetland Restoration. *Restoration Ecology* **5,** 135–146. ISSN: 1526-100X (June 1, 1997).
22. Cameron, G. N. Analysis of Insect Trophic Diversity in Two Salt Marsh Communities. *Ecology* **53,** 58–73. ISSN: 00129658 (Jan. 1972).
23. Cavalieri, A. J. & Anthony H. C. Huang. Evaluation of Proline Accumulation in the Adaptation of Diverse Species of Marsh Halophytes to the Saline Environment. *American Journal of Botany* **66,** 307–312. ISSN: 00029122, 15372197 (1979).

24. Chen, S. S., Wambsganss, M. W. & Jendrzejczyk, J. A. Added Mass and Damping of a Vibrating Rod in Confined Viscous Fluids. *Journal of Applied Mechanics* **43,** 325–329. ISSN: 0021-8936 (June 1, 1976).
25. Cloern, J. E. & Nichols, F. H. *Temporal Dynamics of an Estuary: San Francisco Bay* OCLC: 840305978. ISBN: 978-94-009-5528-8 978-94-010-8940-1. `http://public.eblib.com/choice/publicfullrecord.aspx?p=3103981` (Springer Netherlands, Dordrecht, 1985).
26. Collins, J. I. Prediction of shallow-water spectra. *Journal of Geophysical Research* **77,** 2693–2707. ISSN: 01480227 (May 20, 1972).
27. Cooper, N. J. Wave Dissipation Across Intertidal Surfaces in the Wash Tidal Inlet, Eastern England. *Journal of Coastal Research* **211,** 28–40. ISSN: 0749-0208, 1551-5036 (Jan. 2005).
28. Cowardin, L., Carter, V., Golet, F. & LaRoe, E. *Classification of Wetlands & Deepwater Habitats of the U. S.* FWS/OBS-79/31 (U.S. Fish and Wildlife Service, Washington, D. C., 1979).
29. Craft, C. B., Broome, S. W. & Seneca, E. D. Nitrogen, phosphorus and organic carbon pools in natural and transplanted marsh soils. *Estuaries* **11,** 272–280. ISSN: 0160-8347 (Dec. 1, 1988).
30. Crusius, J. & Wanninkhof, R. Gas transfer velocities measured at low wind speed over a lake. *Limnology and Oceanography* **48,** 1010–1017. ISSN: 00243590 (May 2003).
31. Dalrymple, R. A., Kirby, J. T. & Hwang, P. A. Wave Diffraction Due to Areas of Energy Dissipation. *Journal of Waterway, Port, Coastal, and Ocean Engineering* **110,** 67–79. ISSN: 0733-950X, 1943-5460 (Feb. 1984).
32. Darby, F. A. & Turner, R. E. Below- and Aboveground Spartina alterniflora Production in a Louisiana Salt Marsh. *Estuaries and Coasts* **31,** 223–231. ISSN: 1559-2723, 1559-2731 (Feb. 2008).
33. Davis, E. F., Klosterhaus, S. L. & Stapleton, H. M. Measurement of flame retardants and triclosan in municipal sewage sludge and biosolids. *Environment International* **40,** 1–7. ISSN: 01604120 (Apr. 2012).
34. Davis, J. A. *et al.* Reducing methylmercury accumulation in the food webs of San Francisco Bay and its local watersheds. *Environmental Research* **119,** 3–26 (2012).
35. Davis, J. A. The long-term fate of polychlorinated biphenyls in San Francisco Bay (USA). *Environmental Toxicology and Chemistry* **23,** 2396. ISSN: 0730-7268, 1552-8618 (2004).
36. Day, J. *et al.* The use of wetlands in the Mississippi Delta for wastewater assimilation: a review. *Ocean & Coastal Management* **47,** 671–691. ISSN: 09645691 (Jan. 2004).
37. De Langre, E. Effects of Wind on Plants. *Annual Review of Fluid Mechanics* **40,** 141–168 (2008).

38. Dean, R. G. & Dalrymple, R. A. *Water wave mechanics for engineers and scientists* (world scientific publishing Co Inc, 1991).
39. Deegan, L. A. *et al.* Coastal eutrophication as a driver of salt marsh loss. *Nature* **490,** 388–392. ISSN: 0028-0836 (Oct. 18, 2012).
40. Dhir, B., Sharmila, P. & Saradhi, P. P. Potential of Aquatic Macrophytes for Removing Contaminants from the Environment. *Critical Reviews in Environmental Science and Technology* **39,** 754–781. ISSN: 1064-3389, 1547-6537 (Aug. 31, 2009).
41. Doaré, O., Moulia, B. & de Langre, E. Effect of Plant Interaction on Wind-Induced Crop Motion. *Journal of Biomechanical Engineering* **126,** 146–151. ISSN: 0148-0731 (May 4, 2004).
42. Edwards, K. R. & Proffitt, C. E. Comparison of wetland structural characteristics between created and natural salt marshes in southwest Louisiana, USA. *Wetlands* **23,** 344–356. ISSN: 0277-5212, 1943-6246 (June 1, 2003).
43. Efron, B. & Tibshirani, R. J. *An introduction to the bootstrap* (CRC press, 1994).
44. Ellison, A. M. Effects of Competition, Disturbance, and Herbivory on Salicornia Europaea. *Ecology* **68,** 576–586. ISSN: 00129658 (June 1987).
45. Fagherazzi, S. *et al.* in *Treatise on Geomorphology* (ed Shroder, J. F.) 182–200 (Academic Press, San Diego, 2013). ISBN: 978-0-08-088522-3. (2014).
46. *Principles and Standards for Measuring Primary Production* (eds Fahey, T. J. & Knapp, A. K.) (Oxford University Press, Aug. 1, 2007). 268 pp. ISBN: 978-0-19-516866-2. (2014).
47. Feagin, R. A., Irish, J. L., *et al.* Short communication: Engineering properties of wetland plants with application to wave attenuation. *Coastal Engineering* **58,** 251–255. ISSN: 0378-3839 (Mar. 2011).
48. Feagin, R. A., Lozada-Bernard, S. M., *et al.* Does vegetation prevent wave erosion of salt marsh edges? *Proceedings of the National Academy of Sciences* **106,** 10109–10113. ISSN: 0027-8424, 1091-6490 (June 23, 2009).
49. Fearnley, S. The Soil Physical and Chemical Properties of Restored and Natural Back-Barrier Salt Marsh on Isles Dernieres, Louisiana. *Journal of Coastal Research,* 84–94. ISSN: 0749-0208 (Jan. 1, 2008).
50. Finnigan, J. J. Turbulence in Waving Wheat. *Boundary-Layer Meteorology* **16,** 181–211. ISSN: 0006-8314, 1573-1472 (Sept. 1, 1979).
51. Fitter, A. H. The ecological significance of root system architecture: an economic approach. 229–243 (1991).
52. Flesch, T. & Grant, R. Corn Motion in the Wind during Senescence: 11- Effect of Dynamic Plant Characteristics. *Agronomy Journal* **84,** 748. ISSN: 0002-1962 (1992).

53. Freitas, D. & Chakrabarti, A. *Annual 40 CFR 503 Report submitted to EPA Region 9* (East Bay Municipal Utility District, Special District No. 1, Oakland, Calif., 2015).

54. García-Orenes, F. *et al.* Factors controlling the aggregate stability and bulk density in two different degraded soils amended with biosolids. *Soil and Tillage Research* **82,** 65–76. ISSN: 0167-1987 (May 2005).

55. Gardner, S. C., Grue, C. E., Major, W. W. & Conquest, L. L. Aquatic invertebrate communities associated with purple loosestrife (Lythrum salicaria), cattail (Typha latifolia), and bulrush (Scirpus acutus) in central Washington, USA. *Wetlands* **21,** 593–601. ISSN: 0277-5212, 1943-6246 (Dec. 1, 2001).

56. Gedan, K. B., Kirwan, M. L., Wolanski, E., Barbier, E. B. & Silliman, B. R. The present and future role of coastal wetland vegetation in protecting shorelines: answering recent challenges to the paradigm. *Climatic Change* **106,** 7–29. ISSN: 0165-0009, 1573-1480 (May 1, 2011).

57. Ghisalberti, M. & Nepf, H. M. Mixing layers and coherent structures in vegetated aquatic flows. *Journal of Geophysical Research: Oceans* **107,** 3–1–3–11. ISSN: 2156-2202 (C2 2002).

58. Gibson, K., Zedler, J. & Langis, R. Limited Response of Cordgrass (Spartina foliosa) to Soil Amendments in a Constructed Marsh. *Ecological Applications* **4,** 757–767. ISSN: 1051-0761 (Nov. 1994).

59. Goman, M., Malamud-Roam, F. & Ingram, B. L. Holocene environmental history and evolution of a tidal salt marsh in San Francisco Bay, California. *Journal of Coastal Research* **24,** 1126–1137 (Sept. 2008).

60. Gosselin, F. & de Langre, E. Destabilising effects of plant flexibility in air and aquatic vegetation canopy flows. *European Journal of Mechanics - B/Fluids* **28,** 271–282. ISSN: 0997-7546 (Mar. 2009).

61. Groeneveld, D. P. & French, R. H. Hydrodynamic Control of an Emergent Aquatic Plant (scirpus Acutus) in Open Channels1. *JAWRA Journal of the American Water Resources Association* **31,** 505–514. ISSN: 1752-1688 (1995).

62. Guannel, G. *et al.* Integrated modeling framework to quantify the coastal protection services supplied by vegetation. *Journal of Geophysical Research: Oceans* **120,** 324–345. ISSN: 21699275 (Jan. 2015).

63. Haines, E. Growth Dynamics of Cordgrass, Spartina Alterniflora Loisel., on Control and Sewage Sludge Fertilized Plots in a Georgia Salt Marsh. *Estuaries* **2,** 50–53 (Mar. 1979).

64. Happell, J. D., Chanton, J. P. & Showers, W. J. Methane transfer across the water-air interface in stagnant wooded swamps of Florida: Evaluation of mass-transfer coefficients and isotropic fractionation. *Limnology and Oceanography* **40,** 290–298. ISSN: 00243590 (1995).

65. Harley, C. D. G. & Bertness, M. D. Structural Interdependence: An Ecological Consequence of Morphological Responses to Crowding in Marsh Plants. *Functional Ecology* **10,** 654. ISSN: 02698463 (Oct. 1996).

66. Haynes, R. J., Murtaza, G. & Naidu, R. in *Advances in Agronomy* (ed Donald L. Sparks) 165–267 (Academic Press, 2009). ISBN: 0065-2113. `http://www.sciencedirect.com/science/article/pii/S0065211309040048` (2014).

67. Ho, D. T., Wanninkhof, R., *et al.* Toward a universal relationship between wind speed and gas exchange: Gas transfer velocities measured with ^{3}He/SF$_6$ during the Southern Ocean Gas Exchange Experiment. *Journal of Geophysical Research* **116.** ISSN: 0148-0227. doi:`10.1029/2010JC006854`. `http://doi.wiley.com/10.1029/2010JC006854` (2015) (July 28, 2011).

68. Ho, D. T., Zappa, C. J., *et al.* Influence of rain on air-sea gas exchange: Lessons from a model ocean. *Journal of Geophysical Research: Oceans* **109,** n/a–n/a. ISSN: 01480227 (C8 Aug. 2004).

69. Hodge, A. The plastic plant: root responses to heterogeneous supplies of nutrients. *New Phytologist* **162,** 9–24. ISSN: 0028-646X, 1469-8137 (Apr. 2004).

70. Howes, N. C. *et al.* Hurricane-induced failure of low salinity wetlands. *Proceedings of the National Academy of Sciences* **107,** 14014–14019. ISSN: 0027-8424, 1091-6490 (Aug. 10, 2010).

71. Inc, T. T. E. *Year 5 Monitoring Report for the Western Stege Marsh Restoration Project* (Sept. 30, 2010).

72. Infantes, E. *et al.* Effect of a seagrass (Posidonia oceanica) meadow on wave propagation. *Marine Ecology Progress Series* **456,** 63–72. ISSN: 0171-8630, 1616-1599 (June 7, 2012).

73. Inoue, E. Studies of the phenomena of waving plants (”honami”) caused by wind. Part 1: Mechanism and characteristics of waving plants phenomena. *J. Agric. Meteorol.(Japan)* **11,** 18–22 (1955).

74. Institute, S. F. E. *Dredged Material Testing Thresholds Effective in Calendar Years 2016-2019* Dredged Material Testing Thresholds for San Francisco Bay Area Sediments. `http://www.sfei.org/content/dmmo-ambient-sediment-conditions#sthash.b9yQzZ5H.dpbs`.

75. Jadhav, R. S. & Chen, Q. Field Investigation of Wave Dissipation Over Salt Marsh Vegetation During Tropical Cyclone. *Coastal Engineering Proceedings* **1,** waves.41. ISSN: 0589-087X (Oct. 25, 2012).

76. Jadhav, R. S., Chen, Q. & Smith, J. M. Spectral distribution of wave energy dissipation by salt marsh vegetation. *Coastal Engineering* **77,** 99–107. ISSN: 0378-3839 (July 2013).

77. Janousek, C. *et al.* Potential effects of sea-level rise on plant productivity: species-specific responses in northeast Pacific tidal marshes. *Marine Ecology Progress Series* **548,** 111–125. ISSN: 0171-8630, 1616-1599 (Apr. 21, 2016).

78. Kadlec, R. H. & Wallace, S. *Treatment wetlands* ISBN: 1-4200-1251-7 (CRC press, 2008).

79. Kelley, S. & Mendelssohn, I. A. An evaluation of stabilized, water-based drilled cuttings and organic compost as potential sediment sources for marsh restoration and creation in coastal Louisiana. *Ecological Engineering* **5,** 497–517. ISSN: 0925-8574 (Dec. 1995).

80. Kirwan, M. L., Temmerman, S., Skeehan, E. E., Guntenspergen, G. R. & Fagherazzi, S. Overestimation of marsh vulnerability to sea level rise. *Nature Climate Change* **6,** 253–260. ISSN: 1758-678X, 1758-6798 (Feb. 24, 2016).

81. Knutson, P. L., Brochu, R. A., Seelig, W. N. & Inskeep, M. Wave damping in Spartina alterniflora marshes. *Wetlands* **2,** 87–104. ISSN: 0277-5212, 1943-6246 (Dec. 1982).

82. Knutson, T. R. *et al.* Tropical cyclones and climate change. *Nature Geoscience* **3,** 157–163. ISSN: 1752-0894, 1752-0908 (Mar. 2010).

83. Kobayashi, N., Raichle, A. W. & Asano, T. Wave Attenuation by Vegetation. *Journal of Waterway, Port, Coastal, and Ocean Engineering* **119,** 30–48. ISSN: 0733-950X, 1943-5460 (Jan. 1993).

84. Laan, P., Berrevoets, M. J., Lythe, S., Armstrong, W. & Blom, C. W. P. M. Root Morphology and Aerenchyma Formation as Indicators of the Flood-Tolerance of Rumex Species. *Journal of Ecology* **77,** 693–703. ISSN: 0022-0477 (Sept. 1, 1989).

85. Lacy, J. R. & MacVean, L. J. Wave attenuation in the shallows of San Francisco Bay. *Coastal Engineering* **114,** 159–168. ISSN: 03783839 (Aug. 2016).

86. Lu, Q., He, Z. L. & Stoffella, P. J. Land Application of Biosolids in the USA: A Review. *Applied and Environmental Soil Science* **2012,** 1–11. ISSN: 1687-7667, 1687-7675 (2012).

87. MacIntyre, S. *et al.* Buoyancy flux, turbulence, and the gas transfer coefficient in a stratified lake. *Geophysical Research Letters* **37.** ISSN: 00948276. doi:`10.1029/2010GL044164`. `http://doi.wiley.com/10.1029/2010GL044164` (2015) (Dec. 2010).

88. Mack, S., Day Jr, J. W. & Lane, R. *Restoration of Degraded Wetlands of the Mississippi Delta* (American Carbon Registry, 2012), 26. `http://americancarbonregistry.org/carbon-accounting/standards-methodologies/restoration-of-degraded-deltaic-wetlands-of-the-mississippi-delta/wr-mf-wl_v2-0.pdf`.

89. MacKenzie, R. A. & Dionne, M. Habitat heterogeneity: *Marine Ecology Progress Series* **368,** 217–230. ISSN: 01718630, 16161599 (2008).

90. Mahall, B. E. & Park, R. B. The Ecotone Between Spartina Foliosa Trin. and Salicornia Virginica L. in Salt Marshes of Northern San Francisco Bay: I. Biomass and Production. *The Journal of Ecology* **64,** 421. ISSN: 00220477 (July 1976).

91. Marani, M. *et al.* Spatial organization and ecohydrological interactions in oxygen-limited vegetation ecosystems. *Water Resources Research* **42,** W06D06. ISSN: 1944-7973 (June 1, 2006).

92. Masamba, W. R. L., Gondwe, M. J. & Murray-Hudson, M. Physicochemical controls of diffusive methane fluxes in the Okavango Delta, Botswana. *Wetlands Ecology and Management.* ISSN: 0923-4861, 1572-9834. doi:`10.1007/s11273-015-9407-5`. `http://link.springer.com/10.1007/s11273-015-9407-5` (2015) (Jan. 29, 2015).

93. McKenna, S. & McGillis, W. The role of free-surface turbulence and surfactants in airfffdfffdfffdwater gas transfer. *International Journal of Heat and Mass Transfer* **47,** 539–553. ISSN: 00179310 (Jan. 2004).

94. Melton, J. R. *et al.* Present state of global wetland extent and wetland methane modelling: conclusions from a model intercomparison project (WETCHIMP). *Biogeosciences Discussions* **9,** 11577–11654. ISSN: 1810-6285 (Aug. 27, 2012).

95. Mendelssohn, I. A. & Kuhn, N. L. Sediment subsidy: effects on soilfffdfffdfffdplant responses in a rapidly submerging coastal salt marsh. *Ecological Engineering* **21,** 115–128. ISSN: 0925-8574 (Dec. 1, 2003).

96. Méndez, F. J. & Losada, I. J. An empirical model to estimate the propagation of random breaking and nonbreaking waves over vegetation fields. *Coastal Engineering* **51,** 103–118. ISSN: 03783839 (Apr. 2004).

97. Merino, J. H., Huval, D. & Nyman, A. J. Implication of nutrient and salinity interaction on the productivity of Spartina patens. *Wetlands Ecology and Management* **18,** 111–117. ISSN: 0923-4861, 1572-9834 (Apr. 1, 2010).

98. Miller, R. L., Fram, M., Fujii, R. & Wheeler, G. Subsidence Reversal in a Re-established Wetland in the Sacramento-San Joaquin Delta, California, USA. *San Francisco Estuary and Watershed Science* **6.** ISSN: 1546-2366. `http://www.escholarship.org/uc/item/5j76502x` (2008).

99. Miller, R. L. & Fujii, R. Plant community, primary productivity, and environmental conditions following wetland re-establishment in the Sacramento-San Joaquin Delta, California. *Wetlands Ecology and Management* **18,** 1–16. ISSN: 0923-4861, 1572-9834 (May 26, 2009).

100. Mitsch, W. J. & Gosselink, J. G. *Wetlands* ISBN: 978-0-471-69967-5 0-471-69967-5 (Wiley, Hoboken, N.J., 2007).

101. Mitsch, W. J. & Jørgensen, S. E. *Ecological engineering and ecosystem restoration* 411 pp. ISBN: 978-0-471-33264-0 (Wiley, Hoboken, N.J, 2004).

102. Möller, I. & Spencer, T. Wave dissipation over macro-tidal saltmarshes: Effects of marsh edge typology and vegetation change. *Journal of Coastal Research* **36,** 506–521 (2002).

103. Möller, I., Kudella, M., *et al.* Wave attenuation over coastal salt marshes under storm surge conditions. *Nature Geoscience* **7,** 727–731. ISSN: 1752-0894 (Oct. 2014).

104. Morris, J. T., Shaffer, G. P. & Nyman, J. A. Brinson Review: Perspectives on the Influence of Nutrients on the Sustainability of Coastal Wetlands. *Wetlands* **33,** 975–988. ISSN: 0277-5212, 1943-6246 (Oct. 11, 2013).

105. Morris, J., Sundberg, K. & Hopkinson, C. Salt Marsh Primary Production and Its Responses to Relative Sea Level and Nutrients in Estuaries at Plum Island, Massachusetts, and North Inlet, South Carolina, USA. *Oceanography* **26,** 78–84. ISSN: 10428275 (Sept. 1, 2013).

106. Narayan, S., Beck, M. W., Wilson, P., *et al.* Coastal Wetlands and Flood Damage Reduction: Using Risk Industry-based Models to Assess Natural Defenses in the Northeastern USA. doi:`10.7291/v93x84kh`. `https://doi.org/10.7291/v93x84kh` (2017) (2016).

107. Narayan, S., Beck, M. W., Reguero, B. G., *et al.* The Effectiveness, Costs and Coastal Protection Benefits of Natural and Nature-Based Defences. *PLOS ONE* **11** (ed Chapman, M. (G.) e0154735. ISSN: 1932-6203 (May 2, 2016).

108. Nepf, H. M. Drag, turbulence, and diffusion in flow through emergent vegetation. *Water Resources Research* **35,** 479–489. ISSN: 1944-7973 (1999).

109. Neumeier, U. Quantification of vertical density variations of salt-marsh vegetation. *Estuarine, Coastal and Shelf Science* **63,** 489–496. ISSN: 02727714 (June 2005).

110. Nielsen, P. *Coastal bottom boundary layers and sediment transport* (World Scientific Publishing Co Inc, 1992).

111. Nowacki, D. J., Beudin, A. & Ganju, N. K. Spectral wave dissipation by submerged aquatic vegetation in a back-barrier estuary: Wave dissipation by vegetation. *Limnology and Oceanography* **62,** 736–753. ISSN: 00243590 (Mar. 2017).

112. O'Brien, E. L. & Zedler, J. B. Accelerating the Restoration of Vegetation in a Southern California Salt Marsh. *Wetlands Ecology and Management* **14,** 269–286. ISSN: 0923-4861, 1572-9834 (June 1, 2006).

113. Of Sanitation Agencies, C. A. *Biosolids Fact Sheet* 2015. `http://casaweb.org/wp-content/uploads/2015/12/2015-Biosolids-Fact-Sheet-cm.pdf`.

114. Ouyang, X. & Lee, S. Y. Updated estimates of carbon accumulation rates in coastal marsh sediments. *Biogeosciences* **11,** 5057–5071. ISSN: 1726-4189 (Sept. 19, 2014).

115. Paquier, A.-E., Haddad, J., Lawler, S. & Ferreira, C. M. Quantification of the Attenuation of Storm Surge Components by a Coastal Wetland of the US Mid Atlantic. *Estuaries and Coasts.* ISSN: 1559-2723, 1559-2731. doi:`10.1007/s12237-016-0190-1`. `http://link.springer.com/10.1007/s12237-016-0190-1` (Nov. 18, 2016).

116. Patton, C. *Turning Salt into Environmental Gold: Wetland Restoration in the South San Francisco Bay Salt Ponds* (Save the San Francisco Bay Association, 2002). `https://www.savesfbay.org/sites/default/files/SALT_PONDS_REPORT.pdf`.

117. Pinsky, M. L., Guannel, G. & Arkema, K. K. Quantifying wave attenuation to inform coastal habitat conservation. *Ecosphere* **4,** art95. ISSN: 2150-8925 (Aug. 2013).

118. Poindexter, C. M. & Variano, E. A. Gas exchange in wetlands with emergent vegetation: The effects of wind and thermal convection at the air-water interface. *Journal of Geophysical Research: Biogeosciences* **118,** 1297–1306. ISSN: 2169-8961 (2013).

119. Pontee, N., Narayan, S., Beck, M. W. & Hosking, A. H. Nature-based solutions: lessons from around the world. *Proceedings of the Institution of Civil Engineers - Maritime Engineering* **169,** 29–36. ISSN: 1741-7597, 1751-7737 (Mar. 2016).

120. Py, C., de Langre, E. & Moulia, B. A frequency lock-in mechanism in the interaction between wind and crop canopies. *Journal of Fluid Mechanics* **568,** 425–449. ISSN: 0022-1120 (Dec. 1, 2006).

121. Raupach, M. R., Finnigan, J. J. & Brunei, Y. Coherent eddies and turbulence in vegetation canopies: The mixing-layer analogy. *Boundary-Layer Meteorology* **78,** 351–382. ISSN: 0006-8314, 1573-1472 (Mar. 1, 1996).

122. Redondo-Gomez, S. Bioaccumulation of heavy metals in Spartina. *Functional Plant Biology.* ISSN: 1445-4408. doi:`10.1071/FP12271` (2013).

123. Reimers, R., ENGLANDE, A., Murray, N. & Xu, Y. *Utilization of iron salts to stabilize and/or disinfect biosolids* US Patent 9,199,885. `https://www.google.com/patents/US9199885` (Google Patents, Dec. 2015).

124. Richardson, S. D. & Kimura, S. Y. Emerging environmental contaminants: Challenges facing our next generation and potential engineering solutions. *Environmental Technology & Innovation* **8,** 40–56. ISSN: 23521864 (Nov. 2017).

125. Rohmer, T., Kerr, D. & Hogle, I. *San Francisco Estuary Invasive Spartina Project 2014 ISP monitoring and treatment report* (2015).

126. Ryan, A. B. & Boyer, K. E. Nitrogen further promotes a dominant salt marsh plant in an increasingly saline environment. *Journal of Plant Ecology* **5,** 429–441. ISSN: 1752-993X, 1752-9921 (Oct. 2012).

127. Schoeneberger, P., Wysocki, D. A., Benham, E. C. & Staff, S. S. *Field book for describing and sampling soils. Version 3.0.* (USDA-NRCS, National Soil Survey Center, Lincoln, NE, 2012).

128. Segers, R. & Leffelaar, P. A. Modeling methane fluxes in wetlands with gas-transporting plants: 1. Single-root scale. *Journal of Geophysical Research: Atmospheres* **106,** 3511–3528. ISSN: 2156-2202 (D4 Feb. 27, 2001).

129. Shaffer, G. P. *et al.* The MRGO Navigation Project: A Massive Human-Induced Environmental, Economic, and Storm Disaster. *Journal of Coastal Research* **10054,** 206–224. ISSN: 0749-0208, 1551-5036 (Nov. 2009).

130. Snedden, G. A., Cretini, K. & Patton, B. Inundation and salinity impacts to above- and belowground productivity in Spartina patens and Spartina alterniflora in the Mississippi River deltaic plain: Implications for using river diversions as restoration tools. *Ecological Engineering* **81,** 133–139. ISSN: 0925-8574 (Aug. 2015).

131. Spalding, M., McIvor, A., *et al.* Coastal Ecosystems: A Critical Element of Risk Reduction: Coastal ecosystems and risk reduction. *Conservation Letters* **7,** 293–301. ISSN: 1755263X (May 2014).

132. Spalding, M., Ruffo, S., *et al.* The role of ecosystems in coastal protection: Adapting to climate change and coastal hazards. *Ocean & Coastal Management* **90,** 50–57. ISSN: 0964-5691 (Mar. 2014).

133. Spatz, H.-C. & Speck, O. Oscillation frequencies of tapered plant stems. *American Journal of Botany* **89,** 1–11. ISSN: 0002-9122, 1537-2197 (Jan. 1, 2002).

134. Speck, O. & Spatz, H.-C. Damped oscillations of the giant reed Arundo donax (Poaceae). *American Journal of Botany* **91,** 789–796. ISSN: 0002-9122, 1537-2197 (June 1, 2004).

135. Stagg, C. L. & Mendelssohn, I. A. Restoring Ecological Function to a Submerged Salt Marsh. *Restoration Ecology* **18,** 10–17. ISSN: 1526-100X (Sept. 1, 2010).

136. Stocker, T., Intergovernmental Panel on Climate Change, Intergovernmental Panel on Climate Change & Working Group I. *Climate change 2013: the physical science basis : Working Group I contribution to the Fifth Assessment Report of the Intergovernmental Panel on Climate Change* ISBN: 978-1-107-41532-4 1-107-41532-2 (2014).

137. Streever, W. J. Spartina alternifloramarshes on dredged material: a critical review of the ongoing debate over success. *Wetlands Ecology and Management* **8,** 295–316. ISSN: 0923-4861, 1572-9834 (Oct. 1, 2000).

138. Sullivan, D. Employing Marsh Grass and Compost to Heal the Gulf. *BioCycle* **51,** 24–26. ISSN: 02765055 (Oct. 2010).

139. Sutton-Grier, A., Ho, M. & Richardson, C. J. Organic amendments improve soil conditions and denitrification in a restored riparian wetland. *Wetlands* **29,** 343–352. ISSN: 0277-5212, 1943-6246 (Mar. 1, 2009).

140. Sutton-Grier, A., Wowk, K. & Bamford, H. Future of our coasts: The potential for natural and hybrid infrastructure to enhance the resilience of our coastal communities, economies and ecosystems. *Environmental Science & Policy* **51,** 137–148. ISSN: 14629011 (Aug. 2015).

141. Swanson, K. M. *et al.* Wetland Accretion Rate Model of Ecosystem Resilience (WARMER) and Its Application to Habitat Sustainability for Endangered Species in the San Francisco Estuary. *Estuaries and Coasts* **37,** 476–492. ISSN: 1559-2723, 1559-2731 (Mar. 2014).

142. Sweet, W. *et al. Global and regional sea level rise scenarios for the United States* Report NOS CO-OPS 083 (2017), 75. `http://pubs.er.usgs.gov/publication/70190256`.

143. Takekawa, J. *et al. Final report for sea-level rise response modeling for San Francisco Bay estuary tidal marshes* US Geol Surv Open File Rep 2013-1081 (2013), 161. `http:%20//pubs.%20usgs.gov/of/2013/1081/pdf/ofr20131081.pdf`.

144. Teal, J. M. & Kanwisher, J. W. Gas Transport in the Marsh Grass, Spartina alterniflora. *Journal of Experimental Botany* **17,** 355–361. ISSN: 0022-0957, 1460-2431 (May 1, 1966).

145. Temmerman, S., De Vries, M. B. & Bouma, T. J. Coastal marsh die-off and reduced attenuation of coastal floods: A model analysis. *Global and Planetary Change* **92-93,** 267–274. ISSN: 0921-8181 (July 2012).

146. Tian, G., Franzluebbers, A., Granato, T., Cox, A. & O'Connor, C. Stability of soil organic matter under long-term biosolids application. *Applied Soil Ecology* **64,** 223–227. ISSN: 0929-1393 (Feb. 2013).

147. Tong, C., Baustian, J. J., Graham, S. A. & Mendelssohn, I. A. Salt marsh restoration with sediment-slurry application: Effects on benthic macroinvertebrates and associated soil-plant variables. *Ecological Engineering* **51,** 151–160. ISSN: 0925-8574 (Feb. 2013).

148. Tse, I., Poindexter, C. & Variano, E. Wind-driven water motions in wetlands with emergent vegetation. *Water Resources Research* **52,** 2571–2581. ISSN: 00431397 (Mar. 2016).

149. Turner, R. E. Beneath the Salt Marsh Canopy: Loss of Soil Strength with Increasing Nutrient Loads. *Estuaries and Coasts* **34,** 1084–1093. ISSN: 1559-2723, 1559-2731 (Sept. 2011).

150. Turner, R. E., Swenson, E. M., Milan, C. S., Lee, J. M. & Oswald, T. A. Below-ground biomass in healthy and impaired salt marshes. *Ecological Research* **19,** 29–35. ISSN: 1440-1703 (Jan. 1, 2004).

151. Tyler, A. C., Lambrinos, J. G. & Grosholz, E. D. Nitrogen Inputs Promote the Spread of an Invasive Marsh Grass. *Ecological Applications* **17,** 1886–1898. ISSN: 1051-0761 (Oct. 2007).

152. U.S. Environmental Protection Agency & U.S. Army Corps of Engineers. *Identifying, Planning, and Financing Beneficial Use Projects Using Dredged Material: Beneficial Use Planning Manual* EPA842-B-07-001 (Washington, D. C., Oct. 2007), 114. `http://el.erdc.usace.army.mil/dots/budm/pdf/PlanningManual.pdf`.

153. Valiela, I. & Cole, M. L. Comparative Evidence that Salt Marshes and Mangroves May Protect Seagrass Meadows from Land-derived Nitrogen Loads. *Ecosystems* **5,** 92–102. ISSN: 1432-9840, 1435-0629 (Jan. 1, 2002).

154. Valiela, I. & Teal, J. M. The nitrogen budget of a salt marsh ecosystem. *Nature* **280,** 652–656. ISSN: 0028-0836, 1476-4687 (Aug. 1979).

155. Valiela, I., Teal, J. M. & Persson, N. Y. Production and dynamics of experimentally enriched salt marsh vegetation: Belowground biomass. *Limnology and Oceanography* **21,** 245–252. ISSN: 00243590 (1976).

156. Valiela, I., Teal, J. M. & Sass, W. Nutrient retention in salt marsh plots experimentally fertilized with sewage sludge. *Estuarine and Coastal Marine Science* **1,** 261–269. ISSN: 0302-3524 (July 1973).

157. Valiela, I., Teal, J. M. & Sass, W. J. Production and Dynamics of Salt Marsh Vegetation and the Effects of Experimental Treatment with Sewage Sludge. Biomass, Production and Speies Composition. *Journal of Applied Ecology* **12,** 973–981. ISSN: 00218901, 13652664 (1975).

158. Vance, R. R. *et al.* Effects of Sewage Sludge on the Growth of Potted Salt Marsh Plants Exposed to Natural Tidal Inundation. *Restoration Ecology* **11,** 155–167. ISSN: 1526-100X (June 1, 2003).

159. Wamsley, T. V., Cialone, M. A., Smith, J. M., Atkinson, J. H. & Rosati, J. D. The potential of wetlands in reducing storm surge. *Ocean Engineering* **37,** 59–68. ISSN: 0029-8018 (Jan. 2010).

160. *Concepts and controversies in tidal marsh ecology* (eds Weinstein, M. P. & Kreeger, D. A.) (Kluwer Academic, Dordrecht ; Boston, 2000). 875 pp. ISBN: 978-0-7923-6019-3.

161. Wiberg, P. L. & Sherwood, C. R. Calculating wave-generated bottom orbital velocities from surface-wave parameters. *Computers & Geosciences* **34,** 1243–1262. ISSN: 00983004 (Oct. 2008).

162. Windham, L., Weis, J. & Weis, P. Uptake and distribution of metals in two dominant salt marsh macrophytes, Spartina alterniflora (cordgrass) and Phragmites australis (common reed). *Estuarine, Coastal and Shelf Science* **56,** 63–72. ISSN: 02727714 (Jan. 2003).

163. Wong, J. X., Van Colen, C. & Airoldi, L. Nutrient levels modify saltmarsh responses to increased inundation in different soil types. *Marine Environmental Research.* ISSN: 0141-1136. doi:`10.1016/j.marenvres.2014.12.003` (2015).

164. Ysebaert, T. *et al.* Wave Attenuation by Two Contrasting Ecosystem Engineering Salt Marsh Macrophytes in the Intertidal Pioneer Zone. *Wetlands* **31,** 1043–1054. ISSN: 0277-5212, 1943-6246 (Dec. 1, 2011).

165. *Handbook for restoring tidal wetlands* (ed Zedler, J. B.) (CRC Press, Boca Raton, Fla, 2001). 439 pp. ISBN: 978-0-8493-9063-0.

166. Zedler, J. B. & Callaway, J. C. Tracking Wetland Restoration: Do Mitigation Sites Follow Desired Trajectories? *Restoration Ecology* **7,** 69–73. ISSN: 1526-100X (Mar. 1, 1999).